DISS. ETH NO. 29383

# Online Feedback Optimization for Power Grid Control

A thesis submitted to attain the degree of

DOCTOR OF SCIENCES of ETH ZURICH

(Dr. sc. ETH Zurich)

presented by

Lukas Ortmann

M. Sc. RWTH, RWTH Aachen

born on 18. December 1991

accepted on the recommendation of

Prof. Dr. Florian Dörfler, examiner (ETH Zurich)
Dr. Saverio Bolognani, co-examiner (ETH Zurich)
Prof. Dr. Andreas Ulbig, co-examiner (RWTH Aachen)
Prof. Dr. Christian Rehtanz, co-examiner (TU Dortmund)

2023

ISBN 978-3-907363-34-8
DOI 10.3929/ethz-b-000635318

To my family

*Fortune favors the prepared mind.*

– *Louis Pasteur*

# Acknowledgments

I would like to thank Florian and Saverio for their support, help, and encouragement. You always gave me the freedom and opportunities to explore what I thought was the right way forward. Florian's feedback on papers was always on-point, and Saverio's talent for spot-on formulations helped me write read-worthy papers. Both on a professional and personal level, I could not have asked for better supervisors.

Thank you to Andreas Ulbig and Christian Rehtanz for serving as co-examinators of this thesis.

I want to thank my collaborators from ETH Zurich, Imperial College London, RWTH Aachen, DTU Roskilde, and AEW Energie AG, RTE France, ABB Switzerland for their support during our joint projects.

I also want to thank everyone at the Automatic Control Laboratory (IfA) for making it an outstanding workplace and for creating the "IfA family" spirit. Thanks to Jeremy for being a good friend and the best climbing and mountaineering partner one could ask for. Thanks to Miguel for being a good friend, office mate, collaborator, and climbing buddy. Thanks to Verena for developing "Verena's algorithm", which I used throughout my research, and for being my teaching buddy and boot camp trainer in Ghana. Thanks to Adrian for your work on the mathematical foundation of Online Feedback Optimization and for onboarding me at the lab. Thanks to Irina for going climbing together and to Dominic for the mountain trips. Thanks to Felix and Tasos for being awesome office mates that made it fun to come to the lab. Thanks to Paul for teaching me how to trad climb and for being the Australian rope gun on adventures together with Jeremy. Thanks to Ben, Linda, and the NCCR in general for supporting me throughout my industry outreach, knowledge transfer, and implementation of my research in the real world. Thanks to Sabrina and Tanja for creating a good atmosphere at the lab and for teaching me to understand Swiss German. Thanks to Roy for always providing great advice and for being the very definition of wisdom when it comes to control theory.

I would like to thank the German Academic Scholarship Foundation for their support during my studies and for enabling me to go to Berkeley and Harvard.

Special thanks go to my family. I would not be where I am today if it were not for your support and encouragement. Finally, I want to thank Julia for always supporting me and for being by my side.

# Abstract

Current optimization approaches utilized in the power grid are not equipped to handle the challenges that come with the power grid transformation. New tools are needed that can operate in real-time, handle a large number of volatile generators, and work with the limited model information available in distribution grids. The Online Feedback Optimization (OFO) control method was specifically designed and developed to have these capabilities. It uses optimization algorithms to drive physical systems, e.g., power grids, to the optimal solution of an optimization problem, e.g., Optimal Power Flow (OPF), using limited model information and computation power. Based on optimization and control theory, researchers have developed the mathematical foundation for the OFO control method.

However, there remains a gap between the OFO theory and its application to power systems. The goal of the thesis is to bridge that gap by evaluating the ability of OFO to solve power system problems, improving and extending it, and implementing it in power system laboratories and a real distribution grid.

First, an OFO controller and a simulation of the French transmission grid are derived to evaluate the applicability of OFO controllers to control a heterogenous group of actuators in a subtransmission grid with the ultimate goal of utilizing the grid to its full extent and therefore minimizing the necessary curtailment of renewable generation. Toward that goal, a simulation model was created in close collaboration with the French transmission grid operator, and an OFO controller was extended with the ability to handle discrete actuators. Using this model, it was shown that the newly proposed OFO controller can effectively operate a subtransmission grid, meaning that: 1) the OFO controller tracks the OPF solution, 2) is robust to model mismatch, and 3) enforces the grid constraints.

Second, an OFO controller for the power grid is developed to derive curative actions in real-time and to serve as an example of how OFO controllers could enable curative $N-1$ grid operations. To showcase this, a case study inspired by the 2003 Swiss-Italian blackout is implemented using a dynamic grid simulation tool. Within the simulation environment, an OFO controller has to derive active power setpoints and voltage magnitude setpoints for large generating units to enforce the grid constraints while minimizing the voltage difference over an open circuit breaker. The OFO controller is able to successfully derive effective curative actions in real-time, and the voltage difference is lowered, which would allow for the closing of the circuit breaker.

Third, an algorithm is developed to learn the input-output sensitivity of a system from data while the system is operated by an OFO controller. Given that this is the only model information needed by an OFO controller, it allows building completely model-free OFO controllers. The algorithm is based on a Kalman filter and uses a small white noise to guarantee persistency of excitation. A simulation of the IEEE 123-bus system is used to show the performance of such a model-free OFO controller.

Fourth, an OFO controller using only peer-to-peer communication and local computation is implemented on a laboratory distribution grid feeder. Its task is to minimize the use of reactive power while satisfying the voltage constraints along the feeder. The implementation shows the minimal modeling and communication requirements needed for successful Volt/VAr control.

Fifth, three Volt/VAr control schemes are implemented on a laboratory distribution grid feeder to analyze their capabilities to regulate the voltage along a distribution grid feeder. The schemes are droop control, an OPF-based dispatch, and an OFO controller. The experiment shows that droop control does not utilize the reactive power resources to their full extent and hence cannot enforce the voltage constraints during the experiment. The reactive power setpoints, calculated by the OPF-based dispatch, also lead to constraint violations. The reason behind this is a model mismatch that occurred even though all generation and consumption along the feeder were measured and the grid model of the laboratory is accurately known. Finally, the OFO controller successfully controls the reactive power sources to enforce the voltage constraints and is able to do so with minimal or even no model information.

Sixth, an OFO controller is implemented in the distribution grid of the Canton of Aargau, which supplies 100.000 people. The controller uses off-the-shelf hardware and the reactive power resources of existing inverters to optimize the reactive power flow at the substation connecting the distribution and subtransmission grid. This leads to a financial reward due to a coordination scheme between the distribution grid operator and the subtransmission grid operator. The hardware, software, and controller implementation are presented, and the interaction of an OFO controller with a real distribution grid is analyzed. This successful implementation of an OFO controller in a real distribution grid brings the OFO control method to Technology Readiness Level (TRL) 7.

Overall, the research in this thesis shows that the OFO control method is capable of solving a multitude of power system problems and works well within real power grids.

# Zusammenfassung

Die derzeitigen Optimierungsansätze für das Stromnetz sind nicht in der Lage, die mit der Transformation des Stromnetzes einhergehenden Herausforderungen zu bewältigen. Es werden neue Werkzeuge benötigt, die in Echtzeit arbeiten, eine große Anzahl unbeständiger Generatoren handhaben und mit den begrenzten Modellinformationen arbeiten können, die in Verteilnetzen verfügbar sind. Die OFO-Regelungsmethode wurde speziell für diese Fähigkeiten konzipiert und entwickelt. Sie verwendet Optimierungsalgorithmen, um physikalische Systeme, z. B. Stromnetze, mit begrenzten Modellinformationen und Rechenleistung zur optimalen Lösung eines Optimierungsproblems, z. B. OPF, zu führen. Auf der Grundlage der Optimierungs- und Regelungstheorie haben Forschende die mathematische Grundlage für die OFO-Regelungsmethode entwickelt.

Es bleibt jedoch eine Lücke zwischen der OFO-Theorie und ihrer Anwendung auf Energiesysteme. Ziel dieser Arbeit ist es, diese Lücke zu schließen, indem die Fähigkeit von OFO zur Lösung von Energiesystemproblemen bewertet, verbessert und erweitert und in Labors für Energiesysteme und in einem realen Verteilnetz implementiert wird.

Zunächst werden ein OFO-Regler und eine Simulation des französischen Übertragungsnetzes abgeleitet, um die Anwendbarkeit von OFO-Reglern zur Steuerung einer heterogenen Gruppe von Stellgliedern in einem Teilübertragungsnetz zu bewerten, mit dem Ziel, die Netzinfrastruktur voll auszunutzen und damit die notwendige Abregelung der erneuerbaren Erzeugung zu minimieren. Zu diesem Zweck wurde in enger Zusammenarbeit mit dem französischen Übertragungsnetzbetreiber ein Simulationsmodell erstellt und ein OFO-Regler um die Fähigkeit erweitert, diskrete Aktoren zu steuern. Anhand dieses Modells wurde gezeigt, dass der neu vorgeschlagene OFO-Regler ein Teilübertragungsnetz effektiv betreiben kann, was bedeutet, dass: 1) der OFO-Regler der OPF-Lösung folgt, 2) robust gegenüber Modellfehlern ist und 3) die Grenzen der Netzelemente durchsetzt.

Zweitens wird ein OFO-Regler für das Stromnetz entwickelt, um kurative Maßnahmen in Echtzeit abzuleiten und als Beispiel dafür zu dienen, wie OFO-Regler einen kurativen $N-1$-Netzbetrieb ermöglichen könnten. Um dies zu demonstrieren, wird eine Fallstudie, inspiriert durch den Stromausfall in der Schweiz und Italien im Jahr 2003, mit Hilfe eines dynamischen Netzsimulationstools implementiert. Innerhalb der Simulationsumgebung muss ein OFO-Regler Wirkleistungssollwerte und Spannungsgrößensollwerte für große Erzeugungseinheiten ableiten, um die Grenzen der Netzelemente einzuhalten und gleichzeitig die Spannungsdifferenz über einen offenen Leistungsschalter zu minimieren. Der

OFO-Regler ist in der Lage, wirksame Abhilfemaßnahmen in Echtzeit abzuleiten, und die Spannungsdifferenz wird gesenkt, was das Schließen des Leistungsschalters ermöglicht.

Drittens wird ein Algorithmus entwickelt, um die Eingangs-/Ausgangsempfindlichkeit eines Systems aus Daten zu lernen, während das System von einem OFO-Regler betrieben wird. Da dies die einzige Modellinformation ist, die ein OFO-Regler benötigt, ermöglicht er den Aufbau völlig modellfreier OFO-Regler. Der Algorithmus basiert auf einem Kalman-Filter und verwendet ein kleines weißes Rauschen, um die Beständigkeit der Erregung zu gewährleisten. Anhand einer Simulation des IEEE 123-Bussystems wird die Leistungsfähigkeit eines solchen modellfreien OFO-Reglers gezeigt.

Viertens wird ein OFO-Regler, der nur Peer-to-Peer-Kommunikation und lokale Berechnungen verwendet, in einem Laborverteilnetzabzweig implementiert. Seine Aufgabe ist es, den Einsatz von Blindleistung zu minimieren und gleichzeitig die Spannungsvorgaben entlang des Abzweigs zu erfüllen. Die Implementierung zeigt die minimalen Modellierungs- und Kommunikationsanforderungen, die für eine erfolgreiche Volt/VAr-Regelung erforderlich sind.

Fünftens werden drei Volt/VAr-Regelungsschemata auf einem Laborverteilnetzabzweig implementiert, um ihre Fähigkeiten zur Regelung der Spannung entlang eines Verteilnetzabzweigs zu analysieren. Bei den Verfahren handelt es sich um eine Droop-Regelung, einen OPF-basierten Dispatch und einen OFO-Regler. Das Experiment zeigt, dass die Droop-Regelung die Blindleistungsressourcen nicht in vollem Umfang nutzt und daher die Spannungsbeschränkungen während des Experiments nicht durchsetzen kann. Auch die vom OPF-basierten Dispatch berechneten Blindleistungssollwerte führen zu Grenzwertverletzungen. Der Grund dafür ist ein Modellfehler, der auftrat, obwohl alle Erzeugungs- und Verbrauchsdaten entlang des Netzes gemessen wurden und das Netzmodell des Labors genau bekannt ist. Schließlich steuert der OFO-Regler erfolgreich die Blindleistungsquellen, um die Spannungsbeschränkungen durchzusetzen, und er ist in der Lage, dies mit minimalen oder sogar ohne Modellinformationen zu tun.

Sechstens wird ein OFO-Regler im Verteilnetz des Kantons Aargau implementiert, das 100.000 Menschen versorgt. Der Regler nutzt handelsübliche Hardware und die Blindleistungsressourcen vorhandener Wechselrichter, um den Blindleistungsfluss im Unterwerk, das das Verteil- und Teilübertragungsnetz verbindet, zu optimieren. Dies führt zu einer finanziellen Belohnung durch ein Koordinationsschema zwischen dem Verteilnetzbetreiber und dem Teilübertragungsnetzbetreiber. Die Hardware, die Software und die Implementierung des Reglers werden vorgestellt und die Interaktion eines OFO-Reglers mit einem realen Verteilnetz wird analysiert. Diese erfolgreiche Implementierung eines OFO-Reglers in einem realen Verteilnetz bringt die OFO-Regelungsmethode auf TRL 7.

Insgesamt zeigt die Forschung in dieser Arbeit, dass die OFO-Regelungsmethode in der Lage ist, eine Vielzahl von Stromnetzproblemen zu lösen und in realen Stromnetzen gut funktioniert.

# Contents

CHAPTER 1

# Introduction

ELECTRIC power is a core essential of our modern society, and the electric power grid is the most important critical infrastructure we have. Its continuous and safe operation is of the utmost importance. Until now, the power grid consisted of predictable and controllable power generation from large fossil or nuclear power plants, a transmission grid planned around these power plants, and distribution grids that distributed the power to the consumers. Due to planning the transmission grid specifically to transfer the power production from the large power plants to areas of large consumption, only a limited amount of control and automation was needed in the transmission grid to guarantee safe and continuous operation. No or very little automation was needed in distribution grids, which was possible because they were largely oversized.

Lately, and even more in the near future, the power grid has and will undergo significant changes. Among those changes are: 1) the power consumption is going to increase drastically as we transition from fossil fuels to electric power in the mobility and heating sectors, and 2) the power generation is shifting from the transmission grid to the distribution grids. The latter is the case because many countries are phasing out their nuclear plants, and large fossil fuel power plants are substituted with a large number of small and volatile decentralized energy resources connected to the distribution grids like wind turbines and solar panels. This affects both the transmission and distribution grids. [Age21; Age22]

For the transmission grid, this means it will need to transfer more power than today because of the increased consumption and production. Also, this larger amount of power will enter the transmission grid in locations for which it was not built. Finally, the power production will partly be unpredictable and volatile as it is affected by weather conditions, which means the power flows will change rapidly and often.

For the distribution grid, this means that it will move from delivering power to consumers to also providing generation capacity to the transmission grid, depending on the generation level of its power producers, which depends on the weather. Also, it does not have the capacity to transfer large amounts of power generation and consumption. Finally, just as in the transmission grid, volatile and unpredictable power generation will

lead to rapidly changing power flows.

Both the transmission grid and the distribution grid will therefore have to be physically enforced, which is an enormous investment and time-intensive process. Fortunately, the changes that bring about these problems also come with the opportunity to solve some of them. Nearly all new consumption and generation is interfaced with the power grid through power electronics that can control their active and reactive power consumption or generation. By utilizing these and other controllable devices in the grid to always enforce the grid limits, the amount of physical enforcement needed to guarantee safe and continuous operation can be reduced. This is referred to as virtual grid reinforcement. [Höf+12; RTE19]

To facilitate such virtual reinforcement, methods are needed that can control large numbers of devices in real-time and with a limited amount of model information because no good models of distribution grids are available [IA09]. Given that the core of the problem is enforcing the grid constraints, optimization tools are a natural solution as they allow us to take these constraints explicitly into account. For that reason, optimization problems are already being solved in transmission grids [COC+12].

The state-of-the-art in solving these optimization problems is Offline Optimization, meaning that the optimization problem is solved on a computer using a model of the power grid. Afterward, the calculated setpoints are deployed onto the grid. A famous example of this is Optimal Power Flow (OPF) solvers. Today, Offline Optimization works well in transmission grids because good models are available to optimize over. This is not the case in distribution grids, and creating those models would be challenging due to missing documentation. Also, deriving such models from data would be difficult as measurements within these grids are sparse. Even if models for the distribution grid were available as well, the main problem with Offline Optimization remains, which is the lack of robustness that stems from it being a feedforward control approach: Decisions are based on a model, which inevitably introduces a model mismatch. Robustification to deal with model mismatch is possible but leads to solutions that do not utilize the power grid to its full extent, meaning that more physical reinforcement is again needed. Other drawbacks of Offline Optimization include that it is computationally intensive, and to solve power grid problems, all generation and consumption needs to be measured or estimated, which is difficult in distribution grids.

Lately, Online Optimization methods have been developed that use measurements as feedback to circumvent the drawbacks of Offline Optimization [Mol+17]. This thesis will focus on a specific method, called Online Feedback Optimization (OFO). It uses optimization algorithms as feedback controllers and iteratively drives a physical system to the solution of an optimization problem. This enables it to be robust to model mismatch, to operate with minimal model information and computation power, and to guarantee constraint satisfaction [Hau+21]. These are features that are well suited to control a large number of decentralized energy resources in a volatile environment.

OFO was designed with power system applications in mind and is based on a strong mathematical foundation. However, there remains a gap between the OFO theory and its application to power systems.

The goal of this thesis is to bridge that gap by evaluating the ability of OFO to solve power system problems, improving and extending it, and implementing it in power system laboratories and a real distribution grid.

## 1.1 Introduction to Online Feedback Optimization

> *OFO is a control method that uses optimization algorithms as feedback controllers to drive physical systems to the optimal solution of an optimization problem.*
>
> *OFO controllers solve optimization problems, e.g., OPF, in real-time and with limited model information. Constraint violations, if they occur, are temporary and bounded even in the presence of model mismatch.*

This section presents a tutorial on OFO[1]. For a detailed review, see [Hau+21]. First, the problem setup is introduced, and then the OFO control method is explained, i.e., how to turn optimization algorithms into feedback controllers. Then, the necessary model information and the controller tuning are discussed. Afterward, possible extensions of an OFO controller are described, and the method is compared with Offline Optimization.

### 1.1.1 Definition of the System and Optimization Problem

We begin by defining the system and the optimization problem. Let $u$ be the vector of control inputs that can be actuated, e.g., voltage setpoints of large generators, tap changers positions, active and reactive power injections, as well as controllable demand. Let $y$ be the output vector of all the values one wants to control, e.g., voltage magnitudes and current flows on lines. Finally, let $d$ be the disturbance vector that contains the remaining physical quantities, e.g., active and reactive power consumptions. The steady-state relation between $u$, $d$, and $y$ is determined by the power flow equations. An explicit mapping $y = h(u, d)$ locally exists, but its functional form is usually unknown [BD15]. We now formulate an optimization problem, in which we minimize a possibly non-convex cost function $f(u, y)$, e.g., minimize losses, economic operation, or deviation from a setpoint. We can add constraints on the input $u$, e.g., $u_{min} \leq u \leq u_{max}$, to enforce that the input is within the capabilities of the actuators. Also, we can add constraints on

[1] To provide the reader with a one-stop and concise overview of OFO, this tutorial includes results obtained by the research presented later on in this thesis.

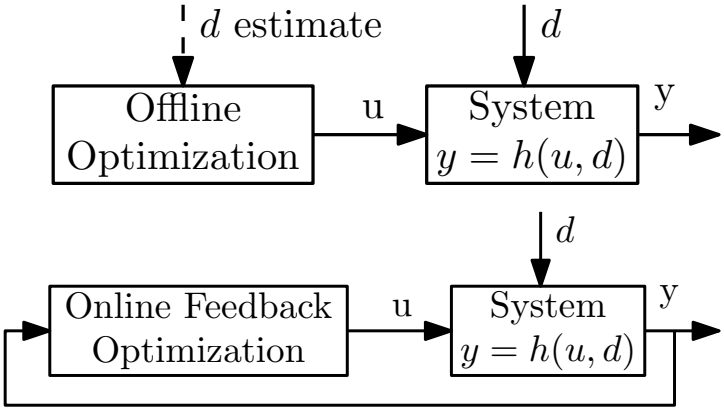


Figure 1.1: Offline vs. Online Feedback Optimization.

the output $y$, e.g., $y_{min} \leq y \leq y_{max}$, to enforce the grid constraints on maximum power flow on a line or voltage at a bus. Mathematically, we write this as possibly non-convex constraint sets $\mathcal{U}$ for $u$ and $\mathcal{Y}$ for $y$. Finally, we define the optimization problem as

$$\begin{aligned} \min_{u} \; & f(u, y) \\ \text{s.t. } & y = h(u, d) \\ & u \in \mathcal{U} \\ & y \in \mathcal{Y} \end{aligned} \tag{1.1}$$

A local optimum $(u^\star, y^\star)$ of (1.1) satisfies the constraints on $u$ and $y$ and locally minimizes the cost function. Note, that this optimization problem is very general and can accommodate many different problems. For example, minimizing losses, angle differences over lines, active power curtailment, voltage differences, or the determinant of the load flow Jacobian, while all being subject to operational constraints and the power flow equations.

### 1.1.2 Optimization Algorithms as Feedback Controllers

The state-of-the-art in solving optimization problems like (1.1) is Offline Optimization using a model $y = h(u, d)$. The resulting setpoints $u^\star$ are then deployed onto the system, see Figure 1.1. The disadvantage of this procedure is that an accurate model $h(u, d)$ needs to be known, and also $d$ needs to be measured or estimated. If there are any errors in $h(u, d)$ or $d$, the calculated setpoints $u^\star$ can lead to suboptimality and, more importantly, constraint violations of $y$ which could trigger protection devices or result in equipment damage. This is due to the feedforward nature of such an offline model-based control approach: The control actions are taken based on a model $y = h(u, d)$ and not on feedback from the real system.

The core idea behind OFO is to use feedback from the system through measurements

of $y$ to drive the power system to the locally optimal solution $(u^\star, y^\star)$ of the optimization problem without (or with very limited) model knowledge. Using this feedback from the system, we can perform closed-loop feedback control instead of model-based feedforward control, see Figure 1.1. This enables us to profit from closed-loop feedback control advantages such as robustness to model mismatch.
Now, we explain how to drive a power system to the optimal solution using feedback. To do so, we turn an optimization algorithm into a feedback controller, which is the core idea of OFO. This has been done with several different optimization algorithms which, all lead to different system behaviors with different advantages. For an overview, see [Hau+21].

Here we explain the idea with an illustrative example, i.e., an optimization problem with no constraints, and the optimization algorithm is gradient descent. In particular, to minimize a function $f(u, y) = f(u, h(u, d))$ one takes gradient steps with step size $\alpha$ which eventually lead to a local minimum of the optimization problem:

$$\begin{aligned} u(k+1) &= u(k) - \alpha \nabla_u f(u(k), h(u(k), d(k))) \\ &= u(k) - \alpha H(u(k))^T \nabla f(u(k), y(k)). \end{aligned} \tag{1.2}$$

The term $H(u, d)^T := \left[ I_p \, \nabla_u h(u, d)^T \right]$ occurs due to the chain rule where $\nabla_u h(u, d)$ is the sensitivity of the output with respect to the input.[2] In model-based Offline Optimization a model $y(k) = h(u(k), d(k))$ with an estimate of $d(k)$ is used, and the update in (1.2) (or of another optimization algorithm) is run over and over again until $||u(k+1) - u(k)||$ is smaller than some tolerance $\epsilon$. Then $u(k+1)$ is considered to be close enough to $u^\star$ and this input is deployed onto the power grid.

In OFO, the model $y = h(u, d)$ is replaced with a real-time measurement $y_m$. To be able to get a new measurement $y_m(k)$ we deploy $u(k)$ onto the grid and then measure $y_m(k)$. This leads to the integral controller

$$u(k+1) = u(k) - \alpha H(u(k), d(k))^T \nabla f(u(k), y_m(k)), \tag{1.3}$$

with gain $\alpha H(u(k), d(k))^T$. This integral controller keeps changing $u$ until the gradient of the cost function $\nabla f(u(k), y_m(k))$ is zero, and therefore the controller drives the system to a locally optimal solution, as intended. Just as with standard integral controllers and due to using feedback, this works for a wide range of gains and is therefore robust against a model mismatch in $H(u(k), d(k))^T$, which depends on the sensitivity $\nabla_u h(u, d)$. Overall, the model $h(u, d)$ is not needed and $d$ is only needed if the sensitivity highly depends on it because the controller is robust against model mismatch in the sensitivity $\nabla_u h(u, d)$.

An OFO controller based on standard gradient descent like (1.3) does not satisfy any constraints. To ensure that the power system always does satisfy the constraints on the

[2] $I_p$ is an identity matrix of size $p$ where $p$ is the size of the input vector $u$.

input $u$ and output $y$, we can use projected gradient descent. An OFO controller derived from projected gradient descent was presented in [Häb+20]. The update law is

$$u(k+1) = u(k) + \alpha\, \sigma_\alpha(u(k), d(k), y_m(k)) \tag{1.4}$$

with

$$\begin{aligned} \sigma_\alpha(u, d, y_m) = \arg\min_{w \in \mathbb{R}^p} \; & \| w + G^{-1} H(u,d)^T \nabla f(u, y_m)^T \|_G^2 \\ \text{subject to} \quad & A(u + \alpha w) \leq b \\ & C(y_m + \alpha \nabla_u h(u,d) w) \leq c, \end{aligned} \tag{1.5}$$

where $G$ is a positive-definite weighting matrix, $\alpha$ is a scalar, and both can be used to adjust the control gain. The matrices $A$ and $C$ and vectors $b$ and $c$ are the linearization of $\mathcal{U}$ and $\mathcal{Y}$ from (1.1) at the current operating point $(u, y)$, respectively. This is also an integral controller that does not need to know the model $h(u, d)$, the disturbance $d$, and is robust to model mismatch in $H(u(k), y_m(k))$. It keeps changing $u$ until $\sigma_\alpha(u, d, y_m)$ is zero, which is only zero when the system has converged to a local optimum that satisfies the constraints.
This controller is essentially the online feedback version of sequential dynamic programming and became known as "Verena's algorithm".

### 1.1.3 Necessary Model Information

A key information in OFO is the sensitivity $\nabla_u h(u, d)$ that describes the effect of a change in the input $u$ on the output $y$. Note that, for example, the sensitivities of power flows (outputs) with respect to active power injections (inputs) are the well-known power-transfer-distribution-factors (PTDFs). Power system sensitivities can be computed with the implicit function theorem using the admittance matrix of the grid, the grid state, and the power flow equations [BD15]. The sensitivity $\nabla_u h(u, d)$ depends on both $u$ and $d$ and the system parameters, e.g., topology and line impedances. Fortunately, it can be approximated with a constant matrix [Ort+20a]. Due to the feedback nature of OFO, the controllers are robust against such approximations. This means that even with an approximate sensitivity the system converges to an operation point $(u, y)$ that satisfies the constraints and enables the safe operation of the power grid. The suboptimality of this operating point is bounded [CSB19] and also temporary constraint violations are bounded [Häb+20]. There do exist methods to learn the sensitivity online from measurements [Pic+22b; Dom+23; Zag+23] and there also exist OFO controllers that do not use any sensitivity whatsoever but rely on zeroth order optimization algorithms [He+22].

### 1.1.4 Controller Tuning

The tuning of an OFO controller consists of two parts. First, the control objective, like minimizing losses while satisfying operational constraints, is encoded in the cost function

$f(u, y)$ and constraint sets $\mathcal{U}$ and $\mathcal{Y}$ of the overarching optimization problem (1.1). Those determine the local optimum that the OFO controller is tracking. Second, the tuning matrix $G$ and scalar $\alpha$ are used to adjust the transient behavior of how the system is driven to the local optimum. The bigger the entry in $G$, corresponding to a certain input $i$, is, the less it will be used during the transient. Changing an entry $g_i$ to $g_i + \lambda$ is ultimately equivalent to adding the term $\lambda w_i^2$ to the cost function in (1.5) which adds a weight to the change of input $i$. Note that this only affects how the system converges to the local optimum, not the local optimum itself. The local optimum is solely defined through the cost function and the constraint sets.

### 1.1.5 Possible Extensions

OFO controllers offer great flexibility and possible extensions.

#### State estimation

Instead of feeding the raw measurement into an OFO controller, one can run the measurements through a state estimation and provide the result of the state estimation to the controller instead. The convergence of this feedback system was proven in [PBD20].

#### Time-varying constraints

The constraints in the control law (1.5) can be different at every time step. This allows to include time-varying constraints of the overarching optimization problem (1.1), e.g. dynamic line ratings or reactive power capabilities of an inverter that depend on its current active power. Furthermore, changing the constraints in the controller can be used to temporarily block tap changers, make the controller reduce the power flow on a line, or lower the voltage angle over a circuit breaker.

#### Updating the sensitivity

The sensitivity depends on the topology, the tap changer positions, the line parameters, the generation, and the consumption. These may change over time, and therefore, the sensitivity can also change over time. Luckily, OFO controllers are robust to an inaccurate sensitivity, but nevertheless, one should use the most accurate sensitivity available. If, for example, the topology is changed, the sensitivity could be recomputed. Also, when a new state estimation is run, its result can be used to update the sensitivity. Last but not least, the sensitivity could be learned from data, see [Pic+22b; Dom+23; Zag+23].

| | Offline Optimization | Online Feedback Optimization |
|---|---|---|
| Without model mismatch | Locally optimal solution | Same locally optimal solution |
| With model mismatch | Constraint violations or suboptimal | Constraints are satisfied, converges to best achievable solution given the model mismatch |
| Computation | Solving a computationally intense non-convex problem | Calculating an easy update step that is computationally light |
| Tracking behavior | No tracking (only adjusts the inputs when a new estimate of $d$ becomes available) | Tracks the time-varying optimal solution |
| Communication infrastructure | Sending setpoints | Sending setpoints & receiving measurements |
| Control strategy | Feedforward | Feedback |
| Decision basis | Model-based | Measurement-based |
| Necessary information | Model $h(u,d)$, disturbance $d$, and sensitivity $\nabla_u h(u,d)$ | Only sensitivity $\nabla_u h(u,d)$ |

Table 1.1: Comparison of Offline Optimization like OPF solvers and Online Feedback Optimization

### 1.1.6 Comparison of Offline Optimization and OFO

The key difference between Offline Optimization and OFO is that the former makes decisions based on a model, whereas the latter makes decisions based on a measurement, see Figures 1.1. With perfect model information, both approaches converge to the optimal operation point $(u^\star, y^\star)$. For that, Offline Optimization needs to know the sensitivity $\nabla_u h(u,d)$, the model $h(u,d)$, and disturbance $d$. OFO, only requires the sensitivity $\nabla_u h(u,d)$ (and $d$ if the sensitivity highly depends on it) because it substitutes the model with a measurement. In the presence of model mismatch, Offline Optimization, OFO, and generally no method can converge to the optimal operation point. Instead, the approaches converge to suboptimal points. This suboptimality arises from the lack of accurate system information and not from the methods using the information. Therefore, suboptimality cannot be avoided under imperfect knowledge. When using Offline Optimization this can result in constraint violations and potential damage to equipment. OFO controllers, however, guarantee constraint satisfaction at steady-state even in the presence of model mismatch thanks to including feedback from the system. For a more in-depth comparison between OPF and OFO see Table 1.1.

## 1.2 Outline and contributions

This is a cumulative thesis with the goal to bridge the gap between the OFO theory and its application to power system problems. Toward that goal

- the OFO control method is evaluated in terms of its capability to solve different power system problems.
- the OFO control method is extended upon and tailored such that it can solve certain power system problems.
- the OFO control method is implemented in a laboratory environment to analyze its interaction with a power system setup.
- the OFO control method is implemented in a real distribution grid to evaluate its performance in a real power grid.

Chapter 2 (based on [Ort+23b]) uses an OFO controller and a simulation of the French transmission grid to evaluate the applicability of OFO controller to control a heterogenous group of actuators in a subtransmission grid with the ultimate goal of utilizing the grid to its full extent and therefore minimizing the necessary curtailment of renewable generation. Chapter 3 (based on [Ort+23a]) uses an OFO controller to derive curative actions for a power grid in real-time and serves as an example of how OFO controllers could enable curative $N-1$ grid operations. Chapter 4 (based on [Pic+22b]) presents a method to learn the input-output sensitivity that the controller needs from data. This allows building completely model-free OFO controllers. Chapter 5 (based on [Ort+20b]) presents the implementation of a distributed OFO controller in a laboratory distribution grid setup. Chapter 6 (based on [Ort+20a]) presents the implementation of a centralized OFO controller in a laboratory distribution grid setup. Chapter 7 (based on [Ort+23c]) presents the implementation of an OFO controller in a Swiss distribution grid for 24/7 operation. Finally, the thesis is concluded with Chapter 8. Below are the detailed contributions of each chapter.

### Chapter 2: Online Feedback Optimization for Subtransmission Grid Control

The Blocaux area is a part of the subtransmission grid in the north of France. Recently, it has seen a large increase in installed wind farm capacity. The power generated by these wind farms can exceed the grid capacity, and curtailment of the wind farms becomes necessary. Usually, wind farms are curtailed by setting their maximum power output to a fixed level. However, this solution will most likely curtail more renewable generation than necessary to operate the grid safely. Instead, the wind farms could be curtailed dynamically, and further actuators like on-load tap changers or reactive power injections

of the wind farms can be used to guarantee the safe operation of the grid. The goal of this chapter is to analyze the ability of OFO controllers to utilize such heterogeneous actuators to control and optimally operate a subtransmission grid. Toward that goal, a simulation model was created in close collaboration with the French transmission grid operator, and an OFO controller was extended with the ability to handle discrete actuators. Using this model, it was shown that the newly proposed OFO controller can effectively operate a subtransmission grid, meaning that: 1) the OFO controller tracks the OPF solution, 2) is robust to model mismatch, and 3) enforces the bus voltages and line limits.

### Chapter 3: Real-time Curative Actions for Power Systems via Online Feedback Optimization

Transmission grids are the backbone of the electric power system, and they need to work robustly and reliably. Therefore, their operation is according to the $N-1$ criteria, meaning that the grid can continue to operate even if any single element (power plant, transformer, transmission line) fails. This can be guaranteed in a preventive manner, meaning that measures are taken such that the grid is always operated at a point where a failure of an element leads to a safe system state in which the grid can keep operating. Alternatively, the grid can be operated in any state, and measures to guarantee safe system operation are only taken if an element actually fails. This is referred to as curative $N-1$ and enables more economic grid operations. This chapter presents a case study in which an OFO controller is used to derive curative actions in real-time for operating the grid in a curative $N-1$ manner. The case study is inspired by the 2003 Swiss-Italian blackout, and the OFO controller is able to successfully derive curative actions.

### Chapter 4: Adaptive Real-Time Grid Operation via Online Feedback Optimization with Sensitivity Estimation

The OFO control method does not need to know a lot of model information. The only model information needed is the input-output sensitivity. The research in this chapter goes one step further and combines an OFO controller with a Kalman filter and persistent excitation to design an OFO controller that is able to continuously learn the input-output sensitivity from data while it is controlling the system. This makes it possible to use OFO controllers that are completely model-free.

### Chapter 5: Fully Distributed Peer-to-Peer Optimal Voltage Control with Minimal Model Requirements

An OFO controller using distributed communication and local computation is implemented on a laboratory distribution grid feeder. Its task is to minimize the use of

reactive power while satisfying the voltage constraints along the feeder. The implementation shows the minimal modeling and communication requirements needed for successful Volt/VAr control.

**Chapter 6: Experimental Validation of Online Feedback Optimization in Power Distribution Grids**

Three Volt/VAr control schemes are implemented on a laboratory distribution grid feeder to analyze their capabilities to regulate the voltage along the feeder. The schemes are droop control, an OPF-based dispatch, and a centralized OFO controller. The experiment shows that droop control does not utilize the reactive power resources to their full extent and hence cannot enforce the voltage constraints during the experiment. The reactive power setpoints, calculated by the OPF-based dispatch, also lead to constraint violations. The reason behind this is a model mismatch that occurred even though all generation and consumption along the feeder were measured and the grid model of the laboratory is accurately known. Finally, the OFO controller successfully controls the reactive power sources to enforce the voltage constraints and is able to do so with minimal or even no model information.

**Chapter 7: Deployment of an Online Feedback Optimization Controller for Reactive Power Flow Optimization in a Distribution Grid**

An OFO controller was implemented in the distribution grid of the Canton of Aargau, which supplies 100.000 people. The controller uses off-the-shelf hardware and the reactive power resources of existing inverters to optimize the reactive power flow at the substation connecting the distribution and subtransmission grid. This leads to a financial reward due to a coordination scheme between the distribution grid operator and the subtransmission grid operator. The chapter presents the hardware, software, and controller implementation and analyzes the interaction of an OFO controller with a real distribution grid. The successful implementation of an OFO controller in a real distribution grid brings the OFO control method to Technology Readiness Level (TRL) 7.

## 1.3 Publications

The research conducted during the author's time as a doctoral candidate involved close collaboration with several colleagues and collaborators, and this section lists all research output during that time.

### Journal publications

[Häb+20] V. Häberle, A. Hauswirth, L. Ortmann, S. Bolognani, and F. Dörfler. "Non-convex feedback optimization with input and output constraints". In: *IEEE Control Systems Letters* 5.1 (2020), pp. 343–348.

[Ort+20a] L. Ortmann, A. Hauswirth, I. Caduff, F. Dörfler, and S. Bolognani. "Experimental validation of feedback optimization in power distribution grids". In: *Electric Power Systems Research* 189 (2020), p. 106782.

[Ort+20b] L. Ortmann, A. Prostejovsky, K. Heussen, and S. Bolognani. "Fully distributed peer-to-peer optimal voltage control with minimal model requirements". In: *Electric Power Systems Research* 189 (2020), p. 106717.

[Pic+22b] M. Picallo, L. Ortmann, S. Bolognani, and F. Dörfler. "Adaptive real-time grid operation via Online Feedback Optimization with sensitivity estimation". In: *Electric Power Systems Research* 212 (2022), p. 108405.

[Zag+23] M. Zagorowska, M. Degner, L. Ortmann, A. Ahmed, S. Bolognani, E. del Rio Chanona, and M. Mercangöz. "Online Feedback Optimization of Compressor Stations with Model Adaptation using Gaussian Process Regression". In: *Journal of Process Control* 121 (2023), pp. 119–133.

### Conference publications

[Hal+22] S. Hall, L. Ortmann, M. Picallo, and F. Dörfler. "Real-time Projected Gradient-based Nonlinear Model Predictive Control with an Application to Anesthesia Control". In: *2022 IEEE 61st Conference on Decision and Control (CDC)*. IEEE. 2022, pp. 6193–6198.

[Hau+20b] A. Hauswirth, L. Ortmann, S. Bolognani, and F. Dörfler. "Limit behavior and the role of augmentation in projected saddle flows for convex optimization". In: *IFAC-PapersOnLine* 53.2 (2020), pp. 5511–5517.

[Ort+23a] L. Ortmann, G. Hotz, S. Bolognani, and F. Dörfler. "Real-time Curative Actions for Power Systems via Online Feedback Optimization". In: *accepted at PowerTech* (2023).

### Preprints

[Kle+23] F. Klein-Helmkamp, F. Böhm, L. Ortmann, A. Winkens, F. Schmidtke, S. Bolognani, F. Dörfler, and A. Ulbig. "Providing Curative Distribution Grid Flexibility Utilizing Online Feedback Optimization - Laboratory Evaluation". In: *submitted to IEEE PES ISGT EUROPE 2023* (2023).

[Mat+23] J. G. Matt, L. Ortmann, S. Bolognani, and F. Dörfler. "Virtual Power Grid Reinforcement via Coordinated Volt/VAr Control". In: *arXiv preprint arXiv:2305.04666* (2023).

[Ort+23b] L. Ortmann, J. Maeght, P. Panciatici, F. Dörfler, and S. Bolognani. "Online Feedback Optimization for Subtransmission Grid Operation". In: *arXiv preprint arXiv:2212.07795* (2023).

[Ort+23c] L. Ortmann, C. Rubin, A. Scozzafava, J. Lehmann, S. Bolognani, and F. Dörfler. "Deployment of an Online Feedback Optimization Controller for Reactive Power Flow Optimization in a Distribution Grid". In: *arXiv preprint arXiv:2305.06702* (2023).

**Toolboxes**

[Ort23] L. Ortmann. *SimulinkMATPOWER*. https://github.com/Lukas738/SimulinkMATPOWER. 2023.

[RO23] C. Rubin and L. Ortmann. *Neplan to PandaPower*. https://gitlab.ethz.ch/ortmannl/neplan-to-pandapower. 2023.

CHAPTER 2

# Online Feedback Optimization for Subtransmission Grid Control

This chapter presents how an Online Feedback Optimization (OFO) controller can be used to control a subtransmission grid. The controller derives active and reactive power setpoints for wind farms and tap positions for onload tap changers. To be able to calculate discrete inputs like tap positions, the OFO control method is extended with the capability to handle discrete actuators. The proposed OFO controller is then tasked to extract the maximum amount of renewable generation from the subtransmission area while satisfying grid constraints. The simulation environment, used in this chapter, was developed in close cooperation with the French transmission grid operator and includes a real test case and a toolbox that was made available to the public.

## 2.1 Introduction

More and more renewable power is installed in the grid to achieve the climate goals [Age21; Age22] and energy independence. In some areas, the capacity of the grid is partly reached and renewable power needs to be curtailed to mitigate overloaded lines [RTE19] and overvoltages. The typical approach to prevent overloaded lines is to curtail the renewable generation to a fixed maximum value, depending on the seasonal thermal ratings of the lines, without taking consumption and other generation into account. For example, these actions currently need to be implemented in the Blocaux area in France which we will use as a benchmark in this chapter. However, this solution leads to unnecessary curtailment of renewable generation [RTE19].
The current practice for voltage control depends on the country and ranges from manual to automatic control with large sampling times. The fast-changing power injections of renewable energy sources like wind and solar require higher control rates to enforce

This chapter is based on the publication [Ort+23b].

voltage and current limits in the grid. Because of this, manual operation strategies or automatic control with sampling times in the minutes will be incapable of safely operating a highly loaded, uncertain, and variable grid in the future. This problem is becoming more severe with increasing renewable integration and is affecting more areas of power grids worldwide [RTE19]. Hence, increasing real-time automation is needed with control actions taken every few seconds.

Real-time control does not only allow to operate the grid under variable renewable generation, but it can also mitigate the need to physically reinforce the grid by virtual reinforcement through automatic control. A report by the French transmission grid operator RTE estimates possible savings of 7 billion Euros over 10 years through using real-time control for active power instead of building new power lines [RTE19]. This opportunity comes from the higher degree of controllability of the grid, given by the flexibility of a fine network of renewable generators connected to almost every bus. Virtual grid reinforcement can be phrased as an optimization problem. However, such optimization is inherently an offline decision-making method, e.g., solving an Optimal Power Flow (OPF) problem and deploying the solution on the grid, see Figure 2.1. This is a feedforward control approach that lacks robustness to unknown disturbances and model uncertainties. Further, it is difficult to run in real-time and can be (at best) implemented repeatedly. While some degree of uncertainty can be tackled via robust optimization tools, such an approach would increase the computational load (thus leading to longer sampling rates) and would jeopardize the efficiency of the solution (due to prioritizing robustness against model mismatch). In contrast, Online Optimization approaches have been analyzed for power system problems, see [Mol+17]. Online Optimization methods combine feedback-based real-time control and optimal operation with respect to an optimization problem. An Online Optimization controller tracks the solution of a nonlinear optimization problem that, at each time, depends on the instantaneous availability of generation, loads, etc. From a control perspective, we want to design a control policy so that this optimal state is an attractive equilibrium for the controlled power grid. We choose the Online Optimization method, called OFO to steer the grid to the optimal operating point using feedback, see Figure 2.1. This method was specifically developed to drive power systems to the solution of an optimization problem while guaranteeing constraint satisfaction [Hau+21; BDS19; LSM20; CDB19; Bia+21a; Sim+20]. It needs minimal model information, and it was experimentally validated in different distribution microgrids [Ort+20a; Ort+20b; Kro+20a].

Related earlier works also use Online Optimization and optimization algorithms as feedback controllers to drive a power system to an optimal operation point. Such algorithms have been analyzed for optimal frequency control, optimal voltage control, and optimal power flow, see [Mol+17] for an extensive review. Most papers analyze the Volt/VAR problem, e.g. [LWL22; QL19; LSZ17] and until now nearly all publications have dealt with distribution grids, e.g. [Guo+23; Oli+23; Dom+23; NCW20b; Pic+22b].

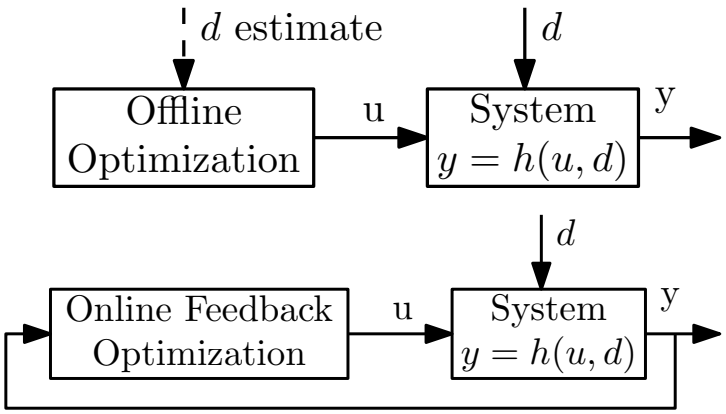


Figure 2.1: Offline vs. Online Feedback Optimization.

Recently, the publication [Tan+20] analyzed such algorithms for transmission grids but again only consider voltage control. For a distribution grid setup the authors of [THL20] include tap changers in their algorithm but again only voltage control is considered.

Overall, the Online Optimization algorithms are mostly used for voltage control in distribution grids and up until now are, except one, limited to continuous inputs whereas inputs in a real power grid can also be discrete, e.g. tap changers. Furthermore, most of them assume to have perfect model information and only consider a subset of available control inputs. Also, synthetic grid models are usually used to analyze the performance. However, these models lack important properties of real power grids e.g., locally controlled tap changers or independently operating voltage-controlled generators. Therefore, important features of these algorithms like constraint satisfaction, tracking of a time-varying optimum, and robustness to model mismatch have not yet been analyzed on a real grid benchmark which is essential to pave the way toward a deployment. In summary, previous approaches to OFO for voltage control had an academic focus, considered synthetic case studies, and relied upon idealistic assumptions. Our contributions are to present and make publicly available a novel subtransmission benchmark model that represents the real French transmission and subtransmission grid. We extend and tailor OFO methods with the capability to handle discrete actuators like tap changers and demonstrate how such controllers can be tuned. We design a uniform controller utilizing active and reactive power injections as well as tap changers. On the provided benchmark, we show the tracking performance, the constraint satisfaction, and the robustness to model mismatch of our OFO controller, and compare it to Offline Optimization.

## 2.2 The Unicorn 7019 Benchmark

In this section, we present the Unicorn 7019 benchmark which is a real benchmark in the French subtransmission grid. We use it to show the performance of our OFO controller.

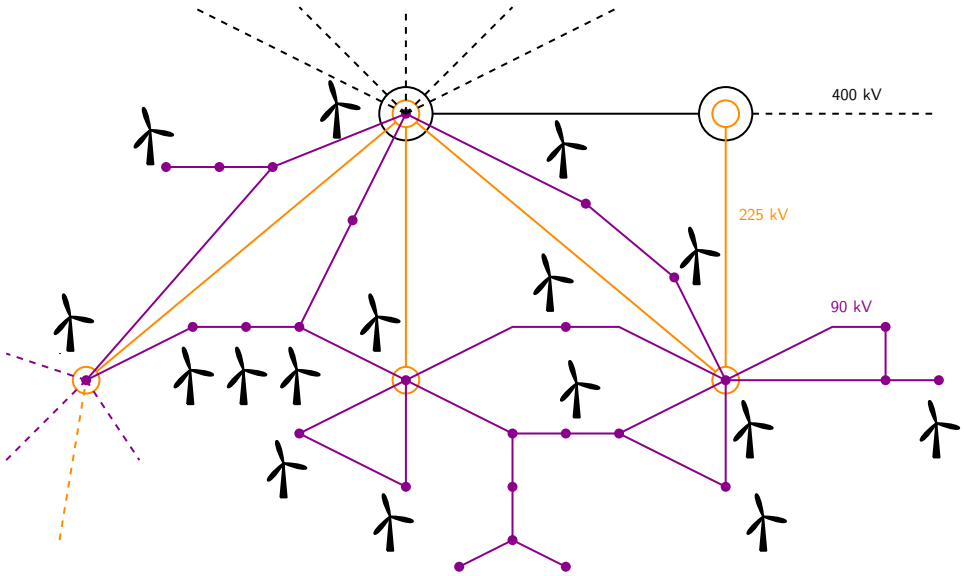


Figure 2.2: The Blocaux area with 31 buses, 58 branches, and 42 wind farms with a total power of 1274 MW. Connections to the rest of France are indicated with dashed lines. The tap changers are on the transformers connecting the different voltage levels.

The benchmark is implemented in MATPOWER [ZMT10] and Matlab Simulink through the toolbox SimulinkMATPOWER [Ort23]. The grid model for the benchmark is the real French transmission and subtransmission grid, which consists of 7019 buses, 9657 branches, 1465 generators, and 907 tap changers. We simulate the steady-state behavior of the whole grid. That means whenever the controller has updated its control setpoints $u$, a power flow is solved. Afterward, all tap changers, which are not controlled by our controller, determine whether their secondary voltage is within bounds. Otherwise, they switch taps and the power flow is solved again with the updated tap ratios. This is done iteratively until no further tap changes occur. This mimics the operating behavior of the real power system. Figure 2.2 shows the Blocaux area, which is located in the north of France. The wind power exceeds the capacity of the grid, and during the summer of 2021, the wind farms were curtailed at a fixed level to prevent overloaded lines. This sometimes leads to unnecessary curtailment.
The task in the benchmark is to minimize the losses and active power curtailment in the Blocaux area using the active and reactive power injections of the wind farms and the on-load tap changers, while satisfying the grid constraints, i.e., voltage magnitude limits at the buses and power flow limits on the lines. During the simulation the wind power produced by the wind farms is changing rapidly, see the blue line in the upper right panel of Figure 2.4. This leads to a time-varying optimum that the controller has to track while guaranteeing the satisfaction of the constraints. For the wind profile, we use real measurements from a wind farm taken in a location close to the Blocaux area. We chose this specific wind profile because the fast change of power makes tracking the

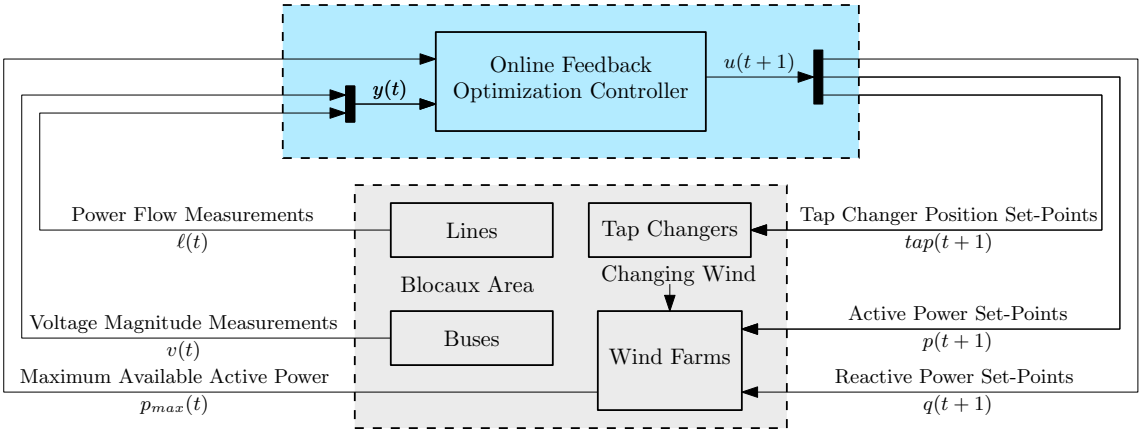


Figure 2.3: Block diagram of the control setup with the controller in blue and the grid in gray.

optimum difficult and satisfying the constraints hard.
The Blocaux area consists of 31 buses, 58 branches, and there are 10 on-load tap changers on the transformers between the transmission grid (225 kV and 400 kV) and the sub-transmission grid (90 kV). There are 42 wind farms with power ratings between 0.5 MW and 102 MW, and a total installed wind power of 1274 MW. We assume the active and reactive power of the 42 wind farms and the position of all 10 tap changers can be controlled. The control architecture can be seen in Figure 2.3 and is as follows. Measurement devices take voltage magnitude measurements $v$ and measure the absolute value of the complex power flow $\ell$, respectively. These are sent to a centralized location, a regional SCADA system, or one of the substations, where the controller is implemented. The controller calculates the reactive and active power setpoints and tap changer positions. These are then communicated to the wind farms and tap changers. Note, that the wind farms accept continuous setpoints, whereas the tap changers are discrete actuators and only accept 33 equally spaced values between 0.9 and 1.1. We assume that the wind farms cannot only accept setpoints, but they can also communicate the currently available wind power to the controller. This could for example be based on a wind speed measurement. To showcase the capabilities of the controller, we define two tasks with which we challenge the controller.

*Optimal and Safe Curtailment:* The goal is to minimize the active power curtailment of renewable wind generation and losses while guaranteeing grid constraints at all times.

*Providing Auxiliary Services:* In addition to the goals of task 1, the wind farms must provide voltage support as an ancillary service. More precisely, the goal is to keep the voltage level at the 225 kV buses below 1.05 p.u.

The benchmark is available online [Ort22], and we invite other researchers to evaluate their control methods on it.

## 2.3 Online Feedback Optimization with Integer Constraints

In this section, we define the control and optimization setup we choose for the benchmark. Then we present our new OFO controller, and comment on the necessary model information and its tuning before we compare it with Offline Optimization.

### 2.3.1 Input, Output, and Optimization Problem

The input $u = [q^T, p^T, tap^T]^T$ consists of the reactive power setpoints $q \in \mathbb{R}^{42}$ and active power setpoints $p \in \mathbb{R}^{42}$ for the 42 wind parks, and the tap positions $tap \in \mathbb{Z}^{10}$ for the 10 tap changers within the Blocaux area, for a total of 94 signals. The output $y = [v^T, \ell^T]^T$ consists of the voltage magnitudes $v \in \mathbb{R}^{31}$ at the 31 buses and the magnitudes of the complex power flows $\ell \in \mathbb{R}^{58}$, for a total of 89 signals. Let $d$ be the disturbance vector which contains active and reactive power consumptions and the generation that we do not control. The steady-state relation between $u$, $d$, and $y$ is determined by the power flow equations. An explicit mapping $y = h(u, d)$ locally exists but its functional form is usually unknown [BD15]. The actuators that will implement our control input $u$ are limited in their capabilities and the bus voltages and line flows have lower and upper limits due to safety constraints. Therefore, we introduce a constraint set $\mathcal{U}$ for the input and $\mathcal{Y}$ for the output. The tap changer positions need to be an element of $\mathbb{Z}$, which is the set of integers. We now formulate an optimization problem, in which the goal is to minimize the losses in the grid and the curtailment that is necessary to satisfy line limits

$$\begin{aligned} \min_{u,y} \quad & f(u,y) := losses(u,y) + curtailment(u) \\ \text{s.t.} \quad & y = h(u,d) \\ & u \in \mathcal{U}, \quad y \in \mathcal{Y} \\ & u_i \in \mathbb{Z} \quad \forall \text{ discrete inputs } i \end{aligned} \tag{2.1}$$

At a local optimum $(u^\star, y^\star)$ the system satisfies the constraints on $u$ and $y$, which means that we have a feasible operating point. Furthermore, the cost function is locally minimized. We do not perform frequency control because we consider this to be done at the transmission grid level. For a paper analyzing the interaction of frequency control with OFO, see [Oli+23].

### 2.3.2 The Proposed Controller

All proposed OFO controllers cannot handle integer constraints. To solve this issue we build up on work from [Häb+20] which we extend with the capabilities to handle discrete

inputs and rate limits. The resulting OFO controller is

$$u(k+1) = u(k) + \sigma(u(k), d(k), y_m(k)) \tag{2.2}$$

$$\begin{aligned} \sigma(u, d, y_m) = \arg\min_{w \in \mathbb{R}^p} \; & \|w + G^{-1} H(u,d)^T \nabla f(u, y_m)^T\|_G^2 \\ \text{subject to} \quad & A(u+w) \leq b \\ & C(y_m + \nabla_u h(u,d) w) \leq c \\ & w \in \mathcal{W} \\ & w_i \in \mathbb{Z} \quad \forall \text{ discrete inputs } i, \end{aligned} \tag{2.3}$$

with $H(u,d)^T := \left[ I \; \nabla_u h(u,d)^T \right]$ where $\nabla_u h(u,d)$ is the sensitivity of the output with respect to the input and $I$ is the identity matrix. The gradient of the cost function from (2.1) is $\nabla f(u,y)$. The set $\mathcal{W}$ can be used to enforce rate constraints on the input $u$ by constraining the change of the input $w$ and $G$ is the tuning matrix. The matrices $A$ and $C$ and vectors $b$ and $c$ are the linearization of $\mathcal{U}$ and $\mathcal{Y}$ from (2.1) at the current operating point, respectively. Problem (2.3) is a mixed integer quadratic optimization problem (MIQP) that needs to be solved at every time step. The main difference that makes (2.3) easier to solve compared to (2.1) is the lack of the nonlinear equality constraint that describes the power flow equations. The heart of the controller is repeatedly solving this optimization problem. This is similar to sequential quadratic programming (SQP). Essentially, OFO is the real-time feedback version of SQP.

### 2.3.3 Controller Tuning

The tuning of an OFO controller consists of two parts. First, the control objective is encoded in the cost function $f(u,y)$ and constraint sets $\mathcal{U}$ and $\mathcal{Y}$ of the overarching optimization problem (2.1). Those determine the local optimum that the OFO controller is tracking. Second, the tuning matrix $G$ is used to adjust the transient behavior of how the system is driven to the local optimum. This is explained in more detail in the following two paragraphs.

#### Tuning the rate of change of different inputs

The tuning matrix $G$ can be used to tune how the grid is converging to the local optima. The bigger an entry $g_i$ of $G$ is, the less aggressively the corresponding input $u_i$ will be used during the transient. Changing an entry $g_i$ to $g_i + \lambda$ is ultimately equivalent to adding the term $\lambda w_i^2$ to the cost function in (2.3) which adds a weight on the change of input $i$. Without discrete actuators, this only affects how the system converges to the local optimum and not the local optimum itself.

#### Tuning the tap changer usage

Tap changer usage comes at a cost because they slowly deteriorate with every tap change. This deterioration is irrelevant when tap changes are needed to enforce constraints. However, one might want to limit the number of tap changes used to minimize the cost function. The proposed OFO controller conveniently provides a tuning option for this which is the matrix $G$. While $G$ does not affect the constraint enforcement it does affect how often discrete inputs are used. The higher the values in $G$ corresponding to a discrete actuator like tap changers, the less they are used. Numerical results will be shown in Section 2.5.

### 2.3.4 Necessary Model Information

OFO is a mostly model-free approach aside from one key piece of model information: the sensitivity $\nabla_u h(u, d)$ that describes the effect of a change in the input $u$ on the output $y$. Note, that for example, the sensitivity of power flows (outputs) with respect to active power injections (inputs) are the well-known power-transfer-distribution-factors (PTDFs). Power system sensitivities can be computed with the implicit function theorem using the admittance matrix of the grid, the grid state, and the power flow equations [BD15]. The sensitivity $\nabla_u h(u, d)$ depends on both $u$ and $d$ and the system parameters, e.g. topology and line impedances. Fortunately, for many applications it can be approximated with a constant matrix [Ort+20a]: due to the feedback nature of OFO, the controllers are robust against such approximations and drive the system to an operating point $(u, y)$ that satisfies the constraints and enables the safe operation of the power grid. The suboptimality of this operating point can be bounded [CSB19]. Additionally, there exist methods to learn the sensitivity online from measurements [Pic+22b; Dom+23; NCW20b] and there also exist OFO controllers that do not use any sensitivity but instead rely on zeroth order evaluation of the cost [He+22].

### 2.3.5 Comparison of Offline Optimization and OFO

The key difference between Offline Optimization and OFO is that the former makes decisions based on a model, whereas the latter makes decisions based on a measurement, see Figure 2.1. With perfect model information, both approaches converge to a locally optimal operation point $(u^\star, y^\star)$. For that, Offline Optimization needs to know the sensitivity $\nabla_u h(u, d)$, the model $h(u, d)$, and disturbance $d$. OFO, instead, only requires the sensitivity $\nabla_u h(u, d)$ because it substitutes the model with a measurement. In the presence of model mismatch, both Offline Optimization and OFO necessarily converge to suboptimal points. When using Offline Optimization this suboptimally can result in constraint violation and potential damage to equipment. OFO controllers instead guarantee constraint satisfaction at steady-state thanks to including repeated measurements

as feedback from the system. For a more in-depth comparison between OPF and OFO see Table 2.1. For a comparison with extremum seeking, model predictive control, and modifier adaptation, see [Hau+21].

| | Offline Optimization | Online Feedback Optimization |
|---|---|---|
| Without model mismatch | Locally optimal solution | Same locally optimal solution |
| With model mismatch | Constraint violations or suboptimal | Constraints are satisfied, converges to the best achievable solution given the model mismatch |
| Computation | Solving a computationally intense non-convex problem | Calculating an easier update step that is computationally lighter |
| Tracking behavior | No tracking (only adjusts the inputs when a new estimate of $d$ becomes available) | Tracks the time-varying optimal solution using measurements |
| Communication infrastructure | Sending setpoints | Sending setpoints & receiving measurements |
| Control strategy | Feedforward | Feedback |
| Decision basis | Model-based | Measurement-based |
| Necessary information | Model $h(u,d)$, disturbance $d$, and sensitivity $\nabla_u h(u,d)$ | Only sensitivity $\nabla_u h(u,d)$ |

Table 2.1: Comparison of Offline Optimization like OPF solvers and Online Feedback Optimization

## 2.4 Controller Design for the Blocaux Area

In this section, we present how the newly proposed algorithm is tailored to the Blocaux area.

### 2.4.1 Constraint Sets and Integer Constraints

The constraint set of the input is $\mathcal{U} = \{u \in \mathbb{R}^{94} \,|\, u_{min} \leq u \leq u_{max}\}$, where $u_{min} = [q_{min}^T, p_{min}^T, tap_{min}^T]^T$ and $u_{max} = [q_{max}^T, p_{max}^T, tap_{max}^T]^T$. The limits on $q$ and $tap$ are the real grid limits and can be found in the MATPOWER case file of the benchmark [Ort22]. The lower limit for $p$ is $p_{min} = 0$ because the wind farms cannot consume power. The upper limit $p_{max}$ depends on the wind, and we assume that the wind farms provide this information to the controller, see the block diagram in Figure 2.3. Therefore, the constraints on the active power are different at every time step. An equivalent definition of the constraint set $\mathcal{U}$ is $\mathcal{U} = \{u \in \mathbb{R}^{94} \,|\, Au \leq b\}$ with $A = [I_{94}, -I_{94}]^T \in \mathbb{R}^{188\times 94}$, where

$I_{94}$ is the identity matrix of size 94, and $b = [u_{max}^T, u_{min}^T]^T \in \mathbb{R}^{128}$. This matrix $A$ and vector $b$ are used in the controller in (2.3). Note, that we do not include rate limits on the input though this is possible.
The constraint set of the output is $\mathcal{Y} = \{y \in \mathbb{R}^{89} \,|\, y_{min} \leq y \leq y_{max}\}$, where $y_{min} = [v_{min}^T, \ell_{min}^T]^T$ and $y_{max} = [v_{max}^T, \ell_{max}^T]^T$. The limits on $v$ and $\ell$ are the real French grid limits for these buses and lines and can be found in the MATPOWER case file of the benchmark [Ort22]. An equal definition of the constraint set $\mathcal{Y}$ is $\mathcal{Y} = \{y \in \mathbb{R}^{89} \,|\, Cy \leq c\}$ with $C = [I_{89}, -I_{89}]^T \in \mathbb{R}^{178 \times 89}$, where $I_{89}$ is the identity matrix of size 89, and $c = [y_{max}^T, y_{min}^T]^T \in \mathbb{R}^{178}$. This matrix $C$ and vector $c$ are used in the controller in (2.3). The tap changers can take 33 discrete positions, and the change of a tap position has to be an integer. When calculating (2.3) the solver must be informed about these integer constraints on a subset of $w$. How this is done is solver specific.

### 2.4.2 Sensitivities

The OFO controller needs the sensitivity $\nabla_u h(u, d)$ to drive the system to the optimum. Namely, these are the sensitivities of the outputs $v$ and $\ell$ with respect to the inputs $q$, $p$, and $tap$. We calculate the sensitivity once initially for a grid state with high power generation and approximate the true time-varying sensitivity with this fixed sensitivity. Note, that the constraints will still be satisfied even with an approximate sensitivity.

### 2.4.3 Cost Function

The cost function encodes our control goal, which is to minimize the losses and the curtailment. This corresponds to the cost function $f(u, y) = losses(u, y) + curtailment(u)$. Furthermore, the regularization of tap changers or other inputs could be added to the cost function. Generally, the cost function specifies how the system is controlled, and it should be chosen judiciously. Note, that for the implementation of the controller only the gradient of the cost function $\nabla f(u, y)$ will be needed, see (2.3). Note that, Offline Optimization would need this gradient as well. To calculate this gradient an exact model and all active and reactive consumption and generation need to be known. We, therefore, work with an approximate cost function containing only values the controller measures: $f(u, y) = w_q q^2 - sum(p) + \mathbf{w}_{tap} tap$. The term $w_q q^2$ with the scalar weight $w_q = 0.0026$ approximates the losses due to a reactive power flow on a medium voltage line connecting a wind farm to the high voltage grid. The term $\mathbf{w}_{tap}$ is a vector of size 10 and incorporates that higher tap positions lower the losses. It is the derivative of the losses with respect to the tap changer positions. It is calculated once numerically for a grid state with high power generation and kept constant for the whole simulation. The

gradient of our approximate cost function is

$$\nabla f(u,y) = \begin{bmatrix} \nabla_u f(u,y) \\ \hline \nabla_y f(u,y) \end{bmatrix} \approx \begin{bmatrix} 2\mathbf{w}_q q \\ -I_{42} \\ \mathbf{w}_{tap} \\ \hline 0_{89} \end{bmatrix}.$$

### 2.4.4 Tuning Parameters and Sampling Time

The sampling time of the controller is 1 second. To solve the MIQP in (2.3) we use the Yalmip toolbox [Lof04] with the solver Gurobi. Solving the MIQP takes less than 40 milliseconds on a standard notebook. As the tuning parameter we choose a diagonal matrix $G = diag(0.1 \cdot I_{42}, 0.2 \cdot I_{42}, 2500 \cdot I_{10})$. The high value of 2500 for the tap changers ensures that they are not overused. The small values for $p$ and $q$ ensure fast convergence of the algorithm.

## 2.5 Results

In this section, we use the Unicorn 7019 benchmark to validate our OFO controller and showcase its performance. We show simulations for both tasks (*Optimal and Safe Curtailment* and *Providing Auxiliary Services*). Furthermore, as a benchmark, we simulate our controller with perfect model knowledge to show the effect of the approximations we made. Also, we show the tracking performance of the OFO controller, i.e., how closely it tracks the grand-truth time-varying optimum, and compare it to the state-of-the-art which is curtailing injection at a fixed level. Finally, we present the influence of the tuning matrix $G$ on the tap changer behavior.

### 2.5.1 Results for Optimal and Safe Curtailment

For the task of *Optimal and Safe Curtailment*, we deploy the controller as described in Section 2.4. The results can be seen in Figure 2.4, and the behavior can be separated into two phases. In the beginning, the wind power is low and no curtailment is necessary. Therefore, the controller aims to minimize the losses. This is done by increasing the voltage with high tap ratios. To satisfy the voltage constraints not all tap changers increase their tap positions and some reactive power is used. Note that the sharp steps in the reactive power injections (lower left panel) can arise when a tap is changed. These steps in the reactive power are sometimes needed to enforce the voltage constraints when a tap change occurs. Around minute 15 the wind power sharply increases and passes the grid capacity. Curtailment becomes necessary to satisfy the current limits on some of the lines. Even though the tap changers have a small influence on the power flows,

this influence is used to redirect flow to non-congested lines. This helps to minimize the necessary curtailment. The tap changes lead to voltages well within the constraints and no reactive power is needed anymore. These are highly non-trivial control actions that no human operator would have been able to derive in real-time. While the wind power increases the controller curtails more active power to keep the flows within the constraints. It can be seen in Figure 2.4 that line constraints violations are minimal and most importantly they are temporary. Therefore, the grid is safely operated at its limit allowing a maximum of renewable wind power to be injected. At the end of the simulation 90.2% of the wind power is injected into the grid.

As explained before, the OFO controller is tracking the locally optimal solution of the optimization problem defined in Section 2.4. We have a high cost on active power curtailment and therefore this control action is only used if it is necessary to satisfy line constraints or in the unlikely case that such a high amount of reactive power would need to be used to satisfy voltage limits that a lower value of the cost function could be achieved by curtailing active power. If another behavior is wanted this can be encoded in the cost function.

### 2.5.2 Results for Providing Auxiliary Services

In this task the subtransmission grid has to provide voltage support to the transmission grid as an ancillary service. The goal is to keep the voltages at the 225 kV buses below 1.05 p.u. This can easily be incorporated into our controller by changing the upper voltage constraint of these buses to 1.05. This example shows the versatility of our framework, i.e., defining the control goals through an optimization problem. The results of the simulation can be seen in Figure 2.5. Similar to the previous task the behavior is split into two phases. In the beginning, the losses are minimized and after minute 15 the focus lies on optimizing curtailment as it becomes the predominant part of the cost. The main difference to the previous task is in the usage of the tap changers and reactive power to satisfy the tighter voltage constraints on the 225 kV buses. For that, more reactive power is used and the tap changers are actuated more. After minute 15 the tap changers behave differently than in the previous task because of the tighter voltage constraints. This leads to a slightly higher curtailment and reactive power is still needed to enforce the voltage constraints. At the end of the simulation 89.9% of the wind power can be injected into the grid.

### 2.5.3 The Effect of the Approximations

When designing the controller in Section 2.4 we assumed that the sensitivity $\nabla_u h(u, d)$ and the derivative of the cost function $\nabla f(u, y)$ are not perfectly known, which is always the case in a practical application. This imperfection affects the optimality of the time-

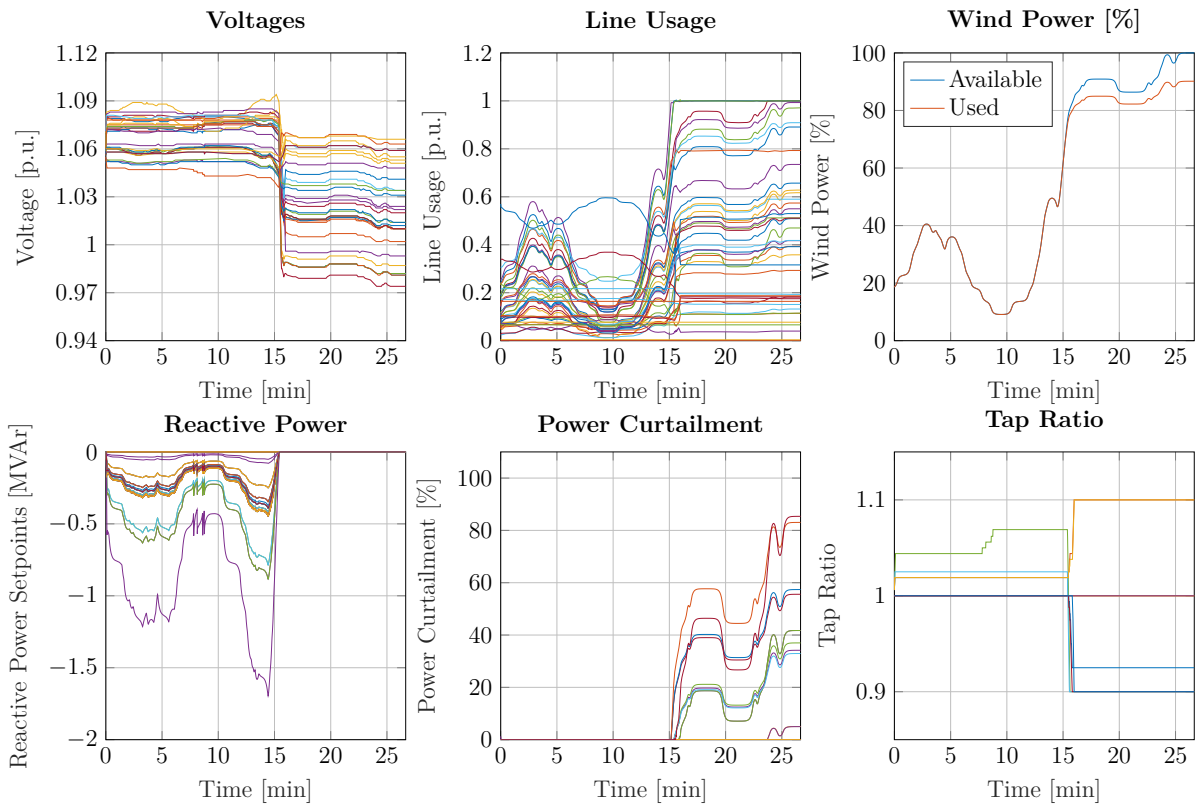


Figure 2.4: Simulation of the Unicorn benchmark under time-varying wind power (blue line in top right plot). The lower three plots show the control inputs and the upper plots show the resulting voltages, line usage, and used wind power. The voltage constraints that the controller has to enforce are the real French grid limits.

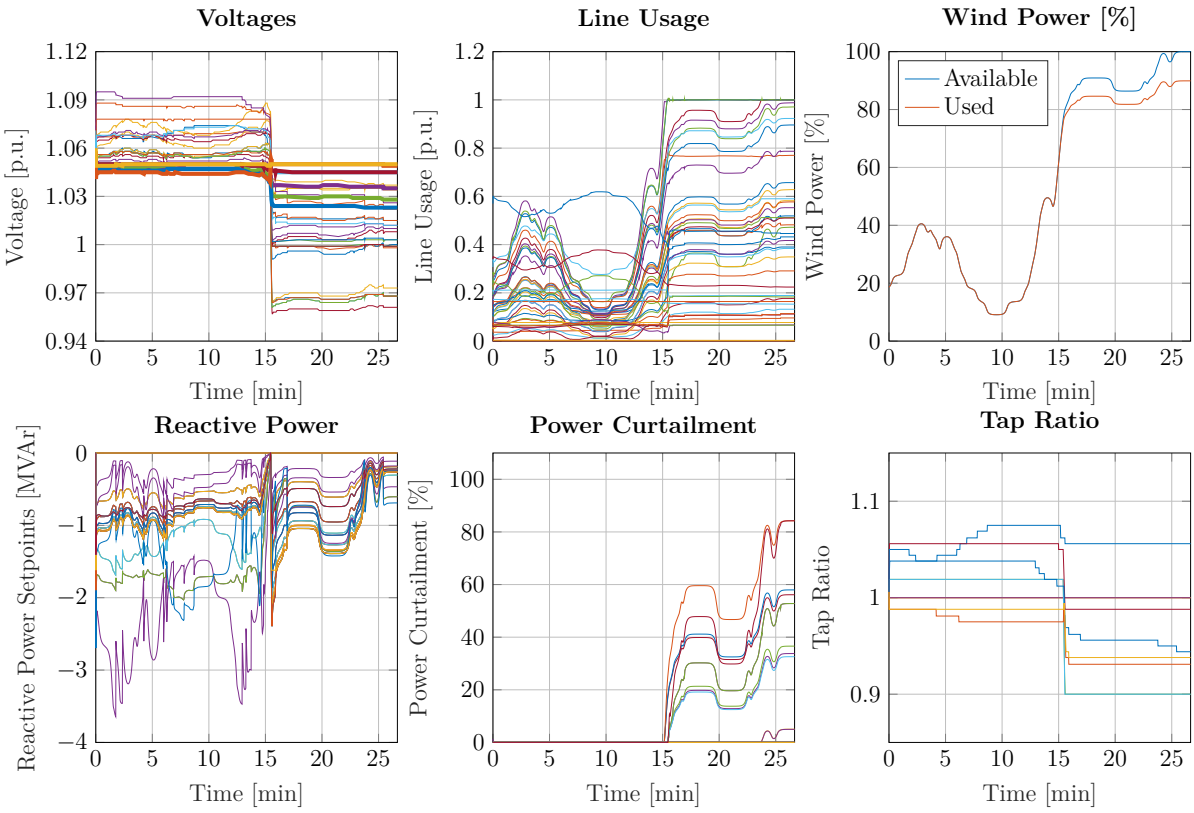


Figure 2.5: Simulation of the Unicorn benchmark under time-varying wind power (blue line in top right plot). The lower three plots show the control inputs and the upper plots show the resulting voltages, line usage, and used wind power. The voltage constraints of the 225 kV buses were set to 1.05 p.u. Those buses are indicated with a thicker line. The controller is enforcing these limits.

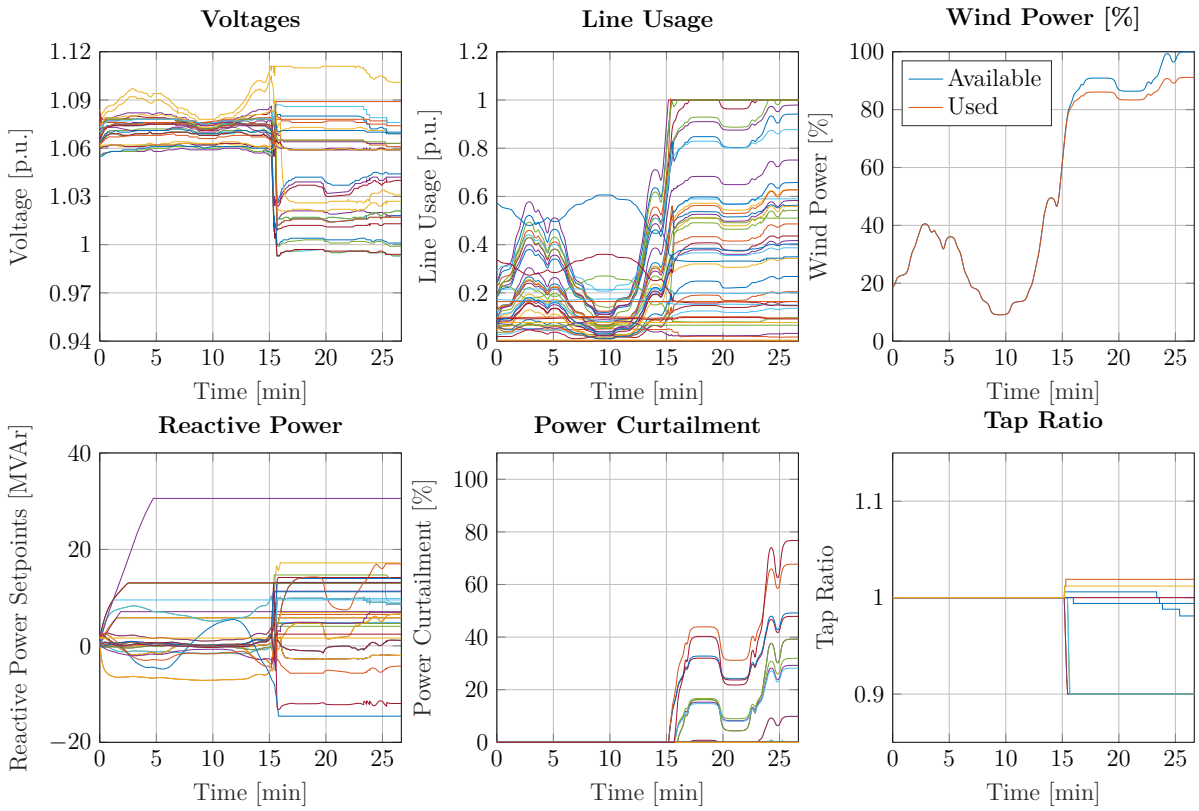


Figure 2.6: Simulation of the Unicorn benchmark under time-varying wind power (blue line in top right plot). The lower three plots show the control inputs and the upper plots show the resulting voltages, line usage, and used wind power. In this simulation, the controller has perfect knowledge of the sensitivity $\nabla_u h(u, d)$ and the derivative $\nabla f(u, y)$.

varying state the controller is tracking. To analyze the sub-optimality we run our OFO controller for *Optimal and Safe Curtailment* again but with perfect information about the sensitivity and derivative of the cost function at every time step. The main difference is in the usage of reactive power and the tap changers, see Figure 2.6. The active power curtailment however is very similar. This is because the approximation of the derivative of the cost function with respect to curtailment is highly accurate as well as the sensitivity of the line flows with respect to the curtailment (those are PTDFs). Overall, 91.14% of the available wind power can be used. This is mostly due to using the reactive power capabilities to reduce reactive power flows on the saturated lines and therefore freeing up capacity for active power flows. Also, the reactive power capabilities are used to reduce reactive power flows in general to lower the losses in the grid. Again, we want to highlight that the suboptimality under model mismatch does not arise from the method but is fundamental to the problem of making decisions based on inaccurate information. Nevertheless, OFO guarantees constraint satisfaction in steady-state while other methods do not.

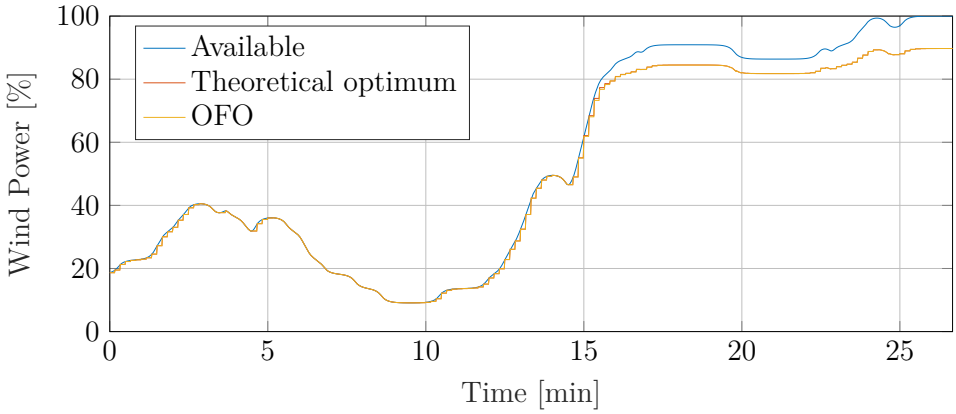


Figure 2.7: Comparison of the available wind power, the wind power that can be theoretically used, fixed curtailment at 60%, and the wind power that the OFO controller can use.

### 2.5.4 Tracking Performance & Comparison to Ground Truth

Changes in the consumption or the production affect the optimal solution of the optimization problem and an OFO controller is constantly trying to track this time-varying local optimum. To analyze the tracking performance we calculate the time-varying optimal solution with an OPF solver that has perfect model knowledge. For a fair comparison, we also provide the OFO controller with perfect model knowledge. We solve the task *Optimal and Safe Curtailment* with both approaches and plot the wind power that they can use. To be able to run the MATPOWER OPF solver we block the tap changers in the Blocaux area at 1. To have a fair comparison we also block the tap changers at 1 for the OFO controller. The result can be seen in Figure 2.7, and show that the optimality of the OFO controller is practically identical to the theoretical optimum that we compute with an omniscient and instantaneous OPF solver. The figure also shows a comparison with the state-of-the-art which is curtailing the wind farms at a fixed level. Here we chose 60% which already leads to one line being loaded at close to 90% meaning that the remaining headroom, for potential lower consumption in the Blocaux and therefore higher line loads, is small. From the figure it becomes apparent that at full wind output, the OFO controller allows the wind farms to inject 50 % more power than the state-of-the-art. The reason behind this large number is that not all lines become saturated and therefore only a few wind parks need to be curtailed. Due to the feedback from the grid, the OFO controller can optimally solve this non-trivial task of deciding which wind park has to be curtailed by which value at what time while making sure all voltages and lines are within their limits.

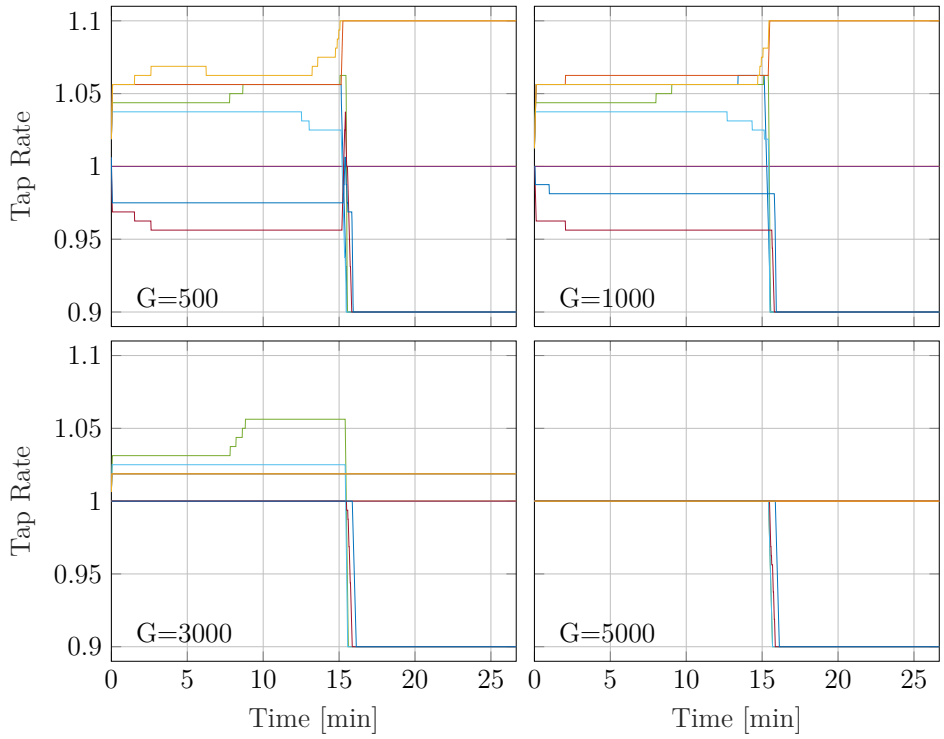


Figure 2.8: Behavior of the tap changers for different values of the entries of G corresponding to the tap changers.

### 2.5.5 Tap changer behavior

The tuning matrix $G$ influences the tap changer behavior. To illustrate this behavior, we simulate the benchmark for different $G$. More precisely, we use the controller for *Optimal and Safe Curtailment* and change the entries of $G$ corresponding to tap changers. The results for different values can be seen in Figure 2.8. With a value of 500, the tap changers are heavily used and might deteriorate quickly. For larger values, their usage decreases and with the value 5000 they are only used once the grid reaches its capacity limit. With a much larger value than 5000, the tap changers would not be used at all unless needed to enforce operational constraints, e.g. voltage limits.

## 2.6 Conclusion

By extending OFO controllers with the capability to handle discrete actuators, we are able to design a real-time controller for a real subtransmission grid benchmark that uses a diverse range of actuators, i.e., active and reactive power capabilities and on-load tap changers. Moreover, this controller operates the grid safely at the locally optimal operation point and tracks the local optimum when it changes over time. We were able to show that this tracking is highly precise and not sensitive to model mismatch. This leads

to the OFO controller being able to extract 50% more wind power in the benchmark than the state-of-the-art. Furthermore, we showed that specifying control objectives in an optimization problem is versatile and allows us to easily include ancillary services like voltage control. Most importantly, however, the simulations on the real benchmark show that OFO can be a powerful tool to safely operate the subtransmission grid in real-time, under model mismatch, and with limited model information. A remaining open question is how several independently controlled subtransmission grids would interact with each other.

CHAPTER 3

# Real-time Curative Actions for Power Systems via Online Feedback Optimization

This chapter describes how an Online Feedback Optimization (OFO) controller could be used to derive curative actions in real-time for power grids operating according to a curative $N-1$ scheme. To showcase the applicability of OFO controllers for this task, a specific situation, that requires the fast dispatch of curative actions, is considered. This situation was inspired by the Swiss-Italian blackout of 2003 and the task of the OFO controller is to change active power and voltage magnitude setpoints of large generating units to lower the voltage difference over an open breaker such that the breaker can be closed again.

## 3.1 Introduction

The electrical power grid is a critical infrastructure and the backbone of modern society. Its uninterrupted operation is crucial and it is essential that security can be guaranteed at all times even when contingencies occur, i.e., a transformer, power plant, or power line is disconnected. Therefore, the grid is operated following the $N-1$ criterion, meaning that the grid must be in a safe state even if any single element fails. This is also referred to as *preventive* $N-1$ security. The ENTSO-E grid code used in Europe allows temporary overloads in case of a contingency if curative or remedial actions are defined upfront to bring the system back to a safe operating point [Com17, Article 32(2)]. The North American Electric Reliability Cooperation (NERC) allows for a *Remedial Action Scheme* that automatically takes corrective actions [NER20]. Permitting such temporary violations relaxes the $N-1$ criterion to *curative* $N-1$ security and enlarges the range of allowed grid configurations, which enables more economical grid operation [Wes+19; MPG87]. This idea of using curative actions dates back at least to the 1980s [MPG87], where security-constraint Optimal Power Flow (OPF) with curative actions were pro-

This chapter is based on the publication [Ort+23a].

posed. Using curative $N-1$ security is an active field of research by, e.g., German Transmission Grid Operators and universities as it helps to utilize the grid to a larger extent [TSO19, Subsection 5.2]. Available curative actions are, e.g., changes of active power generation setpoints, operating points of high-voltage direct current systems, voltage set-points or reactive power injections, and tap changers positions of phase-shifting transformers. Lately, the shift to decentralized generation also enables distribution grids to provide curative actions [KND22]. An overview of curative actions is presented in [Yam+09, Table III].

Currently, the curative actions are decided manually by operators based on long-term experience or based on a library of case studies created by solving OPFs for a set of contingencies so that the actions are available in case they occur. As the share of production from volatile and unpredictable renewable energy sources increases, the grid is expected to operate at different operating points throughout the day, which requires operators to update their curative action plan more often than today. Moreover, determining the best emergency response is already complex nowadays, but it will become more complex in the future because large power plants are being replaced by decentralized energy resources and therefore the number of actuators needed for effective curative actions will increase. Overall, operators will need to determine curative actions more often, and those actions will be more complicated. Last but not least, when a contingency occurs, the operating personnel needs to implement the curative actions quickly while guaranteeing that those actions will not lead to new problems elsewhere.

In contrast to the current practice, we propose to employ a closed-loop control scheme to derive curative actions in real-time after the occurrence of a contingency. This has the following advantages: 1) the current operating point of the grid is taken into account; 2) the feedback nature of closed-loop control provides robustness to model mismatch; 3) due to the low computational complexity, the curative actions are promptly implemented to quickly drive the grid to a feasible operating point.

The control strategy that we propose is based on OFO, a methodology that allows converting iterative optimization algorithms into real-time robust feedback controllers [Hau+21; BDS19; LSM20; CDB19; Bia+21a]. These controllers can then be used to drive a system to the optimum of a constrained optimization problem, which, in the application that we are considering, defines the safe operating region of the grid. Such controllers do not need a full model of the system and guarantee constraint satisfaction even in the presence of model mismatch. There exist several different versions, e.g., distributed, centralized, model-based, and model-free controllers [He+22; Pic+22b]. They are well suited for several real-time optimization problems in power systems [Mol+17, Section IV], and they have also been experimentally validated [Ort+20a; Ort+20b].

To show how an OFO controller could help control the grid during an emergency power system operation, we take inspiration from the 2003 Swiss-Italian blackout. In that blackout, a breaker could not be reclosed because of the excessive voltage angle

difference across the breaker. Using the IEEE 39 bus model we set up a grid in which opening a breaker leads to a high angle difference, which we then reduce using an OFO controller.

The structure of this chapter is as follows. In Section 3.2 we describe the Swiss-Italian blackout and in Section 3.3 we present the simulation setup we are using to reconstruct the underlying problem of this blackout. Afterward, in Section 3.4, we design an OFO controller that determines effective curative actions in real-time. We present the results of our simulations in Section 3.5 and conclude the chapter in Section 3.6.

## 3.2 An example of unsuccessful emergency operations: the 2003 Swiss-Italian Blackout

On September 28th, 2003, Italy was importing a large amount of power from its neighboring countries. At 3:01, a 380 kV line in Switzerland tripped due to a tree flashover. Due to the large power flow toward Italy, there was a high phase angle difference of 42° across the now open circuit breaker. Reclosing this breaker would have resulted in high transient stress for generators located in that region and therefore a local protection system prevented the operators to reclose the line as long as the angle difference was larger than 30°. Meanwhile, because of the open line, power flow increased on other lines, leading to one of them operating at 110% of its capacity. This resulting overload still satisfied the curative $N-1$ criterion, assuming that it could be promptly mitigated. The Swiss operators deployed several control actions to enable reclosing the breaker and to lower the overloading, but did not succeed. The line overheated, which resulted in excessive sag of the conductor. At 3:25, after 24 minutes, a tree flashover occurred and the line was automatically disconnected. The remaining power lines immediately overloaded and were disconnected, leading to the largest Italian blackout in history [UCT04]. The estimated cost of this 18-hour blackout is 1.2 billion Euros [SR16].

## 3.3 Simulation Setup

We reproduce the core phenomena of the Swiss-Italian Blackout using the publicly available IEEE 39 bus test case. It includes 10 generators, 34 lines, and 39 buses, see Figure 3.1. We will trip the power line connecting buses 23 and 24, which we will not be able to reclose unless we make the voltage difference between the two buses sufficiently small. The numerical experiment is done via the dynamic power system simulator *DynPSSimPy* [HUJ21], which models secondary frequency control through Automated Generation Control and the dynamics of synchronous machines, including the excitation system, power system stabilizer, and governor which includes the primary frequency control. Figure 3.2

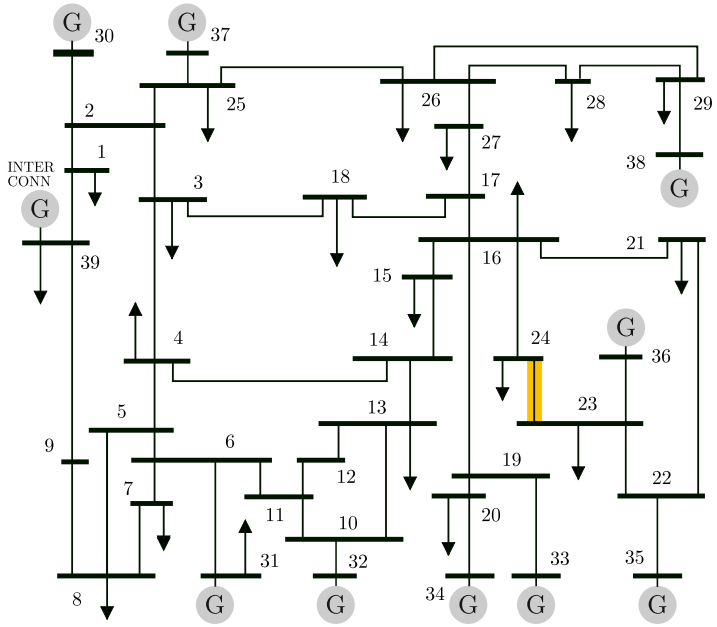


Figure 3.1: IEEE39 test case. The orange line is tripped and needs to be reclosed to bring the system back to a safe state.

shows the interconnection of the different elements. Here we give a short overview of the different components of the model. The synchronous generators are modeled with a sixth-order system

$$\begin{aligned}
\Delta\dot{\omega} =& \frac{1}{2H}\left(\frac{p_m}{\omega} - p_e - D\omega\right) \\
\dot{\delta} =& \Delta\omega \\
\dot{E}'_q =& \frac{E_f - E'_q - I_d(X_d - X'_d)}{T'_{d0}} \\
\dot{E}'_d =& \frac{-E'_d + I_q(X_q - X'_q)}{T'_{q0}} \\
\dot{E}''_q =& \frac{E'_q - E''_q - I_d(X'_d - X''_d)}{T''_{d0}} \\
\dot{E}''_d =& \frac{E'_d - E''_d + I_q(X'_q - X''_q)}{T''_{q0}}
\end{aligned}$$

with the speed deviation of the rotor speed from the nominal frequency $\Delta\omega$, the rotor angle $\delta$ and the internal voltages $E'_q$, $E'_d$, $E''_q$ and $E''_d$. The variables $H$, $D$, $X_d$, $X'_d$, $X''_d$, $X_q$, $X'_q$, $X''_q$, $T'_{d0}$, $T'_{q0}$, $T''_{d0}$, and $T''_{q0}$ are positive, real-valued parameters. Their definition can be found in [Hot21, Table 2.1]. The electrical power output of a synchronous machine is given by

$$p_e = E''_d I_d + E''_q I_q,$$

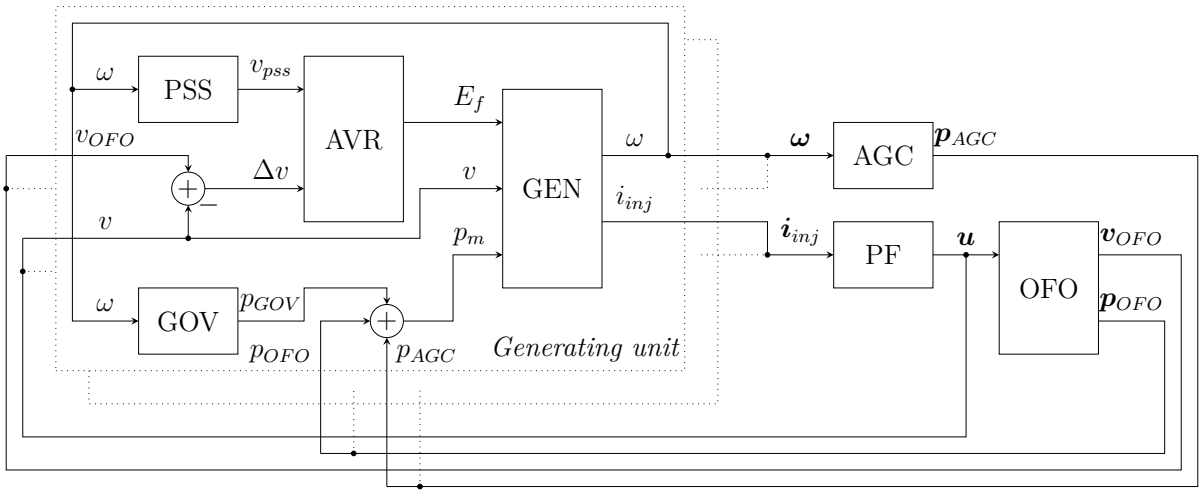


Figure 3.2: Block diagram of the dynamic power system simulator *DynPSSimPy* including the OFO controller. The blocks PSS, AVR, GOV, GEN, AGC, PF and OFO correspond to the power system stabilizer, the automated voltage regulator, the governor, the synchronous machine, the excitation system, the power flow equations and the OFO controller, respectively. The blocks corresponding to one generating unit are grouped by the dotted frame, and possible additional generation units are indicated by the second dotted frame.

where $I_d$ and $I_q$ can be derived from

$$\begin{bmatrix} R & X_d'' \\ -X_d'' & R \end{bmatrix} \begin{bmatrix} I_d \\ I_q \end{bmatrix} = \begin{bmatrix} E_d'' \\ E_q'' \end{bmatrix} - \begin{bmatrix} v_d \\ v_q \end{bmatrix}.$$

Here, $R$ is the armature winding resistance, $v_d = \mathrm{Re}(u)$, and $v_q = \mathrm{Im}(u)$ with the bus voltage $u$. Finally, the current injected by the synchronous generator is

$$i_{inj} = -\left(\frac{E_d''}{X_d''} + j\frac{E_q''}{X_q''}\right) e^{j\delta}.$$

The governors are modeled like in Figure 3.3. They are driven by the frequency deviation $\Delta\omega$ and the steady-state active power fed into the network by the corresponding synchronous machine $p_{m0}$. The parameters of the governors are explained in Table 3.1.

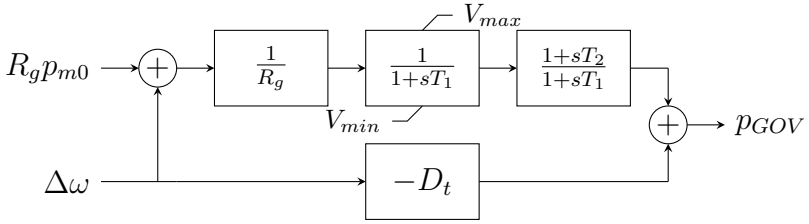


Figure 3.3: Block diagram of the governor model.

Table 3.1: Parameters of the governor model.

| Parameter | Description |
|---|---|
| $T_1$ | Governor time constant |
| $T_2$, $T_3$ | Turbine time constants |
| $R_g$ | Turbine governor droop |
| $D_t$ | Frictional losses factor |
| $V_{min}$, $V_{max}$ | Valve limits |

The excitation systems of the synchronous machines are modeled according to the block diagram in Figure 3.4. The input $v_{pss}$ comes from the power system stabilizer, $\Delta v$ is the deviation of the bus voltage magnitude $v$ from the voltage set point $v_{OFO}$, and $E_{f0}$ is the steady-state field voltage. The parameters of the excitation system are explained in Table 3.2.

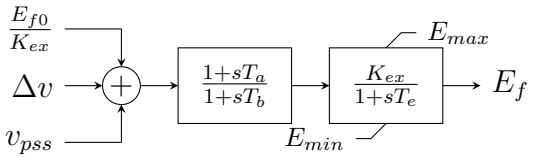


Figure 3.4: Block diagram of the excitation system.

Table 3.2: Parameters of the excitation system model.

| Parameter | Description |
|---|---|
| $K_{ex}$ | Controller gain |
| $T_a$, $T_b$ | Filter time constants |
| $T_e$ | Exciter time constant |
| $E_{min}$, $E_{max}$ | Field voltage limits |

The power system stabilizer can be seen in Figure 3.5 and is driven by the frequency deviation $\Delta\omega$. The parameters of the power system stabilizer are explained in Table 3.3.

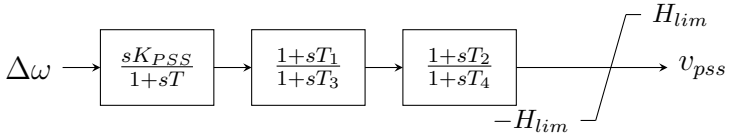


Figure 3.5: Block diagram of the power system stabilizer.

Table 3.3: Parameters of the power system stabilizer model.

| Parameter | Description |
|---|---|
| $K_{PSS}$ | Controller gain |
| $T$ | Washout-filter time constant |
| $T_1$, $T_3$ | Time constants of first lead-lag compensation |
| $T_2$, $T_4$ | Time constants of second lead-lag compensation |
| $H_{lim}$ | Output limit |

The Automated Generation Control can be seen in Figure 3.6. It balances the active power generation and consumption in the power system and is driven by the average frequency deviation over all $g$ generators

$$\Delta\bar{\omega} = \frac{\sum_{i\in[1,g]} \Delta\omega_i H_i S_i}{\sum_{i\in[1,g]} H_i S_i}.$$

The vector $\boldsymbol{\beta}$ contains the participation factor of each generator and the sum of its elements is 1. The parameters of the Automatic Generation Control are explained in Table 3.4.

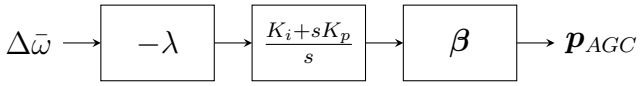


Figure 3.6: Block diagram of the automated generation control.

Table 3.4: Parameters of the automated generation control model.

| Parameter | Description |
|---|---|
| $\lambda$ | Frequency bias factor |
| $K_p$ | Proportional gain |
| $K_i$ | Integral gain |
| $\boldsymbol{\beta}$ | Participation vector |

For more information on the model and the model parameters, the reader is referred to [Hot21].

## 3.4 Curative Actions via Online Feedback Optimization

The curative actions available in the IEEE 39 bus case are changes in the active power generation set-points and voltage set-points of the generators. Hence, we consider the

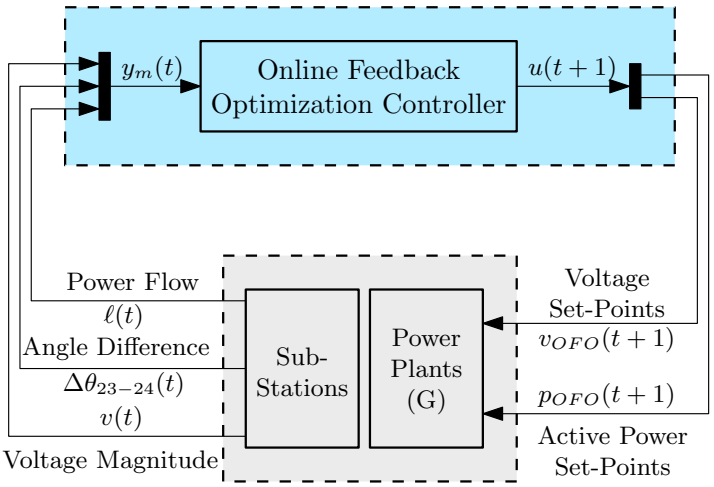


Figure 3.7: Schematic representation of the proposed OFO-based controller. The controller iteratively gathers power system measurements and updates set-points for the controllable power plants in the grid.

controllable active power set-points $p_{OFO}$ and voltage set-points $v_{OFO}$ as our input $u = [p_{OFO}^T, v_{OFO}^T]^T$. We measure the bus voltage magnitudes $v$, all power flows $\ell$, and the phase difference $\Delta\theta_{23-24}$ between buses 23 and 24 and group them in our output $y = [v^T, \ell^T, \Delta\theta_{23-24}]^T$. The block diagram of our controller can be seen in Figure 3.7.

We encode the goal of reclosing the breaker in the following optimization problem

$$\begin{aligned} \min_{u} \quad & (v_{23}(u) - v_{24}(u))^2 + (\theta_{23}(u) - \theta_{24}(u))^2 \\ \text{subject to} \quad & p_{OFO,\min} < p_{OFO} < p_{OFO,\max} && \forall \text{ generators} \\ & v_{OFO,\min} < v_{OFO} < v_{OFO,\max} && \forall \text{ generators} \\ & v_{\min} < v(u) < v_{\max} && \forall \text{ buses} \\ & \ell_{\min} < \ell(u) < \ell_{\max} && \forall \text{ lines} \end{aligned} \tag{3.1}$$

that minimizes the voltage difference subject to actuator limits and grid constraints. Note, that this optimization problem is specific to this emergency situation, and more work is needed to identify optimization problems for other and more general situations. As prescribed by the OFO approach, we then select an optimization algorithm. We choose a projected gradient descent algorithm. An OFO controller derived from such an algorithm was developed in [Häb+20]. The control update is

$$u(t+1) = u(t) + \alpha\, \sigma_\alpha(u(t), y_m(t)) \tag{3.2}$$

with

$$\begin{aligned} \sigma_\alpha(u, y_m) := \ & \arg\min_{w} \ \left\| w + \nabla_u h(u, y_m) \nabla\Phi(y_m)^T \right\|^2 \\ & \text{subject to} \quad A(u + \alpha w) \leq b \\ & \qquad\qquad\ \ C(y_m + \alpha \nabla_u h(u, y_m) w) \leq d\,. \end{aligned} \tag{3.3}$$

In the controller, $\alpha$ is a gradient step-length (that we set to $\alpha = 3$) and $\sigma_\alpha(u, y_m)$ is the projected gradient direction, which is computed via a simple convex quadratic program. Note, that such convex quadratic programs can be efficiently solved for very large numbers of variables and constraints on standard computation hardware. In this auxiliary optimization program, $\Phi(y_m)$ is the cost function of the optimization problem (3.1) where the output $y$ is replaced by the measurement $y_m$. The constants $A$, $b$ $C$, $d$ describe a local linearization of the potentially nonlinear constraints of the optimization problem (3.1), see [Häb+20]. The resulting controller determines curative actions based on measurements and the sensitivity $\nabla_u h(u, y_m)$. Overall, we are solving the highly nonlinear and non-convex optimization problem (3.1) by repeatedly solving the linear and convex problem (3.3) and utilizing feedback measurements. For an in-depth decision of the convergence of this strategy see [Hau+21]. $\nabla_u h(u, y_m)$ is the sensitivity matrix of input (set-points) to output (measurements). These are similar to e.g. power transfer distribution factors and we derive them from the steady-state power flow equations, see [BD15] for details. We recalculate this sensitivity at every time step, which occurs every 5 seconds. Note, that this sensitivity is calculated many times while solving Optimal Power Flow problems. When solving security-constraint Optimal Power Flow Problems, it is calculated for all considered contingencies. Knowing and calculating $\nabla_u h(u, y_m)$, as needed for our controller, is therefore a reasonable assumption. Note that, it can also be estimated and real-time adapted from data [Pic+22b]. Last but not least, the controller is also robust with respect to an inaccurate sensitivity, on which we provide more details in Section 3.5.

## 3.5 Results

The upper panel in Figure 3.8 shows the absolute voltage difference between buses 23 and 24. A small absolute voltage difference implies that both the voltage angle difference and voltage magnitude difference between buses 23 and 24 are small, which allows the breaker to be reclosed. The middle panel shows the generators' voltage set-points and the lower panel shows the generators' active power set-points. After 10 seconds, the line connecting the two buses trips and the absolute voltage difference increases. As described in Section 3.2 local protection might prohibit reclosing the line. Therefore, after 30 seconds, the OFO controller is activated to reduce the absolute voltage difference over the breaker. As can be seen in Figure 3.8, the controller takes effective steps towards minimizing the absolute voltage difference, and within just a few iterations the breaker could be closed again. While the controller is minimizing the absolute voltage difference, the constraints in its update law (3.3) also enforce that the control inputs $u$ are within the actuator capabilities, as can be seen in the lower two panels. Likewise, the constraints on $y$, i.e., bus voltage magnitudes and current flows, can also be enforced.

Overall, the proposed controller quickly reduces the voltage difference. The resulting curative actions include iterative adjustments of the active power and voltage set-points of all generators, showing how complex coordinated interventions may be needed in order to effectively tackle a contingency.

We also analyze the robustness of our controller against model mismatch. The only model information used in an OFO controller is the sensitivity $\nabla_u h(u, y_m)$. The sensitivity might be wrong if it was derived in a different operating state or based on a model with wrong parameters or an incorrect topology. In practice, the sensitivity will always have a model mismatch. For our robustness analysis, we calculate the sensitivity based on grid topologies that are different from the topology of our simulation model. More precisely, we derive the sensitivity for a topology where we erased a line from the grid and then use these wrong sensitivities in our controller. In many power grids, the position of switches and breakers is observed, and therefore a model mismatch due to a wrong topology is unlikely to occur. Nevertheless, we choose this source of model mismatch because we consider it to be the most extreme. The results of our robustness analysis can be seen in Figure 3.9 and show that even with severe model mismatch, the controller is able to reduce the absolute voltage difference and does not become unstable. However, some levels of model mismatch cause very slow performance, and future work should analyze how well the sensitivity needs to be known to guarantee good performance. Generally, the robustness against model mismatch is due to the feedback nature of the approach and the fact that our control law (3.2) is an integrator driven by a gradient step, and integral controllers are known to be robust. This robustness was also observed in experiments [Ort+20a] and analyzed mathematically [CSB19].

Another source of uncertainty that the controller needs to be robust against is that commanded inputs $u$ are not implemented as asked for. For example, the synchronous generators do not follow the commanded input $p_{OFO}$ but the value $p_m$, because the set-points of the governor and the Automatic Generation Control are added on top of $u_{OFO}$, compare Figure 3.2. The lower panel in Figure 3.8 shows the active power generation set-points $p_m$ and one can see that they change continuously and not just every 5 seconds when our controller updates its set-point. Nevertheless, the controller converges because it measures the output $y$ and therefore indirectly the effect of the governor and the Automatic Generation Control.

## 3.6 Conclusion

These preliminary numerical results show that OFO controllers have the potential to derive curative actions in real-time after the occurrence of a contingency and to automate some curative actions in emergency power system operations. Such controllers could either be implemented as a decision support tool for the operator or directly as a closed-

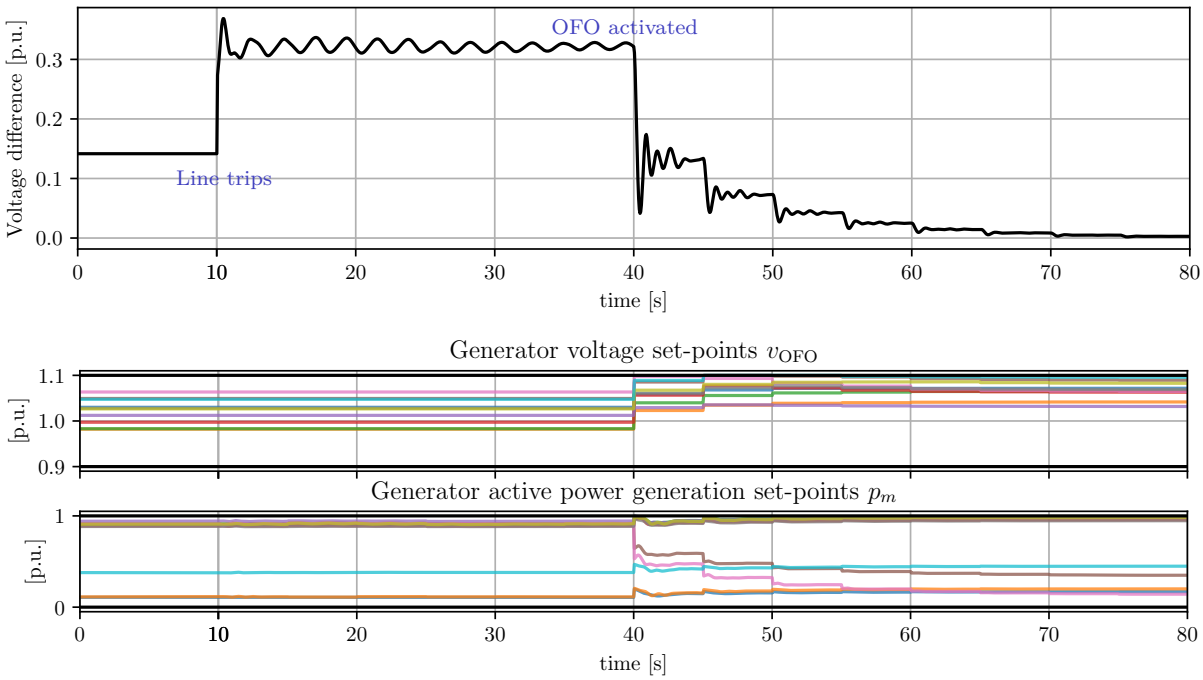


Figure 3.8: Dynamic power system simulation of a line contingency at 10 seconds and activation of the OFO controller at 40 seconds with a sampling time of 5 seconds. $p_m$ is the sum of the OFO controller set-point $p_{OFO}$ and the primary and secondary frequency control. The limits for the voltage set-points are 0.9 p.u. and 1.1 p.u. The limits for the active power set-points are 0 p.u. and 1 p.u. Each color corresponds to one generator.

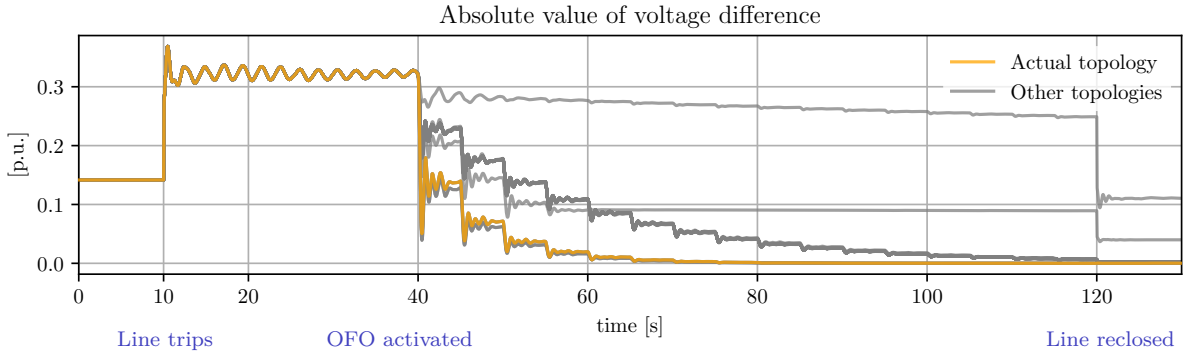


Figure 3.9: Behavior of the closed-loop system for several incorrect sensitivities. The line is tripped at 10 seconds, the controller is activated at 40 seconds, and the line is reclosed at 120 seconds.

loop controller. In our opinion, determining curative actions in real-time is in agreement with the European and North American grid codes, and it definitely reduces the workload in the control room.

Further research is needed to investigate the stability of the interconnection of the controller with the power system dynamics because timescale separation results like those in [Hau+20a] (which assume that grid dynamics are sufficiently faster compared to the rate at which set-points are updated by the controller) turn out to be too conservative for this time-critical application. Furthermore, because we expect the system to work far from nominal operating points during contingencies, robustness to model mismatch needs to be certified for this application more extensively (possibly building on numerical tests like those in [CSB19]). Last but not least, a broader range of emergency situations needs to be analyzed.

CHAPTER 4

# Adaptive Real-Time Grid Operation via Online Feedback Optimization with Sensitivity Estimation

In this chapter, we combine an Online Feedback Optimization (OFO) controller with a Kalman filter and persistent excitation to design an OFO controller that is able to continuously learn the input-output sensitivity from data while it is controlling the system. This makes it possible to use OFO controllers that are completely model-free.

## 4.1 Introduction

The increasing amount of controllable, yet sometimes unpredictable, power resources in electrical grids, e.g., renewable generation, electric vehicles, flexible loads, etc., leads to new challenges and opportunities in the operation of power systems. On the one hand, these new controllable elements allow to minimize the grid operational cost and promote a transition to a more sustainable power system. On the other hand, given the volatility and unpredictability of these resources, fast control decisions are required to avoid constraint violations, e.g., overvoltages. This is especially relevant in distribution grids, where many of these resources are deployed. However, measurement scarcity and poor grid models challenge grid operation at such low voltage levels.

One way to leverage the controllability of these resources and to optimize the grid operation is by solving an AC Optimal Power Flow (AC-OPF) [MH19], an optimization problem to determine the set-points of controllable resources that minimize the operational cost and enforce grid safety requirements, e.g., voltage limits, line thermal limits, etc. Unfortunately, standard AC-OPF requires a) full grid observability, e.g., measure-

This chapter is based on the publication [Pic+22b]. Miguel Picallo and Lukas Ortmann contributed equally to this research with Lukas Ortmann being involved in conceptualization, formal analysis, validation, and writing of the original draft.

ments of all active and reactive power injections and consumptions, and b) an accurate nonlinear grid model, e.g., its admittance matrix [MH19]. Yet, learning the model may require an extensive deployment of measurements across the network [Bol+13; MBV20], usually not available or affordable on the distribution system level. Furthermore, the volatility of renewable energy sources and household loads requires high sampling and control-loop rates to satisfy the grid constraints. Yet, solving a computationally expensive AC-OPF may pose a limit on these rates.

Online Feedback Optimization (OFO) [Mol+17; Hau+17; DS16] is a novel computationally efficient approach that allows to track the solutions of an AC-OPF problem under time-varying conditions using subsecond control-loop rates. OFO is based on a controller that uses grid measurements as feedback to iteratively steer the controllable input set-points towards the AC-OPF solutions, and has already been successfully tested in both simulations and experimental settings [Ort+20a]. Furthermore, OFO neither requires full grid observability [PBD20], nor an accurate nonlinear grid model. It only needs measurements of the outputs that need to be controlled, and the input-output sensitivity that matches a change in the input to a change in the output. This sensitivity is essentially a derivative of the power flow equations at the operating point [BD15], and thus depends on the grid state and exogenous disturbances, e.g., loads. Hence, constructing an accurate sensitivity requires the grid model and full measurements of the grid to evaluate it. To avoid these requirements, some OFO approaches use a constant approximate linear model, and thus a constant approximate sensitivity [DS16; PBD20; Ort+20a]. Even though OFO is robust against small approximation errors in this sensitivity [Ort+20a], an inaccurate sensitivity introduces a model-mismatch that may lower the approach performance [CSB19]. Therefore, some model-free approaches try to operate the system optimally without requiring a model or sensitivity. First, reinforcement learning allows to disregard the model, and instead take decisions based solely on measurements [Che+21]. However, reinforcement learning has limited theoretical guarantees, and may not be able to enforce the grid safety constraints during its learning phase. Second, data-driven control [CLD19; Mug+16; Bia+21b] based on Willems Fundamental lemma [Wil+05] allows to compute the sensitivity after gathering sufficient data. Yet, these approaches estimate a constant linear model, and thus may fail to adapt to different operating points. Finally, zeroth-order gradient-free methods as [CPL21] allow to operate the system while continuously estimating and updating the sensitivity. However, [CPL21] requires a sufficient time-scale separation between the sensitivity estimation procedure and the feedback optimization, which may lower the convergence rate of the entire approach if the measurement sample rate is restricted due to communication limits.

Therefore, in this chapter, with a similar spirit as in the extremum seeking approach [CPL21], we propose a model-free OFO approach that sequentially estimates a time-varying sensitivity while operating the grid, bypassing the need to know the whole grid

model accurately, and to have full grid observability. Our contributions are as follows: First, we design a sensitivity learning approach via recursive least squares [Len99; IM10]. We use as measurements the change in the outputs caused by a change of the controllable inputs. Second, we combine this sensitivity estimation with a persistently exciting OFO that gathers enough information about the sensitivity while driving the control inputs towards the AC-OPF solutions. Third, we certify the convergence of both the estimated sensitivity and the control input towards the true sensitivity and the time-varying solution of the AC-OPF, respectively. Fourth and finally, we simulate the proposed OFO controller with sensitivity estimation on the 3-phase, unbalanced IEEE 123-bus test feeder [Ker91] using real consumption data, and show its superior performance over a state-of-the-art OFO with a constant sensitivity approximation.

The chapter is structured as follows: Section 4.2 presents some preliminaries on grid models, AC-OPF and OFO. Section 4.3 explains our proposed OFO with sensitivity estimation approach, and provides theoretical convergence guarantees. Section 4.4 shows the simulation on a test feeder. Finally, Section 4.5 concludes and discusses further work.

## 4.2 Preliminaries: Grid Model, AC-OPF and OFO

### 4.2.1 Grid Model

For each bus $i$ of a $n$-bus power system we define the voltage magnitude as $v_i \in \mathbb{R}$, the active and reactive power as $p_i \in \mathbb{R}$ and $q_i \in \mathbb{R}$, respectively. We obtain the vectors $v$, $p$, and $q$ of dimension $n$ by stacking the individual bus quantities, i.e., $v = [v_1, \dots, v_n]^T$. We define the control input vector $u \in \mathbb{R}^{n_u}$ consisting of all the controllable resources (e.g. active and reactive generation and flexible loads in $p$ and $q$, slack bus voltage magnitude $v_1$ through tap changers); the output vector $y$ (e.g. voltage magnitude elements in $v$) with all the quantities that we measure and want to control through the inputs; and the disturbance vector $d$ with all uncontrollable power injections (e.g. conventional consumption loads in $p$ and $q$). The grid admittance matrix and the power flow equations allow to define an input-output map $\hbar(\cdot)$ that characterizes the output $y$ as a non-linear function of $u$ and $d$:

$$y = \hbar(u, d). \tag{4.1}$$

The input-output map $\hbar(\cdot)$ is not typically available in closed form, since in general it is not possible to derive an analytical expression of $v$ (in $y$) as a function of $p$ and $q$ (in $u$ and $d$) using the power flow equations [MH19]. Yet, the local existence of a continuous differentiable map $\hbar(\cdot)$ can be guaranteed by the implicit function theorem [KP12].

### 4.2.2 AC Optimal Power Flow for Grid Operation

The operation of a power grid consists of deciding the input $u_t$ at each time instant $t$. An AC-OPF allows to formulate this decision process as an optimization problem:

$$\begin{aligned} u_t^*, y_t^* = &\arg \min_{u \in \mathcal{U}_t, y} f(u) + g(y) \\ &\text{s.t. } y = \hbar(u, d_t), \end{aligned} \tag{4.2}$$

where $f(u)$ is the operational cost on the input $u$; $g(y)$ is a penalty function to enforce some grid specification on the output $y$, e.g., voltage limits; $\mathcal{U}_t$ is the time-varying set of admissible inputs that defines the operational constraints on $u_t$, e.g., power limits $\mathcal{U}_t = \{u \,|\, \underline{u}_t < u < \overline{u}_t\}$; and $d_t$ is the disturbance value at time $t$, e.g., uncontrollable loads or non-dispatchable generation. The nonlinear input-output model (4.1) in (4.2) relates the outputs to the chosen input.

Optimal real-time decision making consists of first taking measurements $d_t$; then, solving the AC-OPF problem (4.2), and finally applying the solution $u_t^*$ to the system. Then, this is repeated at the next time step $t+1$.

### 4.2.3 Linear Power Flow Approximation

Solving AC-OPF problems (4.2) to determine the set-points of power resources is a compelling and valuable tool for grid operators, but it comes with some drawbacks: First, the full nonlinear model of the grid $\hbar(u, d)$ is needed. Second, solving the AC-OPF (4.2) can be computationally expensive, which may jeopardize its use for real-time grid operation. This can be circumvented by linearizing the map $\hbar(\cdot)$ in (4.1) at an operating point [Low14; BZ15; MH19], e.g., the zero-injection point $(u_{\text{op}}, d_{\text{op}}) = (0, 0)$, to obtain the approximation

$$y = H_0 u + D_0 d + y_0, \tag{4.3}$$

where $y_0$ is an offset representing the output value when $u = d = 0$, e.g., 1 p.u. for all voltage magnitudes. The matrices $H_0 = \nabla_u \hbar(u, d)|_{(u_{\text{op}}, d_{\text{op}})}$ and $D_0 = \nabla_d \hbar(u, d)|_{(u_{\text{op}}, d_{\text{op}})}$ are evaluated at the operating point, and represent the sensitivities of the output with respect to changes in the input $u$ and disturbance $d$, respectively. This linear approximation (4.3) can substitute the nonlinear map $\hbar(\cdot)$ in the AC-OPF (4.2) to get

$$\min_{u \in \mathcal{U}_t} f(u) + g(H_0 u + D_0 d_t + y_0). \tag{4.4}$$

### 4.2.4 Online Feedback Optimization (OFO)

Solving the AC-OPF with linear power flow approximation (4.4) is computationally efficient and could be employed in real-time operation. However, this approach does not

take advantage of output measurements $y_t$, since it only feeds $d_t$ through the inaccurate linear model (4.3). Hence, such a *feedforward* approach introduces a model-mismatch that can cause a performance degradation, and even lead to constraint violations, e.g., under and overvoltages.

Instead, OFO is a novel approach [Hau+17; DS16; Mol+17] that uses $y_t$ as *feedback* to achieve a safer grid operation and track the solution of the AC-OPF (4.2) under time-varying conditions. For that, OFO turns a standard optimization algorithm, in our case projected gradient decent [Ber97], into a feedback controller that takes the grid output measurements $y_t$, instead of computing the output $y_t$ via the grid model (4.1) or the linearized one (4.3). Projected gradient decent consists of a gradient step and a projection: First, we compute the gradient of the cost function in (4.4):

$$\nabla_u\Big(f(u)+g(y)\Big) \overset{(4.3)}{=} \nabla_u f(u) + H_0^T \nabla_y g(y).$$

To minimize the operational cost, the current input $u_t$ is pushed along the direction of the negative gradient with a step size $\alpha$, and then it is projected onto the feasible space $\mathcal{U}_t$ to enforce the operational constraints on the input, i.e.,

$$u_{t+1} = \Pi_{\mathcal{U}_t}\Big[u_t - \alpha\Big(\nabla_u f(u_t) + H_0^T \nabla_y g(y_t)\Big)\Big], \tag{4.5}$$

where $\Pi_{\mathcal{U}}\big[u\big] = \arg\min_{z\in\mathcal{U}}\|u-z\|_2^2$ is the projection of $u$ onto $\mathcal{U}$, which is typically easy to evaluate for power grid operation [DS16], especially if $\mathcal{U}_t = \{u \,|\, \underline{u}_t \leq u \leq \overline{u}_t\}$ is a box constraint.

## 4.3 Online Feedback Optimization with Sensitivity Estimation

The OFO controllers are robust, i.e., preserve stability, against using a constant power flow sensitivity approximation $H_0$ instead of the actual one $\nabla_u \hbar(u,d)$ [Ort+20a; CSB19]. Unfortunately, even if the overall system is stable, a model mismatch between $H_0$ and $\nabla_u \hbar(u,d)$ may lead to a difference between the solution $u_t^*$ of the AC-OPF problem and the values $u_t$ produced by the OFO controller (4.5) [CSB19]. Therefore, we propose an approach to sequentially update the sensitivity $H_0$ into a good approximation of the true sensitivity $\nabla_u \hbar(u,d)$, and thus avoid a potential performance degradation. For that, we will consider the sensitivity as a time-varying parameter $H_t = \nabla_u \hbar(u_t, d_t)$, and propose a recursive least-squares approach to generate sensitivity estimates $\hat{H}_t$ using the measured variations of $y$ and $u$ over time, $\Delta u$ and $\Delta y$ respectively. Then, in every time step we feed this estimated sensitivity $\hat{H}_t$ to the OFO as in Figure 4.1.

### 4.3.1 Sensitivity Estimation

Due to the non-linearity of $\hbar(u, d)$, the true sensitivity $\nabla_u \hbar(u, d)$ depends on the values of $u$ and $d$. The temporal variation of the disturbance $d_t$ and the input $u_t$, e.g., due to applying the OFO controller (4.5) in the input case, produces a time-varying sensitivity $H_t = \nabla_u \hbar(u_t, d_t)$. Instead of learning the dependency on $u$ and $d$, we model a time-varying sensitivity $H_t$ with the following random process:

$$h_t = h_{t-1} + \omega_{p,t-1} \tag{4.6}$$

where $h = \text{vec}(H)$ is the column-wise vector representation of the sensitivity matrix $H$, $\Delta u_{t-1} = u_t - u_{t-1}$ denotes a change of the input $u$, and $\omega_{p,t} \sim \mathcal{N}(0, \Sigma_{p,t})$ is a Gaussian process noise with covariance $\Sigma_{p,t} = \Sigma_{p_1} + \Sigma_{p_2} \|\Delta u_t\|_2^2$, that represents how the sensitivity changes over time. We make the part $\Sigma_{p_2}$ of the process noise proportional to $\|\Delta u_t\|_2$, since a large $\Delta u_t$ can trigger a larger change in the true sensitivity $\nabla_u \hbar(u, d)$ that depends on $u$, and the part $\Sigma_{p_1}$ independent of $\Delta u_t$ to account for a uncontrolled random change $\Delta d_t = d_{t+1} - d_t$ that can affect the sensitivity as well.

Next, to derive a measurement equation for the sensitivity $H_t$, consider the first-order Taylor approximation of $y_t$

$$\begin{aligned} \overbrace{\hbar(u_t, d_t)}^{y_t} \approx \overbrace{\hbar(u_{t-1}, d_{t-1})}^{y_{t-1}} + \overbrace{\nabla_u \hbar(u_{t-1}, d_{t-1})}^{H_{t-1}} \Delta u_{t-1} \\ + \nabla_d \hbar(u_{t-1}, d_{t-1}) \Delta d_{t-1}. \end{aligned} \tag{4.7}$$

At each time $t$, we measure $y_t$, and compute the variation $\Delta y_{t-1} = y_t - y_{t-1}$. Based on the Taylor approximation (4.7), we treat this variation $\Delta y_{t-1}$ as a noisy linear measurement of $H_{t-1}$ through a measurement model that depends on $\Delta u_{t-1}$:

$$\Delta y_{t-1} = \underbrace{H_{t-1} \Delta u_{t-1}}_{= U_{\Delta,t-1} h_{t-1}} + \omega_{m,t-1} \tag{4.8}$$

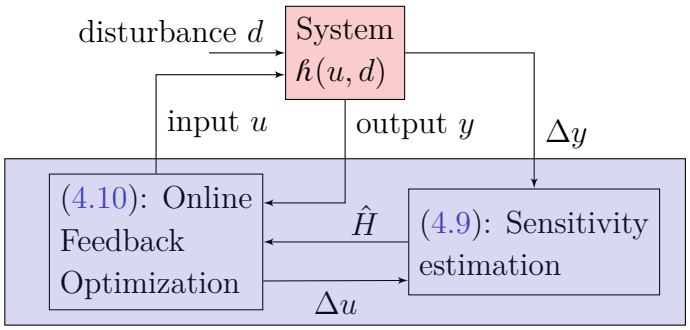


Figure 4.1: Model-free grid operation via Online Feedback Optimization (OFO) with sensitivity estimation.

where $U_{\Delta,t} = \Delta u_t^T \otimes \mathbb{1}$, with the Kronecker product $\otimes$, and $\omega_{m,t} \sim \mathcal{N}(0, \Sigma_{m,t})$ is a Gaussian measurement noise with covariance $\Sigma_{m,t} = \Sigma_{m_1} + \Sigma_{m_2}\|\Delta u_t\|_2^2 + \Sigma_{m_3}\|\Delta u_t\|_2^4$. Again, the part $\Sigma_{m_1}$ independent of $\Delta u_t$ in the measurement noise represents the effect of an uncontrolled random disturbance change $\Delta d_t$, while the other parts $\Sigma_{m_2}$ and $\Sigma_{m_3}$ encapsulate the second-order error of the Taylor approximation (4.7).

To update the sensitivity estimate $\hat{h}_t$, we combine the information given by the previous sensitivity estimate $\hat{h}_{t-1} = \text{vec}(\hat{H}_{t-1})$, and the measurements $\Delta y_{t-1}$ (4.8). We compute the new sensitivity estimate $\hat{h}_t$ through a Bayesian update represented in the following least-squares problem [Len99; IM10]:

$$\hat{h}_t = \arg\min_{\hat{h}} \|\hat{h} - \hat{h}_{t-1}\|^2_{\Sigma^{-1}_{t-1}} + \|\Delta y_{t-1} - U_{\Delta,t-1}\hat{h}\|^2_{\Sigma^{-1}_{m,t-1}},$$

where $\Sigma_t$ is the covariance matrix representing the uncertainty of the sensitivity estimate $\hat{h}_t$, and $\|x\|_A^2 = x^T A x$ is the norm of $x$ with respect to a positive definite matrix $A$. The resulting recursive estimation can be expressed as a Kalman filter [Jaz70]:

$$\begin{aligned} \hat{h}_t &= \hat{h}_{t-1} + K_{t-1}(\Delta y_{t-1} - U_{\Delta,t-1}\hat{h}_{t-1}) \\ \Sigma_t &= \big(\mathbb{1} - K_{t-1}U_{\Delta,t-1}\big)\Sigma_{t-1} + \Sigma_{p,t-1}, \end{aligned} \tag{4.9}$$

where $\mathbb{1}$ is the identity matrix, and $K_t = \Sigma_t U_{\Delta,t}^T(\Sigma_{m,t} + U_{\Delta,t}\Sigma_t U_{\Delta,t}^T)^{-1}$ is the Kalman gain, which is well defined for an invertible $\Sigma_{m,t}$, see later Assumption 1.

**Remark 1.** *Note that for a diagonal measurement noise covariance $\Sigma_{m,t} = \sigma_{m,t}\mathbb{1}$, in the limit $\sigma_{m,t} \to \infty$, the gain is $K_t = 0$, thus the sensitivity is not updated, and we keep the initial sensitivity, i.e., $\hat{h}_t = \hat{h}_{t-1} = \cdots = \hat{h}_0$. Similarly, a large $\Sigma_{m,t}$ diminishes $K_t$, and helps to tune how fast we want to learn or differ from the initial sensitivity. On the other hand, the process noise covariance $\Sigma_{p,t}$ represents our trust in our current model, and it also helps to tune the learning rate.*

### 4.3.2 Persistently Exciting OFO

To learn the time-varying sensitivity $H_t$, we need to capture enough information via the measurement equation (4.8), i.e, we need to use different $\Delta u$ to explore different reactions $\Delta y$ and infer different elements of $H_t$ from them. This can be formalized via the persistency of excitation condition [BS85]: $\Delta u_t$ is persistently exciting if there exists a time span $T > 0$, such that for all $t > 0$, the matrix formed by columns $\Delta u_{t+i}$ for $i \in \{0, \dots, T\}$ has full rank, i.e., $\text{rank}(\Delta u_t, \dots, \Delta u_{t+T}) = n_u$. To achieve persistency of excitation, we perturb the OFO step (4.5) with $\omega_{u,t} \in \mathbb{R}^{n_u}$, a bounded zero-mean white noise with independent and identically distributed elements with standard deviation $\sigma_u$, e.g., a truncated Gaussian distribution. As a result, we obtain the following persistently

exciting OFO with estimated sensitivity $\hat{H}_t$:

$$u_{t+1} = \Pi_{\mathcal{U}_t}\Big[u_t - \alpha\Big(\nabla_u f(u_t) + \hat{H}_t^T \nabla_y g(y_t)\Big) + \omega_{u,t}\Big] \tag{4.10}$$

The resulting interconnected OFO, sensitivity learning and power grid is represented in the block diagram in Figure 4.1. At each time $t$, a complete loop of the online optimization with sensitivity estimation can be represented as:

**Algorithm 4.1** Online Feedback Optimization (OFO) with sensitivity estimation (blue block in Figure 4.1)

1: **Input:** $y_t$ (measured from the grid)
2: Recover from previous step: $y_{t-1}, u_{t-1}, u_t$
3: Sensitivity update using (4.9):
$K_{t-1} = \Sigma_{t-1} U_{\Delta,t-1}^T (\Sigma_{m,t-1} + U_{\Delta,t-1}\Sigma_{t-1}U_{\Delta,t-1}^T)^{-1}$ $\hat{h}_t = \hat{h}_{t-1} + K_{t-1}(\Delta y_{t-1} - U_{\Delta,t-1}\hat{h}_{t-1})$
$\Sigma_t = \Big(\mathbb{1} - K_{t-1}U_{\Delta,t-1}\Big)\Sigma_{t-1} + \Sigma_{p,t-1}$
4: Sample the excitation noise $\omega_{u,t} \sim \mathcal{N}(0, \sigma_u^2 \mathbb{1})$
5: Input optimization using (4.10):
$u_{t+1} = \Pi_{\mathcal{U}_t}\Big[u_t - \alpha\Big(\nabla_u f(u_t) + \hat{H}_t^T \nabla_y g(y_t)\Big) + \omega_{u,t}\Big]$
6: **Output:** $u_{t+1}$

**Remark 2.** *The sensitivity learning approach (4.9) is independent of the method used to update the input $u$, since it only requires the increment $\Delta u$ and the measured $\Delta y$. Hence, it is not only compatible with the projected-gradient-based OFO in (4.10), but can be combined with linearly simplified AC-OPF as (4.4), or other OFO approaches, e.g., primal-dual methods [DS16; Ort+20a], quadratic programming [Häb+20; Pic+22a], which may have other desirable properties, like strict constraint satisfaction or a faster convergence.*

### 4.3.3 Convergence Analysis

In this section we analyze the convergence of the estimated sensitivity $\hat{H}_t$ produced by the sensitivity learning (4.9), and the input $u_t$ produced by the OFO (4.10), towards the true sensitivity $H_t$ and the solution $u_t^*$ of the AC-OPF (4.2), respectively. We certify this convergence assuming that the true sensitivity $H_t$ behaves according to the simplified dynamic process (4.6) and satisfies the linear measurements equation (4.8); and that the projected gradient descent used in (4.10) is a strongly monotone and Lipschitz continuous operator:

**Definition 1** (Monotone and Lipschitz operator)**.** *An operator $F : \mathbb{R}^n \to \mathbb{R}^n$ is $\eta_F$-strongly monotone if $(x_1 - x_2)^T(F(x_1) - F(x_2)) \geq \eta_F \|x_1 - x_2\|_2^2$ for all $x_1, x_2$, and $L_F$-Lipschitz continuous if $\|F(x_1) - F(x_2)\|_2 \leq L_F \|x_1 - x_2\|_2$.*

**Assumption 1.** *The functions $f(\cdot)$ and $g(\cdot)$ in (4.2) are continuously differentiable. The sensitivity satisfies (4.6) and (4.8) with independent $\omega_{p,t}$ and $\omega_{m,t}$. Furthermore, for all $t > 0$, $\Sigma_{p,t}, \Sigma_{m,t}$ have a positive lower and upper bound, i.e., there exists $\gamma, \beta > 0$ such that $\gamma\mathbb{1} \preceq \Sigma_{p,t} \preceq \beta\mathbb{1}$, $\gamma\mathbb{1} \preceq \Sigma_{m,t} \preceq \beta\mathbb{1}$; there exists $L_h > 0$ such that $\|\nabla_y g(\hbar(u_t^*, d_t))\|_2 \leq L_h$; and the operator $F_t(\cdot) = \nabla_u f(\cdot) + H_t^T \nabla_y g(\hbar(\cdot, d_t))$ in (4.10) is $\eta$-strongly monotone and $L$-Lipschitz continuous.*

The continuous differentiability of $f(\cdot)$ and $g(\cdot)$ is common for typical cost functions in power systems, e.g., linear or quadratic $f(\cdot)$, and quadratic penalty functions like $g(\cdot) = \max(0, \cdot)^2$. For strongly convex and Lipschitz smooth cost functions $f(\cdot)$, the strong monotonicity and Lipschitz continuity of the gradient operator $F_t(\cdot)$ holds in certain regions around nominal operating points [CSB19]. In particular, it would hold if using a usual linear approximation for the input-output map (4.1) [PBD20]. Since $u$ and $d$ are restricted by the grid physical limits, e.g., power ratings, the upper bound of $\|\Delta u_t\|_2$ and $\|\nabla_y g(\hbar(u_t^*, d_t))\|_2$ are justified, since $g(\cdot)$ is differentiable in a compact set. The persistency of excitation ensures that $\|\Delta u_t\|_2 > 0$ with high probability. Then, $\Sigma_{p,t} = \Sigma_{p_1} + \Sigma_{p_2}\|\Delta u_t\|_2^2 \succ 0, \Sigma_{m,t} = \Sigma_{m_1} + \Sigma_{m_2}\|\Delta u_t\|_2^2 + \Sigma_{m_3}\|\Delta u_t\|_2^4 \succ 0$ if at least one $\Sigma_{p_i} \succ 0$ and one $\Sigma_{m_j} \succ 0$ for some $i, j$. Finally, even though the true sensitivity is state dependent, i.e., $H_t = \nabla_u \hbar(u_t, d_t)$, the process and measurement noises in (4.6) and (4.8) allow to overapproximate the actual behavior of the sensitivity via these simplifications. In conclusion, Assumption 1 is reasonable. Then, with a persistently exciting $\Delta u$ as in (4.10), we have the following convergence result:

**Proposition 1.** *Under Assumption 1, and the persistently excited OFO updates (4.10), the sensitivity estimates (4.9) satisfy:*

$$\begin{aligned} &\textit{Unbiased mean: } \|\mathbb{E}[h_t - \hat{h}_t]\|_2^2 \leq C_{h,1} e^{-C_{h,2} t} \overset{t\to\infty}{\to} 0 \\ &\textit{Bounded covariance: } \mathbb{E}[\|h_t - \hat{h}_t\|_2^2] = tr(\Sigma_t) \\ &\qquad\qquad \leq C_{h,3} + C_{h,4} e^{-C_{h,5} t} \to C_{h,3}, \end{aligned} \tag{4.11}$$

*where $\mathbb{E}[\cdot]$ denotes the expectation, $C_{h,i} > 0$ are positive constants, and $\overset{t\to\infty}{\to}$ the limit as $t$ goes to infinity. Furthermore, if the step size in (4.10) satisfies $\alpha < \frac{2\eta}{L^2}$, so that $\epsilon = \sqrt{1 - 2\eta\alpha + L^2\alpha^2} < 1$, then we have*

$$\begin{aligned} &\mathbb{E}[\|u_t - u_t^*\|_2] \\ \leq &\tfrac{1}{1-\epsilon}\Big(\sigma_u + \sup_{k<t} \mathbb{E}[\|\Delta u_k^*\|_2] + \sqrt{C_{h,3}}\alpha L_h\Big) \\ &+ \epsilon^t \mathbb{E}[\|u_0 - u_0^*\|_2] + \alpha L_h t \sqrt{C_{h,4}} \max(\epsilon, e^{\frac{-C_{h,5}}{2}})^{t-1} \\ \overset{t\to\infty}{\to} &\tfrac{1}{1-\epsilon}\Big(\sigma_u + \sup_{k} \mathbb{E}[\|\Delta u_k^*\|_2] + \sqrt{C_{h,3}}\alpha L_h\Big). \end{aligned} \tag{4.12}$$

*Proof.* See Appendix. □

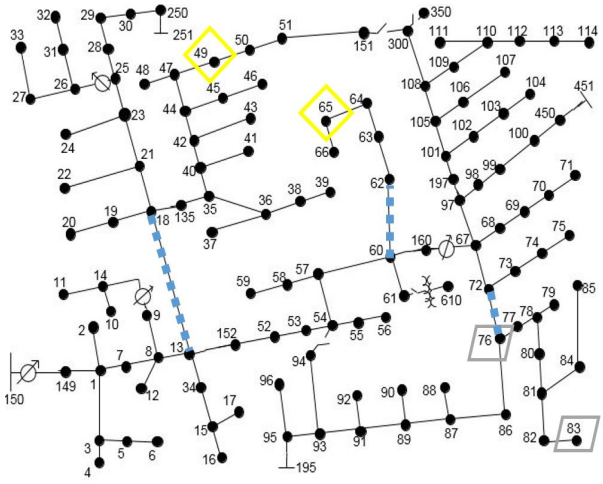

Figure 4.2: IEEE 123-bus test feeder [Ker91]. **Distributed generation:** yellow diamond = solar, grey parallelogram = wind. **Lines with perturbed electrical parameters:** blue square-dotted.

Proposition 1 establishes first that the estimated sensitivity $\hat{h}_t$ converges in expectation to the true sensitivity $h_t$ with a bounded covariance. Additionally, the control input $u_t$ converges to the AC-OPF solution $u_t^*$ from (4.2) with a quantifiable tracking error determined by the bound $C_{h,3}$ of the sensitivity estimation covariance, the variance $\sigma_u$ of the persistency of excitation noise $\omega_u$, and the temporal variation of the AC-OPF solution $\mathbb{E}[\|\Delta u_t^*\|_2^2]$, where $\Delta u_t^*$ can also be bounded by the temporal variation of $d_t$ and $\mathcal{U}_t$ in the AC-OPF (4.2) [SHD21].

## 4.4 Test Case

In this section we validate the proposed OFO with sensitivity estimation. We simulate a benchmark distribution grid under time-varying conditions during a 1-hour simulation with 1-second resolution, hence a 1 second control-loop rate. In particular, we show its superior performance against an OFO approach with a constant sensitivity. First we explain the simulation setup, and then we comment the results obtained.

### 4.4.1 Simulation Setup

- Distribution grid: We use the 3-phase, unbalanced IEEE 123-bus test feeder [Ker91] in Figure 4.2.
- Disturbance $d$: We consider uncontrollable active and reactive loads in our disturbance vector $d$. To generate these load profiles we use 1-second resolution data of the ECO data set [Bec+14], then aggregate households and rescale them to the base loads of

the 123-bus feeder. This gives us values of $d_t$ for every second during simulation time of 1h.

- Controllable input set-points $u$: We add two solar PV systems and two wind turbines to the grid as in [PBD20], see Figure 4.2. They can inject active power, and inject and absorb reactive power on all three phases, which gives us 24 control inputs. We consider a slack bus 150 in Figure 4.2, with a controllable voltage magnitude through, e.g., a tap changer, which makes in total $n_u = 25$. The solar and wind generation profiles are generated based on a 1-minute solar irradiation profile [Hel] and a 2-minute wind speed profile [MER]. Generation is assumed constant between samples. We use these profiles to set the time-varying upper limit of the feasible set $\overline{u}_t$, set the lower limit of active generation to $\underline{u}_t = 0$, and define $\mathcal{U}_t = \{u \,|\, \underline{u}_t \leq u \leq \overline{u}_t\}$.

- Output $y$: We consider as output $y$ the voltage magnitudes of all phases at all buses except the slack bus, given that it is a control input.

- AC-OPF cost function in (4.2): We use a quadratic cost that penalizes deviating from a reference: $f(u) = \frac{1}{2}\|u - u_{\text{ref}}\|_2^2$. The reference $u_{\text{ref}}$ for the voltage magnitude at the slack bus is 1 p.u. The reference for the controllable generation is the maximum installed power to promote using as much renewable energy as possible. The reference for reactive power is 0. Note that the cost function is continuously differentiable, and has a strongly monotone and Lipschitz continuous gradient as required in Assumption 1. We consider the voltage limits [0.94 p.u., 1.06 p.u.] for all nodes as in [Hau+17; PBD20], and use the penalty function $g(y) = \frac{\rho}{2} \max\left( \left[\begin{smallmatrix} \mathbb{1} \\ -\mathbb{1} \end{smallmatrix}\right] y + \left[\begin{smallmatrix} -1.06 \\ 0.94 \end{smallmatrix}\right], 0 \right)^2$, with a sufficiently large penalization parameter $\rho = 100$ to discourage violations. Again, this function is continuously differentiable, and has a monotone and Lipschitz continuous gradient.

- Sensitivity process and measurement noises in (4.6) and (4.8): Under fast sampling rates $\Delta d_t$ may be negligible, especially when compared to $\Delta u_t$. Hence, for the simulation we assign $\Sigma_{p_1}, \Sigma_{m_1}, \Sigma_{m_2}$ to 0, and keep $\Sigma_{p_2}, \Sigma_{m_3} \succ 0$. This ensures that $\Sigma_{p,t}, \Sigma_{m,t} \succ 0$ for all $t$, as required by Assumption 1.

- Persistency of excitation: We use a symmetric truncated Gaussian distribution with $\sigma_u = 0.0001$ p.u. to introduce a low persistency of excitation noise $\omega_{u,t}$ that facilitates our sensitivity learning, but avoids introducing a big deviation in the input convergence, see (4.12).

- Initializing sensitivity and linear model (4.3): We use the zero-injection operating point $u_{\text{op}} = 0, d_{\text{op}} = 0$ to initialize the sensitivity estimation, i.e., $\hat{H}_0 = H_0 = \nabla_u \hbar(u, d)|_{(0,0)}$, see (4.3). In the first simulation (1: true admittance) we use the true admittance to compute $H_0$, in the second (2: perturbed admittance) we use a

perturbed admittance matrix, where we have introduce an up to 20% error in the admittance of the lines indicated in Figure 4.2.

### 4.4.2 Results

We analyze the simulation performance of OFO with sensitivity learning (4.9) and (4.10), and compare it against an OFO with constant sensitivity (4.5). We validate both results in Proposition 1: First, the estimated sensitivity $\hat{H}_t$ converges to the real time-varying sensitivity $H_t$. Second, the input $u_t$ converges to the AC-OPF solution $u_t^*$ (4.2).

#### True admittance

First we perform a simulation where we use the true admittance to derive the initial sensitivity $H_0$ in the linear power flow approximation (4.3). Figure 4.3 shows the norm of the AC-OPF solution $u_t^*$ of (4.2) that we calculate with the correct non-linear model $\hbar(\cdot)$ and the disturbances $d_t$. This optimal input is time-varying due to the changing solar radiation and wind speed in the limits $\overline{u}_t$, and the temporal variation of the loads in $d_t$. Figure 4.3 shows how the OFO control input $u_t$ converges towards the optimal input $u_t^*$ using different sensitivities: The inputs $u_H$ produced by the OFO controller (4.5) with the exact sensitivity $H_t = \nabla\hbar(u_t, d_t)$ succeed in tracking the AC-OPF solution $u^*$, with relatively small differences caused by the time-varying disturbances $d_t$ and/or available energy $\overline{u}_t$. However, when using the constant sensitivity $H_0$ in (4.5), there is a large difference between the generated control input $u_{H_0}$ and the optimal one $u^*$. This gap is closed when using the OFO with sensitivity estimation (4.10), i.e., $u_{\hat{H}}$ is able to converge to the AC-OPF solution $u^*$ of (4.2) with a small tracking error, as predicted by Proposition 1.

Figure 4.4 shows the relative error $\frac{\|\Delta y - H\Delta u\|_2}{\|\Delta y\|_2}$ of the measurement equation (4.8). This helps to understand why OFO with sensitivity learning (4.9) performs better than with a constant sensitivity $H_0$: The linearization error with estimated sensitivity $\hat{H}_t$ gets lower respect to the one with $H_0$. This means that the learned sensitivity becomes a more accurate linear approximation than (4.3), which causes the lower optimization error observed in Figure 4.3. Even though the error $\frac{\|\Delta y - H\Delta u\|_2}{\|\Delta y\|_2}$ does not converge to 0 when using $\hat{H}$, the sensitivity estimation approach (4.9) learns enough to drive the control set-points to the optimum, see Figure 4.3, which is our ultimate objective.

Finally, Figure 4.5 shows that the inputs $u_{\hat{H}}$, produced by the OFO with sensitivity estimation (4.10) result into much less voltage violations than $u_{H_0}$ from the OFO with constant sensitivity (4.5). Actually, the number of voltage violations of $u_{\hat{H}}$ gets close to those of the OFO with true sensitivity $u_H$. Hence, the OFO with sensitivity estimation not only reduces the distance to the AC-OPF solution, see Figure 4.3, but performs a better voltage regulation.

### Perturbed admittance

In Figure 4.6 we show a simulation for which we perturb the admittance of the lines indicated in Figure 4.2 with an up to 20% error. We observe how the OFO with sensitivity learning $u_{\hat{H}}$ (4.10) is still able to track the AC-OPF solution $u^*$ of (4.2) in time-varying conditions. The OFO $u_{H_0}$ with a fixed sensitivity (4.5) and the same step size as $u_{\hat{H}}$ diverges, since it tries to regulate the voltage with a wrong sensitivity that is too far from the actual one. Convergence is recovered with a lower step size in $u_{H_0,\text{slow}}$, but it still performs poorly at tracking the AC-OPF solution. This experiment allows us to conclude that the OFO with sensitivity estimation (4.10) is a model-free approach that does not require an accurate model, but learns it online.

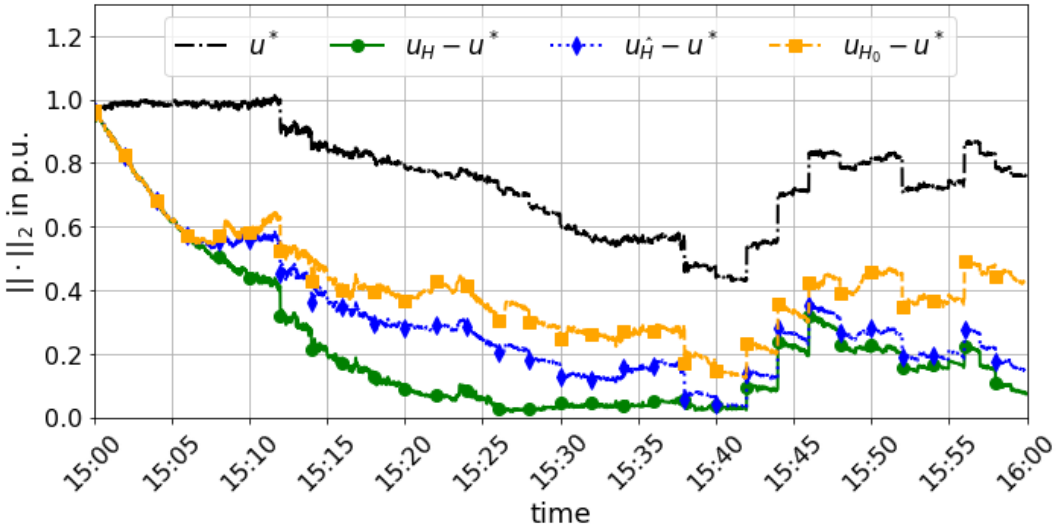


Figure 4.3: Euclidean norm of the AC-OPF solution $u_t^*$, and the optimization error between $u_t^*$ and the set-points $u_t$ produced by the OFO (4.5), using either the true sensitivity $H$ (green with dots), the estimated sensitivity $\hat{H}$ (blue with diamonds), the constant sensitivity at a zero-injection operation point $H_0$ (yellow with squares), with respective set-points $u_H, u_{\hat{H}}, u_{H_0}$.

## 4.5 Conclusion and Outlook

Standard Online Feedback Optimization (OFO) typically uses an approximate input-output sensitivity, which may lower its performance. Alternative, one can compute the actual sensitivity, but that requires, having an accurate grid model and full grid observability, which is usually not available. In this work we have proposed a recursive estimation approach that provides Online Feedback Optimization (OFO) with a tool to learn the model sensitivity without extensive measurements, and thus improves

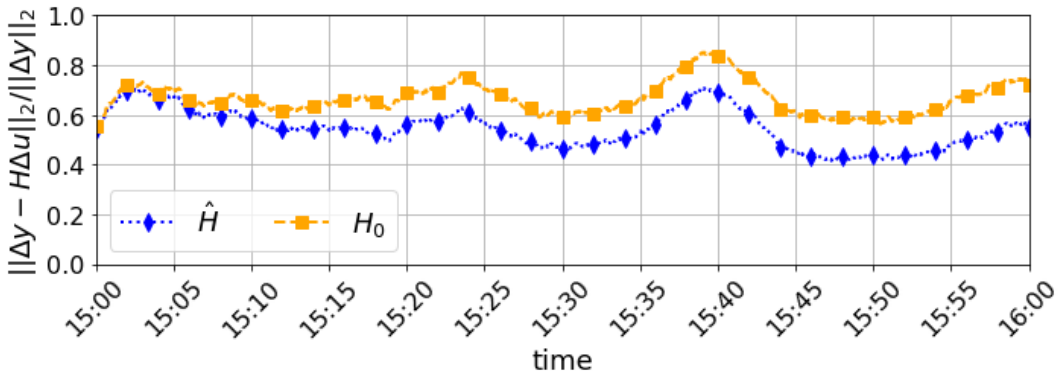


Figure 4.4: Moving average over 5 minutes of the relative error $\frac{\|\Delta y - H\Delta u\|_2}{\|\Delta y\|_2}$ when using the learned sensitivity $\hat{H}$ (blue with diamonds) or the one fixed at an zero-injection operation point $H_0$ (yellow with squares).

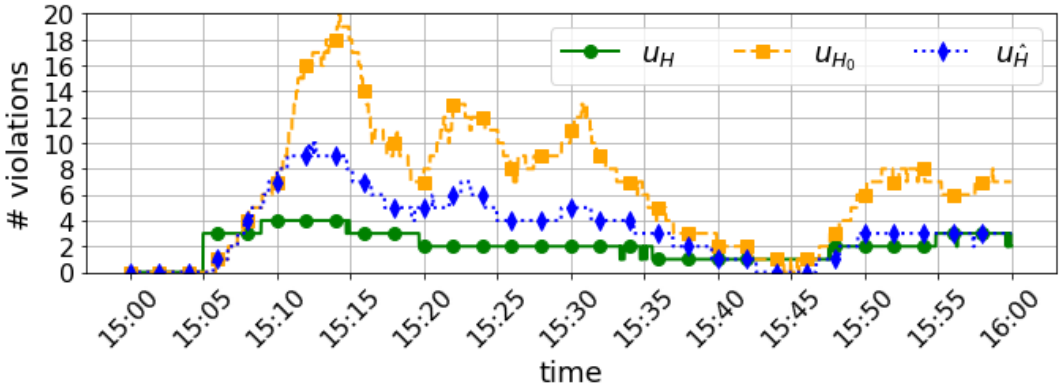


Figure 4.5: Moving average over 5 minutes of the number of voltage violations across all nodes.

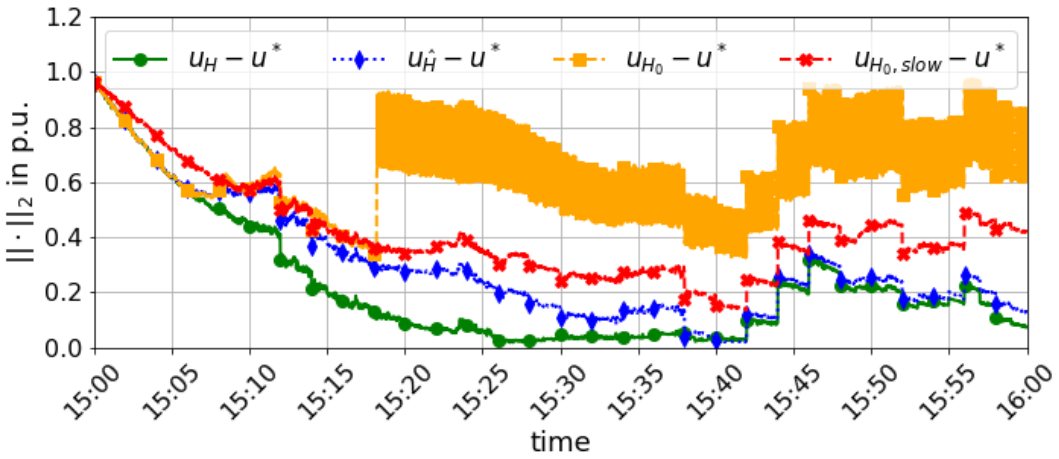


Figure 4.6: Same as Figure 4.3. For the constant sensitivity $H_0$, we plot $u_{H_0}$ (yellow) when using the same step size as $u_H, u_{\hat{H}}$, and $u_{H_0,\text{slow}}$ (red) with a smaller step size. Both $\hat{H}$ and $H_0$ are initialized with an perturbed admittance matrix $Y$.

its performance and turns OFO into a model-free approach. We have provided convergence guarantees when approximating the time-varying sensitivity behavior by a random process with linear measurements. We have established that even under time-varying conditions the estimated sensitivity and the control input converge to a neighborhood of the true sensitivity and the solution of the AC-OPF, respectively. Finally, we have validated with simulations using the IEEE 123-bus test feeder that our proposed OFO controller with sensitivity estimation performs successfully even though the actual sensitivity is state-dependent, i.e., it is able to track a time-varying optimal input while satisfying the grid specifications. In short, the proposed OFO controller with sensitivity estimation can be used as a model-free plug-and-play controller for real-time power grid operation that enables safe and optimal control.

An interesting future addition would be to investigate a more suitable way to design the persistency of excitation, possibly linked to the optimization problem, so that it explores specific directions of interest. Additionally, it would be interesting to observe how the proposed sensitivity estimation approach performs under a sudden change of topology caused by, e.g., a line fault, network split, etc.; under communication problems, e.g., delays, missing packages, recurrent outliers due to, for example, sensor misscalibration.

# Appendix: Proof of Proposition 1

Consider the information matrix $W_I = \sum_{k=t}^{t+T} U_{\Delta,k}^T \Sigma_{m,k}^{-1} U_{\Delta,k} = \sum_{k=t}^{t+T} (\Delta u_k \Delta u_k^T) \otimes \Sigma_{m,k}^{-1}$. Since $\gamma \mathbb{1} \preceq \Sigma_{m,t} \preceq \beta \mathbb{1}$ for all $t$, we have $\frac{1}{\beta}\mathbb{1} \preceq \Sigma_{m,t}^{-1} \preceq \frac{1}{\gamma}\mathbb{1}$, and $(\sum_{k=t}^{t+T} \Delta u_k \Delta u_k^T) \otimes \frac{1}{\beta}\mathbb{1} \preceq W_I \preceq (\sum_{k=t}^{t+T} \Delta u_k \Delta u_k^T) \otimes \frac{1}{\gamma}\mathbb{1}$. Since $\Delta u$ is persistently exciting, there exists a sufficiently

large $T$ and $\gamma_2, \beta_2 > 0$ so that $\gamma_2 \mathbb{1} \preceq \sum_{k=t}^{t+T} \Delta u_k \Delta u_k^T \preceq \beta_2 \mathbb{1}$, and thus $\frac{\gamma_2}{\beta}\mathbb{1} \preceq W_I \preceq \frac{\beta_2}{\gamma}\mathbb{1}$. Hence, the matrix pair $(\mathbb{1}, U_{\Delta,t})$ from the dynamic system (4.6) and (4.8) is uniformly completely observable, and, additionally, uniformly complete controllable given $\Sigma_{p,t} \succ 0$ [Jaz70, Ch. 7]. As a result, the sensitivity converges exponentially in expectation, and is exponentially bounded in mean square [Jaz70; TR76], i.e., there exists positive constants $C_{h,i} > 0$ satisfying (4.11).

Then, under Assumption 1 we have

$$
\begin{aligned}
&\|u_{t+1} - u_{t+1}^*\|_2 \leq \|u_{t+1} - u_t^*\|_2 + \|\Delta u_t^*\|_2 \\
\overset{(4.10)}{\leq} &\|\Pi_{\mathcal{U}_t}\Big[u_t - \alpha\Big(\nabla_u f(u_t) + \hat{H}_t^T \nabla_y g(y_t)\Big) + \omega_{u,t}\Big] \\
&- \Pi_{\mathcal{U}_t}\Big[u_t^* - \alpha F_t(u_t^*)\Big]\|_2 + \|\Delta u_t^*\|_2 \\
\leq &\|\Big(u_t - \alpha\Big(\nabla_u f(u_t) + \hat{H}_t^T \nabla_y g(y_t)\Big) + \omega_{u,t}\Big) \pm H_t \nabla_y g(y_t) \\
&- \Big(u_t^* - \alpha F_t(u_t^*)\Big)\|_2 + \|\Delta u_t^*\|_2 \\
\leq &\|\Big(u_t - \alpha F_t(u_t)\Big) - \Big(u_t^* - \alpha F_t(u_t^*)\Big)\|_2 + \|\omega_{u,t}\|_2 \\
&+ \alpha L_h \|h_t - \hat{h}_t\|_2 + \|\Delta u_t^*\|_2 \\
\leq &\epsilon \|u_t - u_t^*\|_2 + \|\omega_{u,t}\|_2 + \alpha L_h \|h_t - \hat{h}_t\|_2 + \|\Delta u_t^*\|_2,
\end{aligned}
$$

where in the second inequality we use that $u_t^*$ satisfies $u_t^* = \Pi_{\mathcal{U}_t}\Big[u_t^* - \alpha F_t(u_t^*)\Big]$, i.e., due to optimality $u_t^*$ is a fixed point of the operator (4.10) with $\omega_{u,t} = 0$ and the true sensitivity $H_t$ instead of the estimated one $\hat{H}_t$. In the fourth inequality, where $\epsilon^2 = 1 - 2\eta\alpha + L^2\alpha^2$, we use that the operator $F_t(\cdot)$ is $\eta$-strongly monotone and $L$-Lipschitz continuous. Hence, in expectation we have

$$
\begin{aligned}
&\mathbb{E}[\|u_{t+1} - u_{t+1}^*\|_2] \\
\leq &\epsilon \mathbb{E}[\|u_t - u_t^*\|_2] + \sigma_u + \mathbb{E}[\|\Delta u_t^*\|_2] + \alpha L_h \mathbb{E}[\|h_t - \hat{h}_t\|_2] \\
\leq &\epsilon^{t+1} \mathbb{E}[\|u_0 - u_0^*\|_2] + \tfrac{1}{1-\epsilon}\Big(\sigma_u + \sup_{k \leq t} \mathbb{E}[\|\Delta u_k^*\|_2]\Big) \\
&+ \alpha L_h \sum_{k=0}^{t} \epsilon^{t-k} \mathbb{E}[\|h_k - \hat{h}_k\|_2] \\
\overset{(4.11)}{\leq} &\epsilon^{t+1} \mathbb{E}[\|u_0 - u_0^*\|_2] \\
&+ \tfrac{1}{1-\epsilon}\Big(\sigma_u + \sup_{k \leq t} \mathbb{E}[\|\Delta u_k^*\|_2] + \sqrt{C_{h,3}} \alpha L_h\Big) \\
&+ \alpha L_h (t+1) \sqrt{C_{h,4}} \max(\epsilon, e^{\frac{-C_{h,5}}{2}})^t \\
\overset{t \to \infty}{\to} &\tfrac{1}{1-\epsilon}\Big(\sigma_u + \sup_{k} \mathbb{E}[\|\Delta u_k^*\|_2] + \sqrt{C_{h,3}} \alpha L_h\Big),
\end{aligned}
$$

where in the second inequality we apply the first one recursively. In the second and third inequality we bound the geometric series $\sum_{k=0}^{t} \epsilon^{t-k} \leq \frac{1}{1-\epsilon}$, and use that $\sqrt{\cdot}$ is subadditive.

CHAPTER 5

# Fully Distributed Peer-to-Peer Optimal Voltage Control with Minimal Model Requirements

This chapter describes how an Online Feedback Optimization (OFO) controller can be implemented in a distributed way using only peer-to-peer communication. The OFO controller is implemented on a laboratory distribution grid feeder and it is shown that the distributed implementation scales nicely with the number of controlled resources as long as the communication rate is high enough. Furthermore, the implemented controller preserves privacy because only Lagrangian multipliers are communicated.

## 5.1 Introduction

Future power distribution grids are expected to host a significant portion of the total generation capacity, for the most part from renewable energy sources like solar and micro-wind installations. Meanwhile, the deployment of a distributed electric mobility infrastructure will substantially increase the loading of this infrastructure. This transition will inevitably affect the operating regime of distribution feeders, and will increase the risk of both overvoltage and undervoltage contingencies. On the other hand, micro-generators and electric vehicle charging stations will offer unprecedented voltage control flexibility via their power inverters, offering a finely distributed network of reactive power compensators.

For the control of these reactive power compensators, a multitude of decentralized Volt/VAr feedback control strategies have been proposed (e.g., Volt/VAr droop control; cf. [Bol+19] for a literature review) and ultimately incorporated in many grid codes and standards [IEE; VDE18; Com16]. These strategies rely on the control architecture

This chapter is based on the publication [Ort+20b].

schematically represented in Figure 5.1, where each power inverter independently regulates its reactive power injection based on the voltage measurement performed at its point of connection, typically via a static update map

$$q_h(t+1) = f_h(v_h(t)).$$

The update map $f_h$ is usually the outcome of heuristic design procedures. In most cases the design is completely model-free (no grid information is used), although computational design approaches have also been proposed [KAH19].

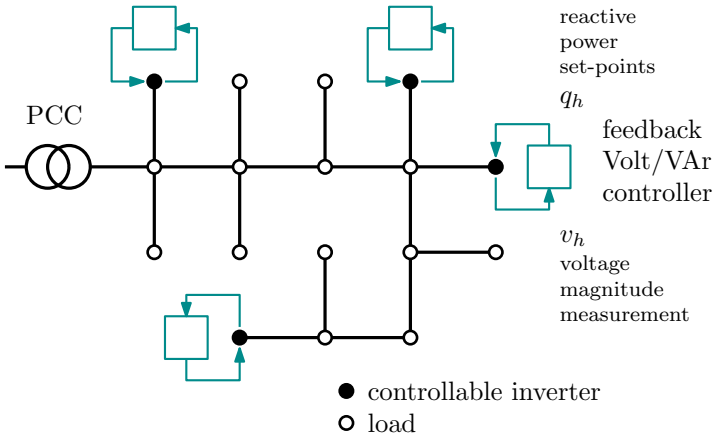


Figure 5.1: Schematic representation of the control architecture employed by fully decentralized Volt/VAr feedback strategies, e.g. [IEE; VDE18; Com16].

Fully decentralized feedback control solutions present multiple advantages, such as:

- high robustness, given by the absence of a single point of failure;
- economical deployment and retrofitting (plug-and-play);
- minimal actuation time delays, due to the absence of any communication;
- modularity and interoperability, as individual inverters do not coordinate their action;
- scalability and computational simplicity.

However, purely decentralized control strategies fail to ensure feasible voltages, even if such a feasible solution exists, as recently proven in [Bol+19]. Conversely, centralized feedback Volt/VAr solutions are guaranteed to drive the system to a feasible voltage profile, using the same measurements collected in the decentralized setting (i.e., only voltage magnitude measurements of the inverters) but processing them in a centralized manner. We refer to [Dör+19; BD19] for a recent review of Online Feedback Optimization methods that can be employed to design these centralized feedback Volt/VAr strategies, and

to [Ort+20a] for an experimental validation that demonstrates a remarkable robustness against model uncertainty.

This chapter is motivated by a fundamental question: is it possible to achieve optimal Volt/VAr regulation without collecting all measurement and all model information in a centralized location? A limited number of recent works contributed towards an answer to this question by proposing feedback control strategies that are extremely parsimonious in terms of information that inverters need to communicate:

- A distributed solution for the voltage regulation and loss minimization problem is proposed in [Bol+15], allowing asynchronous communication between agents (but relying on both angle and magnitude measurements).
- In [Oli+16], power inverters are controlled by individual automata that communicate a "distress signal" only when their regulation problem becomes infeasible; however, this strategy is not guaranteed to converge to the optimal regulation.
- In a similar spirit, [MFL19] proposes a distributed strategy in which inverters communicate only when triggered by local voltage violation rules; an all-to-all communication channel is however assumed.
- A primal-dual method that requires only communication between neighboring inverters is proposed in [QL19];
- The authors of [Mag+19] demonstrate how coordination between inverters can be achieved by only transmitting a few bits of information;
- a distributed dual ascent method is employed in [MQL20], allowing for delayed communication between inverters;
- finally, [Bol+19] proposes a distributed synchronous dual ascent method with a nested quadratic program.

To the best of the authors' knowledge, none of these distributed solutions has been implemented and tested on a real grid with physically distributed computations.

In this work, we provide a proof-of-concept demonstration of how Volt/VAr regulation can be achieved via a distributed feedback control law, namely under the specifications that:

- each inverter can only establish asynchronous peer-to-peer communication with its neighboring inverters;
- each inverter only maintains model information regarding its grid neighborhood;
- no central coordination unit is present.

The reported experiment also validates other important features of this distributed solution such as its robustness against noisy measurements, its real-time computational feasibility, and the viability of algorithm distribution in a peer-to-peer setting with no master algorithm synchronization.

Finally, we investigated scalability of the proposed approach via a series of numerical experiments.

## 5.2 Distributed Voltage Control

In this section we report the procedure proposed in [Bol+19] to design a distributed controller for the Volt/VAr regulation problem. Although a synchronous communication channel was assumed in [Bol+19], it provides the key idea on how to achieve optimal coordination via only short-range exchange of information.

### 5.2.1 Online Feedback Optimization Controller

The controller is derived from the optimization problem

$$\begin{aligned} \min \quad & \frac{1}{2} q^T M q \\ \text{subject to} \quad & v_{\min} \leq v_h(q, w) \leq v_{\max} \quad \forall h \\ & q_{\min} \leq q_h \leq q_{\max} \quad \forall h. \end{aligned} \tag{5.1}$$

where the matrix $M$ is a square, symmetric and positive definite design parameter and $v$ and $q$ are the vectors we obtain by stacking the voltages $v_h$ and reactive power set-points $q_h$ of the different inverters, respectively. The function $v_h(q, w)$ is the steady-state map of the nonlinear power flow equations that defines voltages $v_h$ as a function of both reactive powers $q$ and external influences $w$ (e.g., active and reactive demands, active generation).

Active power injections are not a decision variable in (5.1) for the following reason. Controlling the active power of devices comes with an economic cost, whereas the usage of reactive power is free (neglecting the active power losses generated by the reactive power flows). Therefore, it is typically preferred to use the reactive power capabilities in the network to their full extent before controlling active power injections.

To solve (5.1) we introduce the dual multipliers $\lambda_{h,\min}$ and $\lambda_{h,\max}$ for the voltage constraints of every inverter $h$. Stacking them gives us the vector $\lambda = \left[\begin{smallmatrix} \lambda_{\min} \\ \lambda_{\max} \end{smallmatrix}\right]$ with which

we form the Lagrangian $\mathbf{L}(q, \lambda)$ by dualizing the voltage constraints:

$$\begin{aligned}\mathbf{L}(q,\lambda) = \frac{1}{2} q^T M q + \sum_h \lambda_{h,\min}(v_{\min} - v_h(q,w)) \\ + \sum_h \lambda_{h,\max}(v_h(q,w) - v_{\max}).\end{aligned} \tag{5.2}$$

We thus define the equivalent dual optimization problem

$$\begin{aligned}\max_{\lambda \geq 0} \min_{q} \quad & \mathbf{L}(q,\lambda) \\ \text{subject to} \quad & q_{h,\min} \leq q_h \leq q_{h,\max} \quad \forall h.\end{aligned} \tag{5.3}$$

The optimization problems (5.1) and (5.3) have the same solution (Strong Duality Theorem, [Ber99, Proposition 5.3.2]).[1] We adopt an iterative dual ascent update on $\lambda$ to compute the solution of (5.3), obtaining

$$\begin{aligned}\lambda_{\min}(t+1) &= [\lambda_{\min}(t) + \alpha \nabla_{\lambda_{\min}} \mathbf{L}(q(t), \lambda(t))]_{\geq 0} \\ &= [\lambda_{\min}(t) + \alpha(v_{\min} - v(q(t), w))]_{\geq 0} \\ \lambda_{\max}(t+1) &= [\lambda_{\max}(t) + \alpha \nabla_{\lambda_{\max}} \mathbf{L}(q(t), \lambda(t))]_{\geq 0} \\ &= [\lambda_{\max}(t) + \alpha(v(q(t), w) - v_{\max})]_{\geq 0}.\end{aligned} \tag{5.4}$$

As we can see every inverter integrates its own voltage violation with a gain of $\alpha$. This corresponds to the integral part of a PI-controller and can be done locally, by using feedback from the physical system through voltage magnitude measurements $v(t)$ of the inverters, rather then via a numerical evaluation of $v(q(t), w)$. To find the optimal reactive power set-points we use the newly calculated $\lambda(t+1)$ and solve

$$\begin{aligned}q(t+1) = \quad \arg\min_{q} \quad & \mathbf{L}(q, \lambda(t+1)) \\ \text{subject to} \quad & q_{h,\min} \leq q_h \leq q_{h,\max} \quad \forall h.\end{aligned} \tag{5.5}$$

Towards this goal, we introduce the approximation

$$\frac{\partial v(q,w)}{\partial q} \approx X \tag{5.6}$$

where $X$ is the reduced bus reactance matrix that can be derived from the grid topology and the cable data. The sensitivity described by $X$ is similar to power transfer distribution factors for active power generation on the transmission level. Under no-load conditions and the assumption of negligible cable resistances this approximation is

[1] This holds true if $\mathcal{U}$ is convex, and $f(u)$ and $g(h(u,y))$ are convex over $\mathcal{U}$. Convexity of $f(u)$ can be guaranteed as it is chosen by the designer and $\mathcal{U}$ usually describes box constraints which renders $\mathcal{U}$ convex. Convexity of $g(y) = g(h(u,w))$ is not guaranteed, even for convex $g(\cdot)$, when $h(u,w)$ is non-linear. However, convexity of $g(h(u,w))$ is only required over $\mathcal{U}$ and at least power systems tend to be reasonably linear within the bounds of the available actuation capacity $\mathcal{U}$.

accurate, because the nonlinearity of the power flow equations is mild near this operating point [BD15]. In our application the system can be heavily loaded and the cable resistances are high. It was shown in [Ort+20a] that Online Feedback Optimization is sufficiently robust against this model mismatch.

This approximation makes $v(q, w)$ linearly dependent on $q$, and we can approximate (5.5) with a convex quadratic optimization problem (QP). This QP involves the decision variables of all DERs and can be solved by collecting all the necessary information (the multipliers $\lambda(t+1)$ and the parameters $X$) in a central control unit [Ort+20a]. In the following we use the idea proposed in [Bol+19] to show how (5.5) can also be solved in a distributed manner, without centralized computation or centralized model knowledge.

### 5.2.2 Distributing the Controller

To solve the subproblem (5.5) in a distributed manner we perform $K$ iterative steps, which will have to be executed between the times $t$ and $t+1$. To denote these iterative steps we introduce a new iteration counter $\tau$. We also introduce the dual multipliers $\mu_{h,\min}$ and $\mu_{h,\max}$ for the reactive power constraints of every inverter $h$, which we stack in the vector $\mu = \left[\begin{smallmatrix}\mu_{\min}\\ \mu_{\max}\end{smallmatrix}\right]$. By dualizing the reactive power constraints, we define the Langrangian

$$\begin{aligned}\mathbf{L}_\lambda(q,\mu) = \mathbf{L}(q,\lambda) &+ \sum_h \mu_{h,\min}(q_{\min} - q_h) \\ &+ \sum_h \mu_{h,\max}(q_h - q_{\max})\end{aligned} \tag{5.7}$$

and the following optimization problem:

$$\max_{\mu\geq 0} \min_q \quad \mathbf{L}_\lambda(q,\mu). \tag{5.8}$$

The optimization problems (5.5) and (5.8) have the same solution (Strong Duality Theorem, [Ber99, Proposition 5.3.2]). Similarly as before, we solve this optimization problem via gradient ascent iterations on $\mu$ with step size $\gamma$:

$$\begin{aligned}\mu_{\min}(\tau+1) &= [\mu_{\min}(\tau) + \gamma\nabla_{\mu_{\min}}\mathbf{L}_\lambda(\hat{q}(\tau),\mu(\tau))]_{\geq 0} \\ &= [\mu_{\min}(\tau) + \gamma(q_{\min} - \hat{q}(\tau))]_{\geq 0} \\ \mu_{\max}(\tau+1) &= [\mu_{\max}(\tau) + \gamma\nabla_{\mu_{\max}}\mathbf{L}_\lambda(\hat{q}(\tau),\mu(\tau))]_{\geq 0} \\ &= [\mu_{\max}(\tau) + \gamma(\hat{q}(\tau) - q_{\max})]_{\geq 0}\end{aligned} \tag{5.9}$$

where

$$\hat{q}(\tau) = \arg\min_q \mathbf{L}_\lambda(q,\mu(\tau)).$$

Observe, that the update of $\mu_{\min}$ and $\mu_{\max}$ can be done locally by every inverter by integrating the constraint violation of the virtual quantity $\hat{q}(\tau)$. In order to compute the

unconstrained minimizer $\hat{q}(\tau)$, we take the derivative $\nabla_q \mathbf{L}_\lambda(q, \mu)$ and obtain

$$\nabla_q \mathbf{L}_\lambda(q, \mu) = Mq + \frac{\partial v}{\partial q}(\lambda_{\max} - \lambda_{\min}) + \mu_{\max} - \mu_{\min}. \tag{5.10}$$

As stated before, we approximate the derivative $\partial v / \partial q$ with $X$ and set (5.10) to 0. We then solve for $q$ and obtain

$$\begin{aligned} \hat{q}(\tau) = &-M^{-1}X(\lambda_{\max} - \lambda_{\min}) \\ &+ M^{-1}[\mu_{\max}(\tau) - \mu_{\min}(\tau)]. \end{aligned} \tag{5.11}$$

Equation (5.11) reveals that all the communication requirements of the proposed iterative algorithm are encoded in the sparsity of the matrices $M^{-1}$ and $M^{-1}X$. In fact, off-diagonal non-zero elements of these two matrices determine components of $\lambda$ and $\mu$ that need to be communicated between inverters in order to compute $\hat{q}(\tau)$.

In order to maximize the sparsity of both these matrices, we exploit the structure inherited from the physical system. We inherit the formal definition of neighboring inverters from [Bol+15], see Figure 5.2. Neighbors according to this definition can be conveniently discovered via correlation analysis of the voltage measurements, even without central supervision (see [Bol18; DC18] and references therein).

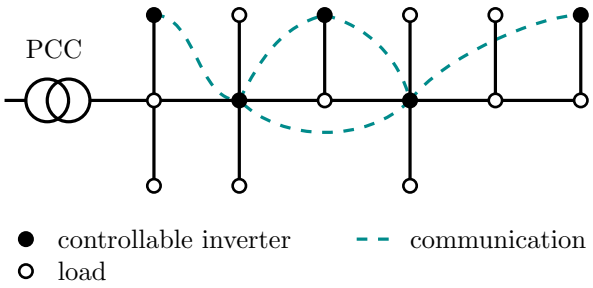


Figure 5.2: Schematic representation of neighbor-to-neighbor communication, where we adopt the definition of neighbors from [Bol+15]: two inverters are neighbors if the electrical path connecting them does not pass through any other bus where a controlled inverter is connected.

Due to the sparsity of the power flow equations, $G = X^{-1}$ is a sparse matrix: namely, $G_{ij}$ of $G$ is non-zero only if the buses $i$ and $j$ are neighbors, and $G_{ij}$ depends only on the electrical impedance of the path between $i$ and $j$.

Based on this observation, we choose $M = X$ which yields

$$\hat{q}(\tau) = \lambda_{\min} - \lambda_{\max} + G\left(\mu_{\min}(\tau) - \mu_{\max}(\tau)\right). \tag{5.12}$$

Therefore inverter $i$ only needs to gather $\mu_{j,\min}$ and $\mu_{j,\max}$ from their neighbors $j$ to calculate $\hat{q}_i(\tau)$. Note that $M = X$ is possibly not the only choice that allows to distribute

the algorithm, if one accepts to use a descent direction in the gradient steps which is not the steepest one [Dör+19, Section III.F]. With a proper choice of the gain $\gamma$ (for which we refer to Section 5.5) the alternate execution of (5.9) and (5.12) is guaranteed to converge to the solution to (5.8). We assume that the number of iterations $K$ is chosen sufficiently large so that, after $K$ iterations, $\hat{q}$ is accepted as the solution to (5.5) and determines the next set-point $q(t+1)$. The effect of this approximation is also studied in Section 5.5.

The resulting control algorithm consists in a main loop, reported hereafter as Algorithm 5.1, and a nested iterative procedure, Algorithm 5.2. Communication between agents only happens as part of Algorithm 5.2, when the dual multipliers $\mu$ of the reactive power constraints need to be communicated with neighbors (steps 7–8). All other steps are basic numerical operations that each inverter performs locally. The resulting control architecture is represented in Figure 5.3.

Note that the implementation of our controller inherits the theoretical guarantees provided in [Bol+19], including Proposition 6 that guarantees asymptotic optimality (under the linearity condition (5.6) and assuming that (5.5) is solved exactly).

**Algorithm 5.1** Online Feedback Optimization controller

1: Initialize: $\lambda_{h,\min}$ and $\lambda_{h,\max}$ with 0
2: **loop**
3: Locally measure the voltage magnitude $v_h$
4: Locally update $\lambda_{h,\min}$ and $\lambda_{h,\max}$ via (5.4)
5: Jointly compute $q_h$ via Algorithm 5.2
6: Locally apply the new set-point $q_h$
7: Wait until next system interrupt
8: ▷ System interrupts generated every $T$ seconds

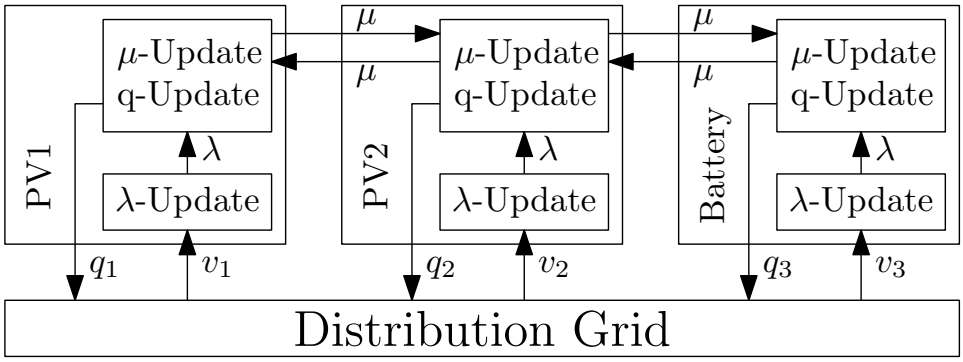


Figure 5.3: Control architecture. Measurement and actuation is performed locally by each controller. Only the dual multipliers $\mu_{\min}$ and $\mu_{\max}$ need to be communicated to neighboring peers.

**Algorithm 5.2** Distributed QP solver

1: **if** Algorithm 5.2 was never executed previously **then**
2: Initialize: $\mu_{h,\min}$, $\mu_{h,\max}$ and $\hat{q}_h$ with 0
3: **else**
4: Keep previous values to warm start
5: counter = 0 ▷ Iteration counter
6: **repeat**
7: Locally update $\mu_{h,\min}$ and $\mu_{h,\max}$ via (5.9)
8: Send $\mu_{h,\min}$ and $\mu_{h,\max}$ to neighbors
9: Receive $\mu_{i,\min}$ and $\mu_{i,\max}$ from all neighbors
10: Locally, compute $\hat{q}_h$ via (5.12)
11: counter = counter + 1
12: **until** counter == K
13: Return the solution $q_h = \hat{q}_h$

## 5.3 Experimental Setup

The experiment has been implemented in the SYSLAB facility located on the Risø campus of the Technical University of Denmark. The setup consists of a 400 $V$ three-phase electric grid connecting a variety of DERs (solar panels, wind turbines, a flow battery, a diesel generator, controllable loads, among others). Each device has an associated computer node running a distributed monitoring and control platform.

### 5.3.1 Algorithm Implementation and Deployment

An existing distributed optimization framework developed at DTU [Sem19] was adopted to implement the proposed distributed optimization controllers over an asynchronous communication channel. Each computer node implements Algorithm 5.1 in major fixed time intervals of $T = 10$ seconds, based on their individual clock. This is therefore the rate at which measurements are collected (line 3) and the system is actuated (line 6). The choice of such a long interval is due to hardware constraints given by the laboratory setup. A more frequent actuation is often possible. However, the actuation interval should be long enough for the system to settle and reach its steady state. The frequency at which the system can be actuated will always be significantly lower than the rate at which inverters can communicate (see Section 5.5 for a discussion on the implications on the algorithm scalability).

Algorithm 5.2 is executed in K iterations. Lines 7 and 8 of this algorithm require communication between neighbours, where the communication time is variable, dependent on uncontrollable influences. Coherency of the algorithm, and thereby a synchronous

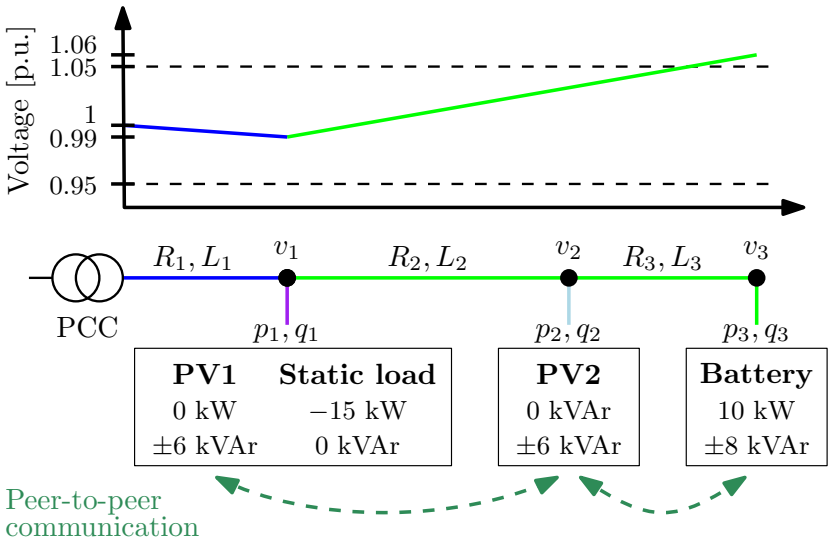


Figure 5.4: Sketch of the voltage profile, the distribution feeder and the peer-to-peer communication. The colors of the voltage profile and the diagram match the colors in the topology in Figure 5.5.

advancement of the algorithm steps, is achieved by letting individual nodes remain idle until data has been received from all neighbours (line 8 of Algorithm 5.2). This way, the synchronous Algorithm 5.2 is transparently implemented on an asynchronous communication channel, which has better scaling properties than a synchronous one in such a setup [Sem19]. ZeroMQ [Hin13] is used as the underlying messaging library with TCP transport, facilitating reliable data delivery. The code comprising the distributed framework and algorithm is deployed to each of the active SYSLAB node computers and operates as a local process.

### 5.3.2 Test Case and Experiment Design

The topology and operational set-points are designed to produce a voltage drop at the beginning and an overvoltage at the end of the feeder. Without proper reactive power control, the feeder's ability to host renewable energy infeed is limited and generation would need to be curtailed. The setup consists of the flow battery, two photovoltaic arrays (PV), an adjustable resistive load, and a utility grid connection (PCC). This test system is illustrated in Figure 5.4, and Figure 5.5 presents the corresponding implementation on the SYSLAB topology view.

The active power injection $p_3$ of the battery is interpreted as a renewable source, which is not to be curtailed; its active power infeed is set to $p_3 = 10$ kW. The static load is set to an active power consumption of 15 kW ($p_1 = -15$ kW) which is larger than the local production, therefore causing a positive active power flow from the substation. PVs

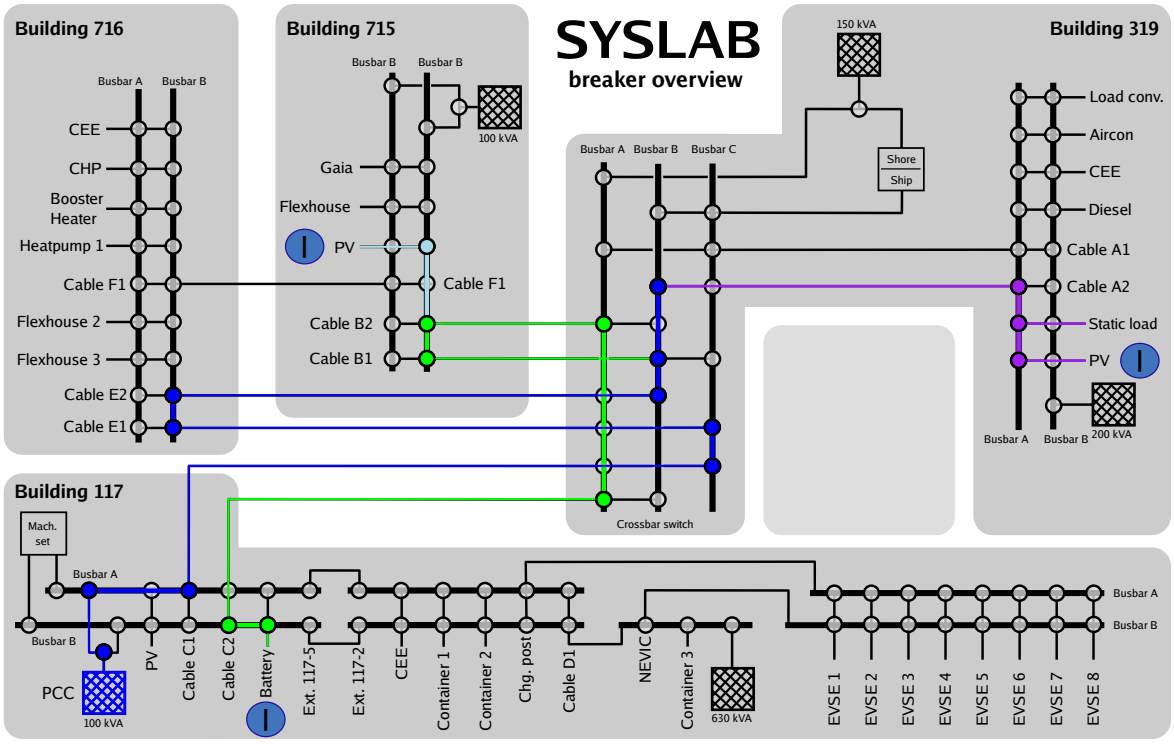


Figure 5.5: SYSLAB infrastructure with the used topology. The colors match the colors in the diagram and in the voltage profile in Figure 5.4. Inverters participating in the control algorithm are marked with an I.

are fluctuating power sources. Therefore, to facilitate repeatability of the experiments and to allow for a comparison between different controllers, the PVs are curtailed to not inject active power ($p_2 = 0$ kW). The different nodes are connected via cables with non-negligible resistance, see Table 5.1. Due to a weak link (resistive) cable connecting the battery to the grid, the battery encounters an overvoltage when the reactive power injection is zero. Both PVs and the battery can measure their voltage magnitudes, and their reactive power injections can be controlled. The PV inverters have a reactive power range of ±6 kVAr and the battery can be actuated with ±8 kVAr. The PVs and the battery can communicate with their neighbors, while the load is uncontrolled and unmeasured. The voltage limits are defined to be 0.95 p.u. and 1.05 p.u.

## 5.4 Experimental Results

In this section, we first demonstrate the suboptimal performance of a decentralized (purely local) controller on the proposed system, by implementing the droop control recommended by the IEEE standard [IEE]. We then execute the proposed distributed controller, evaluate its control performance, examine the nested execution of Algorithm 5.2,

Table 5.1: Parameters of the cables between busbars/devices.

| | Cable | Length [m] | Cross section [mm$^2$] | R [Ω] | X [Ω] |
|---|---|---|---|---|---|
| | C1 | 700 | 240 | 0.085 | 0.054 |
| | E1 | 450 | 240 | 0.055 | 0.035 |
| | E2 | 450 | 240 | 0.055 | 0.035 |
| | A2 | 25 | 95 | 0.0078 | 0.002 |
| | PV1 | 83 | 16 | 0.095 | 0.007 |
| | Static Load | 11 | 95 | 0.002 | 0.001 |
| | B1 | 350 | 95 | 0.11 | 0.027 |
| | PV2 | 8 | 6 | 0.025 | 0.0008 |
| | B2 | 350 | 95 | 0.11 | 0.027 |
| | C2 | 700 | 240 | 0.085 | 0.054 |
| | Battery | 100 | 2.5 | 0.774 | 0.012 |

hint at a windup phenomenon in case of problem infeasibility, and analyze the trade-off between control performance and communication complexity.

### 5.4.1 Local Control

The droop controller that we implement is the one proposed in [IEE] and similar to the ones suggested in the recent grid codes [VDE18; Com16]. Every inverter implements the following piecewise linear control law.

$$q_h = \begin{cases} q_{\max} & v_h < v_1 \\ q_{\max}\dfrac{v_2 - v_h}{v_2 - v_1} & v_1 \le v_h \le v_2 \\ 0 & v_2 \le v_h \le v_3 \\ q_{\min}\dfrac{v_h - v_3}{v_4 - v_3} & v_3 \le v_h \le v_4 \\ q_{\min} & v_4 < v_h \end{cases}$$

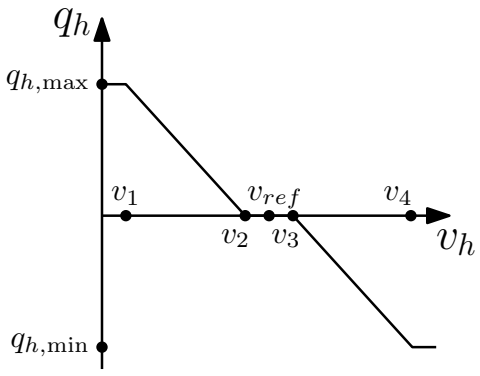


where $v_h$ is the measured voltage magnitude, $q_h$ is the calculated reactive power injection, $q_{\min}$ and $q_{\max}$ are the minimum and maximum reactive power injection. We tune the droop curve to $v_1 = 0.95$ p.u., $v_2 = 0.99$ p.u., $v_3 = 1.01$ p.u. and $v_4 = 1.05$ p.u..

The resulting performance of the controller is reported in Figure 5.6. When the control is activates at minute 3, only the controller at the battery detects a voltage violation and immediately lowers its reactive power injection to the minimum. However, this is not

sufficient to regulate the voltage to the desired voltage range. The PV systems do not detect an overvoltage and therefore do not draw reactive power. Without introducing coordination between the inverters, the persistent overvoltage at the battery cannot be prevented. Therefore, all local control strategies fail in this setup, as established from a theoretical perspective in [Bol+19].

Figure 5.6 also shows that PV1 injects reactive power around minute 4 of the experiment. This worsens the overvoltage at the battery, which shows that local control decisions can in some cases be even detrimental.

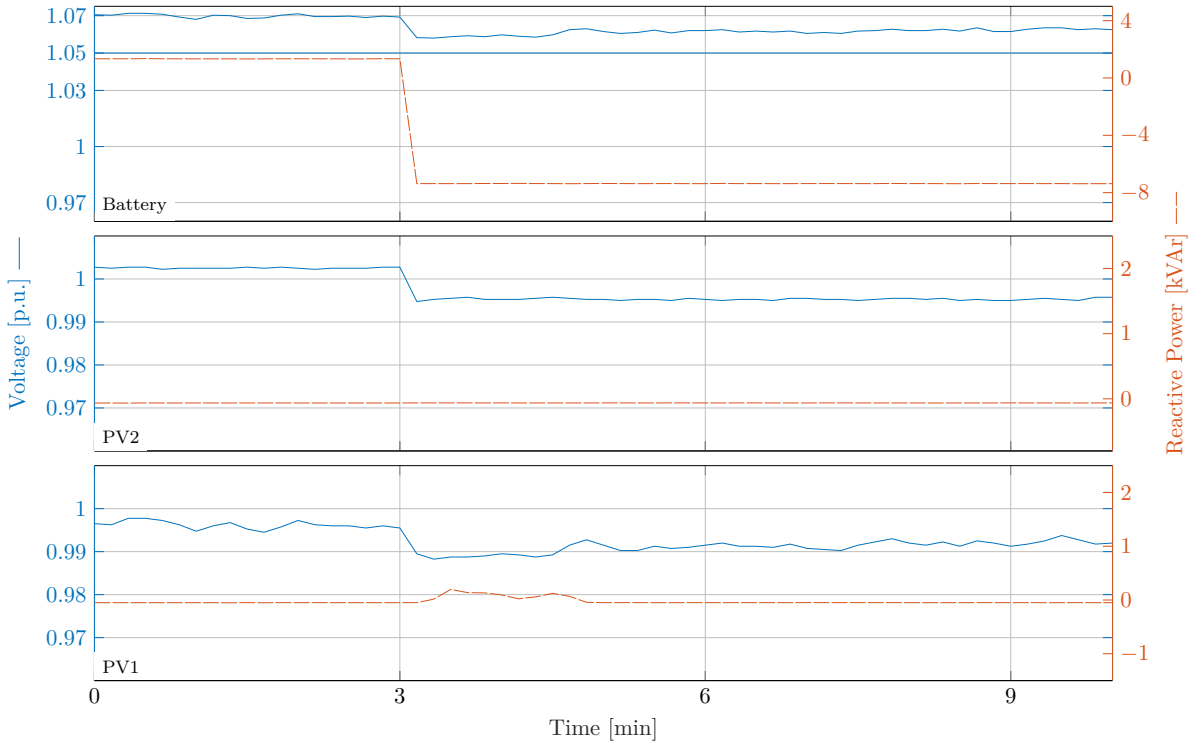


Figure 5.6: Performance of local droop control (IEEE 1547 standard).

### 5.4.2 Controller Evaluation

Figure 5.7 shows the performance of the distributed voltage controller with a gain of $\alpha = 100$, $K = 100$ communication steps to distributively solve the QP, an ascent step length of $\gamma = 0.005$ and with matrices $M = X$ and $G = X^{-1}$:

$$X = \begin{bmatrix} 0.10 & 0.09 & 0.09 \\ 0.09 & 0.11 & 0.11 \\ 0.09 & 0.11 & 0.16 \end{bmatrix}, \quad G = \begin{bmatrix} 48.3 & -40.7 & 0 \\ -40.7 & 61.8 & -18.7 \\ 0 & -18.7 & 19.1 \end{bmatrix}.$$

Cable data have been used to compute the matrix $G$, although the necessary parameters could also be estimated (see [Pro+16] for an experimental demostration on the same

network). Notice that, as expected, the matrix $G$ has the sparsity pattern induced by the topology of the distribution grid (zero elements in the positions corresponding to non-neighbors). The system is initialized with zero reactive power flow.[2] The controller is activated after 3 minutes and drives all voltages to the desired range. After 11 minutes the active power of the battery, which produces the overvoltage, is brought to 0 kW. The algorithm promptly responds by bringing the reactive power injections of all the power inverters to 0 kVAr.

For a more in-depth analysis of the control behavior we provide the data in Figure 5.8 for a controller with $\alpha = 50$ and $K = 50$. We report both the electrical quantities $v$ and $q$ and the controllers' internal variables $\lambda_{\max}$ and $\mu_{\min}$ ($\lambda_{\min}$ and $\mu_{\max}$ remain zero in this experiment). Once the controller is activated at 3 minutes, the voltage violation leads to a growing $\lambda_{3,\max}$ at the battery. As this integral variable grows, the battery starts drawing reactive power. Once the reactive power $q_3$ of the battery reaches the battery's reactive power limit, the corresponding multiplier $\mu_{3,\min}$ starts growing. At each iteration of Algorithm 5.2, this value is communicated to PV2. Ultimately, PV2 starts drawing reactive power as well (thus participating to the voltage regulation task). Once the reactive power limit of PV2 is reached, its $\mu_{2,\min}$ value becomes positive and PV1 starts to draw reactive power. As long as there remains an overvoltage at the battery, the battery keeps integrating its $\lambda_{3,\max}$, which leads to a larger reactive power demand by the inverter that is closer to battery and is not yet saturated. Finally, the voltage converges to the voltage constraint. Once that point is reached the system has settled (not fully represented in Figure 5.8). Three remarks are due.

- There is no central clock signal and the different inverters time their iterations of Algorithm 5.1 independently. Measurements are therefore not perfectly synchronous. We do not observe any detrimental effect in the experiment.
- Each controller gathers raw voltage measurements. No filtering or state estimation is performed (which, in general, would require a system model and further exchange of information). The control performance seems to be unaffected by measurement noise and quantization.
- With a smaller actuation interval (smaller T) and therefore more frequent control actuations the settling time of the algorithm can be reduced.

### 5.4.3 Convergence of Algorithm 5.2

In Figure 5.9, we can see how the internal variables $\hat{q}$ of the three inverters converge during the execution of Algorithm 5.2. The algorithm is started as soon as the multipliers

[2]Due to an inaccuracy of the sensor used by the internal reactive power controller of the battery, we can observe a small tracking error. The reported measurements in the figures are from accurate sensors.

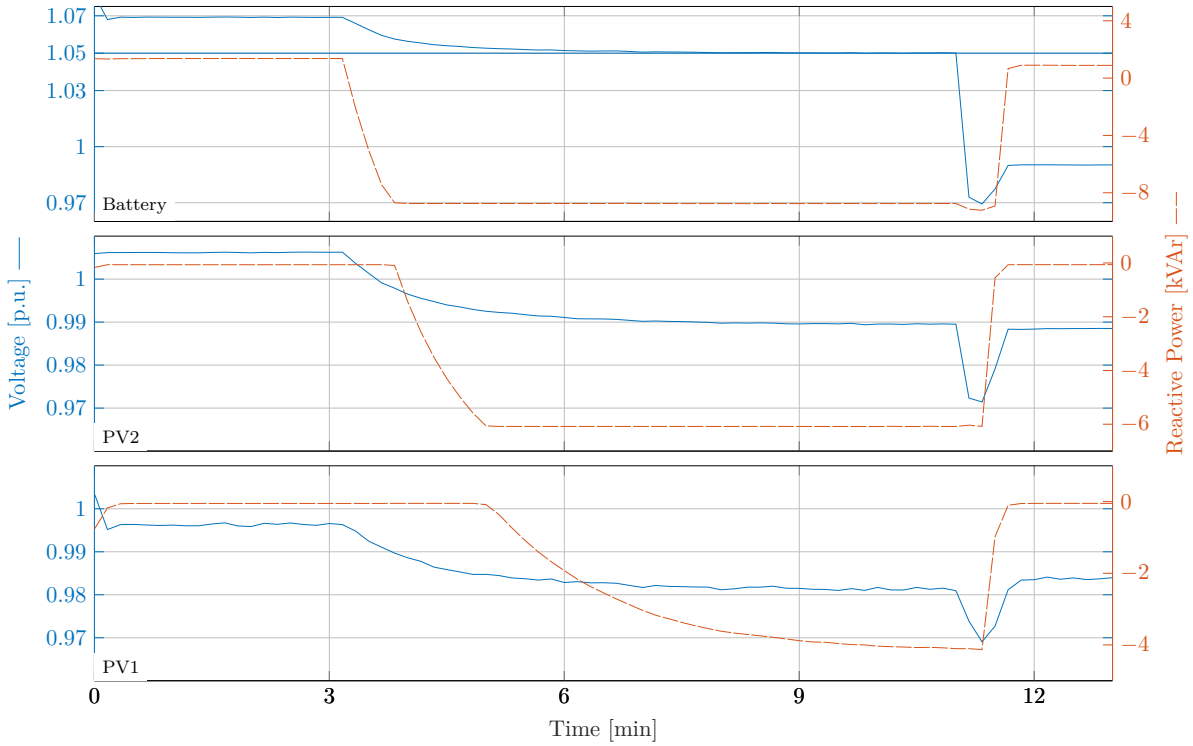


Figure 5.7: Performance of the distributed voltage controller, $\alpha = 100$.

$\lambda_{\max}$ are updated with the measured voltage violation. Agents update their internal variable $\hat{q}_h$ (orange dots in Figure 5.9) and their multipliers $\mu_{h,\min}, \mu_{h,\max}$ (not represented) while communicating with their neighbors at each iteration. After $K$ iterations, the internal value $\hat{q}$ is used to actuate the system by updating the reactive power set-points for the inverters (blue line). A few remarks are due:

- due to the warm start of the algorithm and the relatively small changes in $\lambda_{\max}$, the initialization of $\hat{q}$ is already close to the final (optimal) value;
- $K = 40$ iterations suffice for the convergence of Algorithm 5.2 in this experiment (see Section 5.5 for further discussion on the effect of early termination of Algorithm 5.2);
- the time needed to complete Algorithm 5.2 is significantly shorter than the sampling rate of Algorithm 5.1 (10 s).

### 5.4.4 Controller Windup

Figure 5.10 illustrates the behavior of the proposed scheme when the Volt/VAr regulation problem is temporarily unfeasible. A persistent overvoltage at the battery leads to a

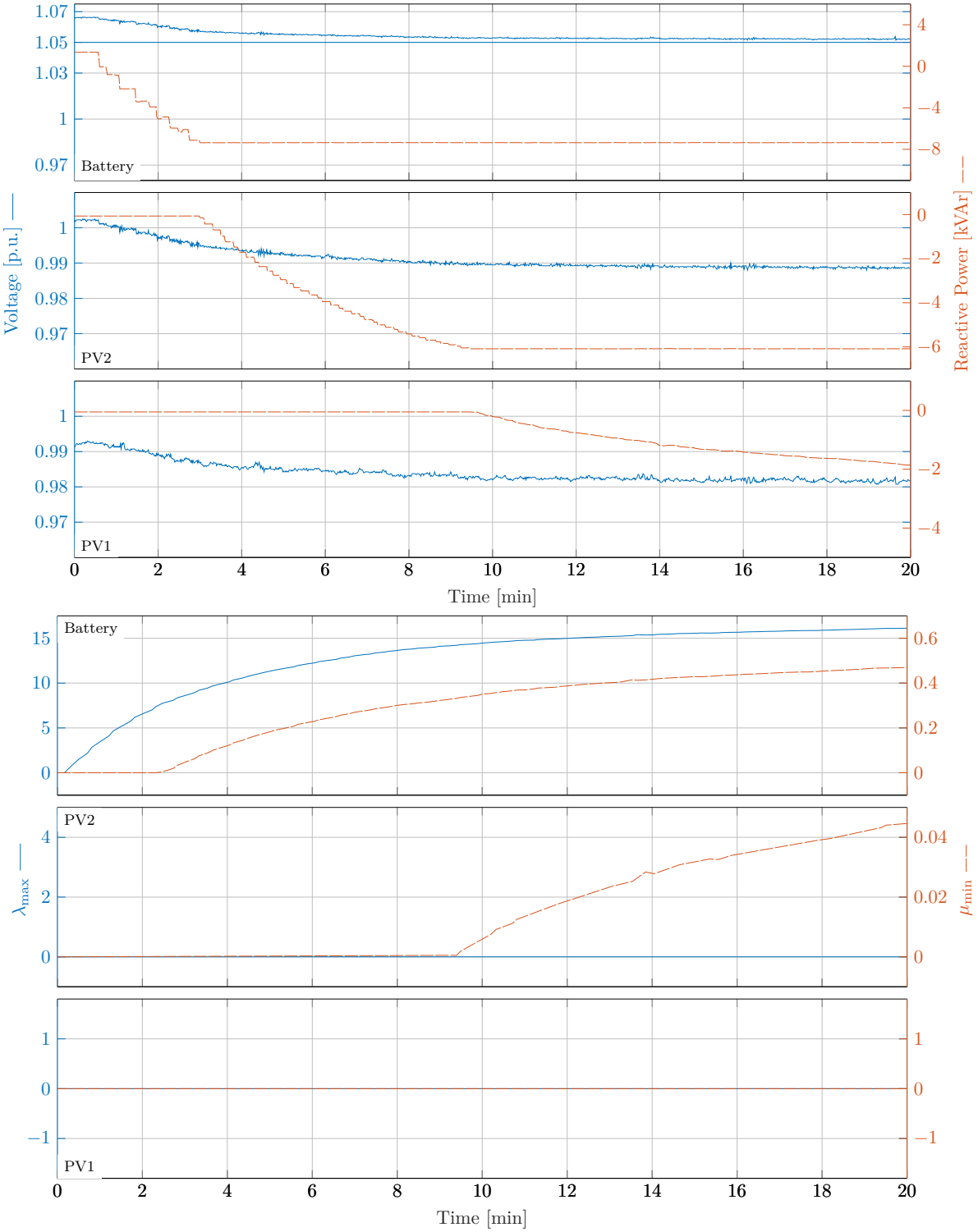


Figure 5.8: Behavior of the distributed controller with control gain $\alpha = 50$. Upper panels: electrical quantities $v, q$. Lower panel: dual multipliers $\lambda_{\max}$ and $\mu_{\min}$ (evaluated at the last step of Algorithm 5.2).

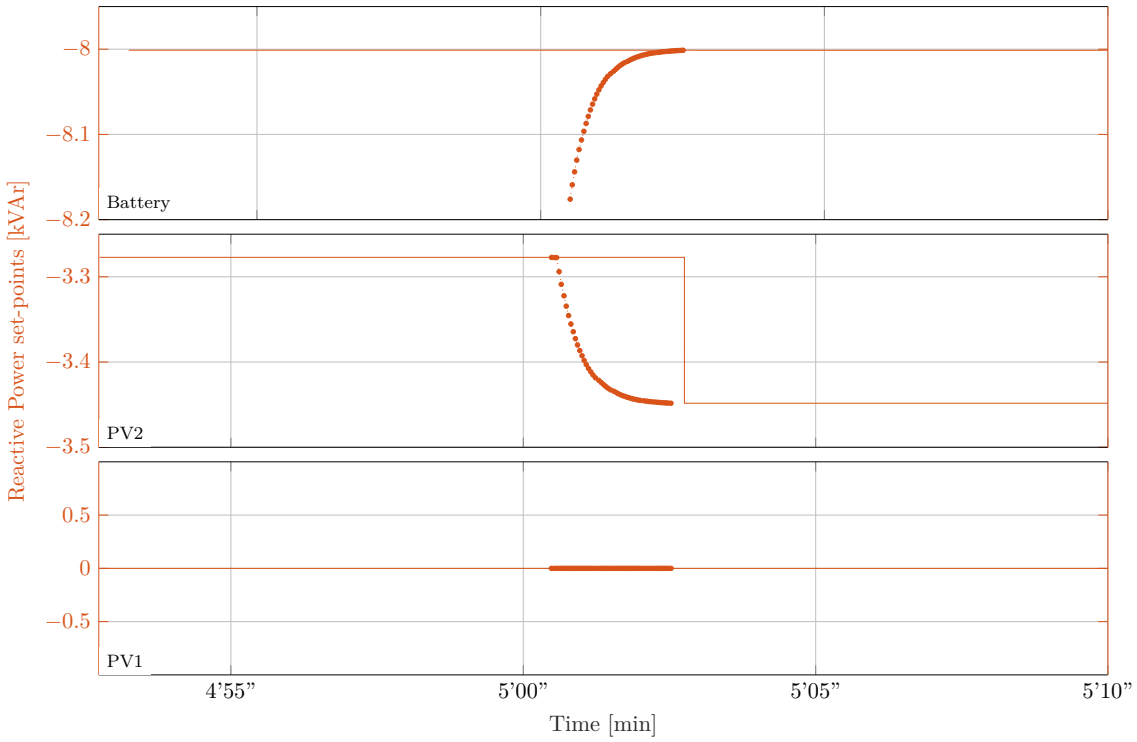


Figure 5.9: Convergence of one execution of Algorithm 2. Reactive power set-points (solid) and updates of the internal variable $\hat{q}$ (dotted).

constantly growing $\lambda_{3,\max}$. All inverters are drawing their maximum reactive power, which confirms that the voltage cannot be regulated: there does not exist a feasible reactive power input such that all voltages are within the voltage limits.

Once we remove the cause of the overvoltage (at approx. 4 minutes) and the voltage drops, the inverters do not adjust their reactive power injection, but remain saturated at their limit value for several minutes. This phenomenon corresponds to the windup behavior that is often observed in integral controllers. Here, the integrator is $\lambda_{3,\max}$ of the battery.

One solution to this windup problem is to stop the integration of the voltage violation once all inverters have saturated. While this is an easy modification for a centralized controller (see [Ort+20a]), a more sophisticated anti-windup scheme is needed in a distributed setup, where no single agent is aware of the infeasibility of the optimization problem. The design of an effective distributed anti-windup scheme is an interesting and open problem *per se*.

### 5.4.5 Control Performance vs Communication Complexity

The ability of performing optimal voltage control without global communication comes at a price. As detailed in Section 5.2.2, in order to obtain an iterative update that

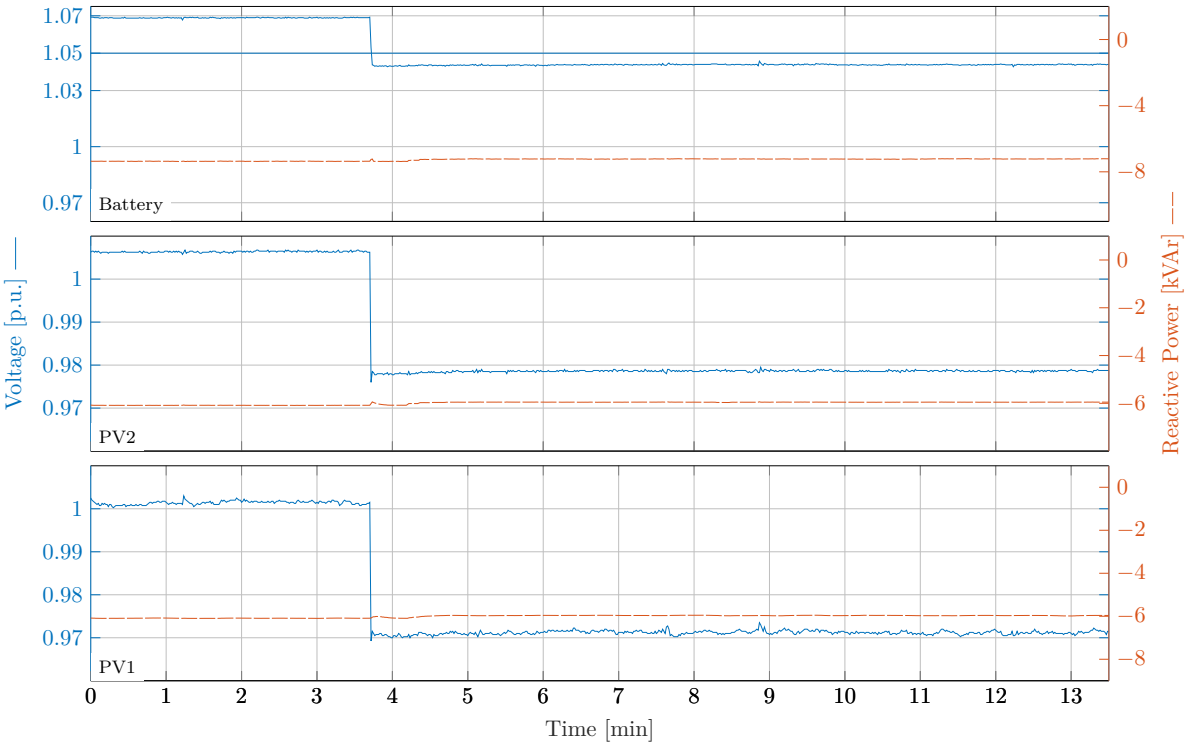


Figure 5.10: Controller windup due to a persistent overvoltage.

only requires neighbor-to-neighbor communication we had to constrain the choice of the quadratic cost parameter $M$ in (5.1).

We showed that $M = X$ is a valid choice, $X$ being the grid susceptance matrix. As discussed in [Bol+15], the minimization of $q^T Xq$ is connected to the minimization of power losses caused by reactive power flows (under the assumption of homogeneous X/R ratio). Moreover, as discussed in [Bol+19], the cost $q^T Xq$ can then be rewritten as $(Xq)^T GXq$, where $Xq$ is the first order approximation of the voltage drop caused by reactive power injection. Therefore, because $G$ has the structure of a Laplacian, $q^T Xq$ promotes equal voltage drops in the network.

In general, however, a network operator may be interested in minimizing a different cost function, e.g.

$$J_{\text{fair}} := \sum_i (q_i / q_i^{\max})^2 \tag{5.13}$$

which promotes proportional fairness in the use of the reactive power capacity of each inverter. The difference in the reactive power set-points and in the resulting cost is reported in Table 5.2. Given the inexpensive nature of reactive power, these differences are in most cases acceptable.

Table 5.2: Comparison between the steady-state of the distributed algorithm and the maximal-fairness set-points that minimize (5.13).

| | $\arg\min\ q^T X q$ | $\arg\min\ J_{\text{fair}}$ | difference |
|---|---|---|---|
| $J_{\text{fair}}$ | 2.12 | 1.98 | 6.9% |
| PV1 $q_1$ | -2.06 kVAr | -3.76 kVAr | 0.28 [p.u.] |
| PV2 $q_2$ | -6 kVAr | -4.6 kVAr | 0.23 [p.u.] |
| Battery $q_3$ | -8 kVAr | -8 kVAr | 0 [p.u.] |

## 5.5 Scalability

In this section we investigate how the performance of the proposed feedback scheme scales with the number of nodes. In order to perform this analysis, we consider a fictitious scenario which is identical to the one described in Section 5.3.2, but where $N'$ extra "dummy" nodes have been added on the line connecting PV2 to the Battery (see Figure 5.11). These nodes are equally spaced and have zero reactive power capability. They can communicate one to the next one, so that the entire communication graph becomes a line of $N = N' + 3$ nodes. Their presence therefore affect the execution of the algorithm without affecting the optimal solution of the problem.

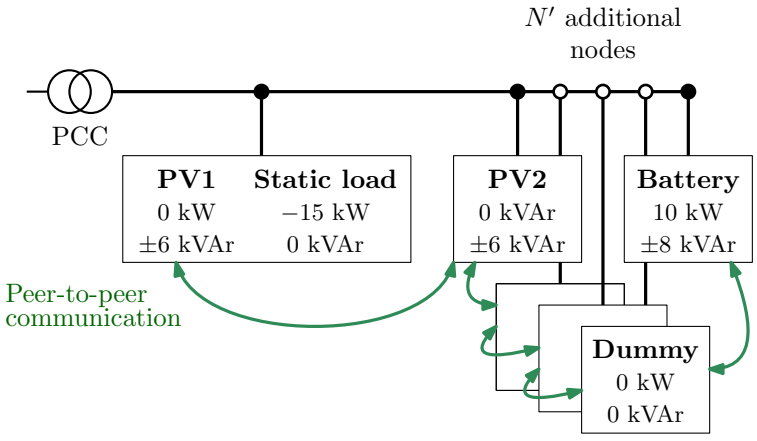


Figure 5.11: Diagram of the electrical topology and of the communication graph used in the numerical analysis of the algorithm scalability.

We compare two implementations of our method: in the first case (that we denote as $K \gg 1$), we allow an arbitrarily large number $K$ of communication steps between each actuation step (namely, we allow communication until convergence up to a tolerance of 10 VAr); in the second case, we only allow one communication step for each actuation step ($K = 1$).

This second case closely resembles what was proposed [Bol+15]. More generally, we

consider it as a prototype for the other distributed methods available in the literature, where communication and actuation are always interleaved one-to-one. These include for example the primal-dual methods proposed in [Mag+19] or in [QL19]. The other methods reviewed in the Introduction also share the same interleaving between communication and actuation. We will see in this section how this appears to be a design choice that limits performance as the network grows in size. In the comparison, it is important to keep in mind that iterations that only require computation and communication can be executed much faster than iterations that require actuation of the system and measurement. We therefore counted and reported them separately, as *communication steps* and *actuation steps*.

We executed the algorithm with $K \gg 1$ and $K = 1$ for networks of different sizes, and these are the main findings.

**Ease of tuning:**

- If $K$ is large, then the tuning of the inner optimization gain $\gamma$ becomes very simple; Figure 5.12 shows how a large $K$ gives a plateau of valid choices for $\gamma$.
- An optimal value of $\gamma$ as a function of the grid parameters has been suggested in [Bol+15, Corollary 2] when $K$ is unbounded, and seems to be an excellent choice also for $K$ finite but sufficiently large. In the specific case of Figure 5.12, the recommended $\gamma$ is $1/(2\sigma(G)) = 0.004$.
- For large $K$, tuning $\alpha$ becomes significantly simpler. All the executions of $K \gg 1$ in Table 5.3 use the same parameter $\alpha = 100$ and attain similar time to convergence, while $\alpha$ needed to be substantially re-tuned when $K = 1$.

**Controller performance:**

- By allowing many communication steps, the number of actuation steps required for convergence is significantly reduced (see Table 5.3).
- The number of communication steps required for convergence of the nested subproblem increases with the size of the network (although not exponentially). Remember that these steps only require communication and computation, and we showed that they may also be performed asynchronously (in contrast to the actuation steps, which need to be synchronous). By using an asynchronous implementation of the inner loop data exchange, the time needed for a single communication step is only determined by the communication speed between two neighbouring nodes [Sem19].
- The performance of the controller degrades gracefully if an upper bound on the communication steps is imposed (see Table 5.4).

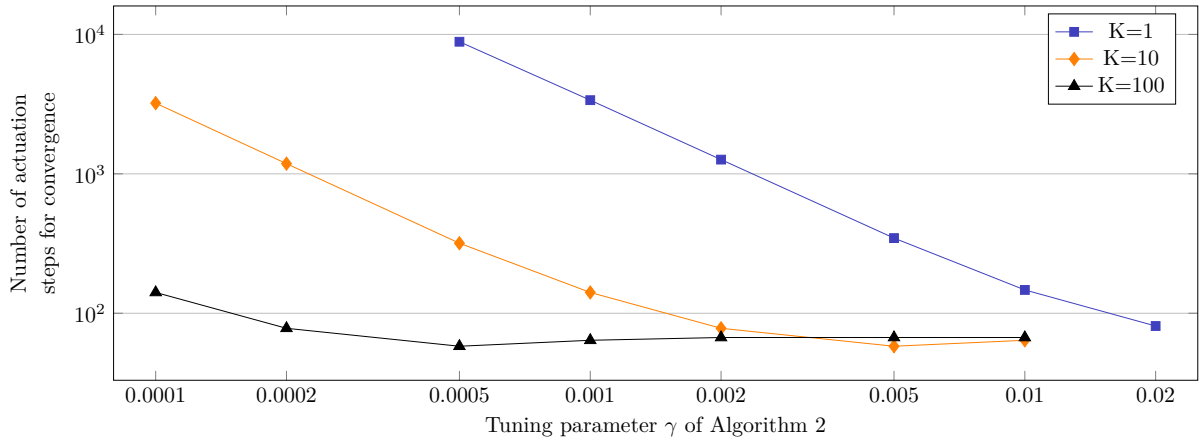


Figure 5.12: Number of actuation steps required for convergence as a function of $\gamma$ and of the number of communication steps $K$. Network with 3 inverters and $\alpha = 100$. Each curve stops, at the right end, at the largest $\gamma$ that does not cause instability.

Table 5.3: Actuation steps required for convergence. For $K \gg 1$, parameters are constant and are $\alpha = 100$, $\gamma = 1/(2\sigma(G))$. For $K = 1$, $\alpha$ has been optimized for every instance.

| | $K \gg 1$ | | $K = 1$ |
|---|---|---|---|
| nodes | communication steps | actuation steps | actuation steps |
| 3 | 35 | 46 | 258 ($\alpha = 40$) |
| 7 | 566 | 46 | 2975 ($\alpha = 3.1$) |
| 10 | 1417 | 47 | 5972 ($\alpha = 1.6$) |
| 30 | 14515 | 51 | >30000 |
| 100 | 19848 | 61 | >30000 |

Table 5.4: Actuation steps required for convergence, for different values of $K$ (communication steps) in a network of 30 nodes.

| $K$ | 100 | 300 | 1000 | 3000 | 10000 | 30000 |
|---|---|---|---|---|---|---|
| actuation steps | 724 | 211 | 67 | 39 | 50 | 51 |

These findings indicate how the decomposition of the iterative optimization scheme into an iteration that requires actuation of the grid (and therefore cannot be executed too frequently) and a nested sequence of communication steps is fundamental for the overall scalability of the solution.

## 5.6 Conclusion

We implemented for the first time a fully distributed peer-to-peer Volt/VAr controller on a real low-voltage distribution network. The controller at each inverter only uses local voltage measurements and the required model knowledge is only the electrical distance to its neighbors. No filtering or centralized estimation is needed, and the controller is able to drive the system to an optimal point where all voltage and reactive power constraints are satisfied. Each inverter is allowed to communicate only with its neighbors in the electric topology. We also showed that the performance of such a distributed strategy scales nicely with the size of the grid, as long as the communication rate is substantially higher than the measurement/actuation rate. Moreover, we highlight some directions for future investigation, such as optimizing the trade-off between communication complexity and performance, detecting problem infeasibility, and analyzing finite-time convergence of the nested algorithm.

CHAPTER 6

# Experimental Validation of Online Feedback Optimization in Power Distribution Grids

This chapter describes work that implemented an Online Feedback Optimization (OFO) controller in a laboratory distribution grid feeder to analyze its interaction with power grid hardware. The results show the performance of an OFO controller in Volt/VAr control and compares it with droop control and Optimal Power Flow (OPF)-based dispatch.

## 6.1 Introduction

The shift towards distributed microgeneration and the change in power consumption (electric mobility, storage, flexible loads) poses unprecedented challenges to power distribution grids. One important concern is the occurrence of over- and undervoltages in distribution feeders, which may force the distribution system operator to curtail generation or to shed loads, respectively. The flexibility of the power inverters of distributed energy resources (DERs), and more precisely their reactive power capabilities, can be used to avoid these extreme remedial actions. Control of reactive power flows is a relatively inexpensive way to regulate the feeder voltage and should therefore be fully exploited in order to avert taking action on the active power flows in the grid.

Many *local control strategies* have been proposed towards this goal. In these strategies, each DER only measures the voltage at its point of connection in order to decide its own reactive power set-point. No communication infrastructure is needed because the controllers are fully decentralized. An example of local control strategies are static control laws like droop control with dead band and saturation, which have been included in the recent grid codes [IEE; VDE18; Com16]. Incremental local control strategies have also been proposed, where the reactive power set-point is calculated as a function of the voltage magnitude and the past reactive power set-point [CC17; FZC15]. The main

This chapter is based on the publication [Ort+20a].

advantage of local control strategies is that they are easy to implement due to being fully decentralized. However, it was recently shown that they are suboptimal [Bol+19]. Namely, they do not necessarily regulate the voltage to the admissible range, even with sufficient reactive power capability of the inverters.

An alternative solution to the voltage regulation problem is to use an optimal power flow (OPF) solver to calculate the optimal reactive power set-points (see [EGH16] and references therein). This optimization-based method requires an accurate grid model and full observability of the grid state, neither of which are usually available in distribution grids. Estimating the real-time state of a distribution grid is only possible if enough sensors are deployed which adds significant complexity and cost to this approach.

A third and more promising option is *Online Feedback Optimization* (OFO) or *autonomous optimization*. OFO has been recently proposed as a strategy to adjust DER set-points in real-time and to drive the system to an optimal operating point without measuring or estimating the power demands [BD15; DS16; Hau+17; QL19; Mag+19; Mol+17; TDL17; BD19]. To the best of the authors' knowledge, there is no publicly available report of testing of these solutions on a real grid, and their robustness to model mismatch and measurement noise has been conjectured but never verified in experiments.

This chapter presents an experimental verification of the effectiveness of OFO for Volt/VAr control on a simple, yet plausible testbed. The experiment shows that the grid state converges to the optimal reactive power flow, and it allows to assess the performance in the presence of:

- *model mismatch*, especially in comparison to standard OPF-based dispatch, showing that OFO performs well with an extremely rudimentary model of the grid;
- realistic *measurement accuracy*, based on off-the-shelf sensors and without any state-estimation stage.

Additionally, the experiment illustrates the suboptimality of the local Volt/VAr control strategies included in recent grid codes. As predicted in [Bol+19], they can be ineffective and even detrimental in regulating under- and overvoltages, leading to more loads being shed or renewable generation being curtailed than necessary.

The rest of the chapter is structured as follows: In Section 6.2 the general concept of OFO is presented and the assumptions are introduced that make the implementation more tractable. Afterwards a OFO controller is designed for the Volt/VAr problem. The experimental setup and the controller implementation are explained in Section 6.3 and Section 6.4, respectively. Finally, the experimental results are presented in Section 6.6 and the chapter is concluded in Section 6.7.

## 6.2 Online Feedback Optimization

Consider the problem of determining the values of some set-points $u$ (e.g, reactive power injections) in order to minimize a given cost function (typically a cost of the control effort) while satisfying some constraint on an output signal $y$ (e.g, voltage bounds). The output $y$ is also affected by an exogenous uncontrollable input $w$ (e.g, power demand of the loads), and depends on these inputs via a nonlinear map $y = h(u, w)$.

The aforementioned decision problem is mathematically represented by the possibly non-convex optimization problem

$$\begin{aligned} \min_{u} \ & f(u) && \text{cost of actuation effort} \\ \text{s.t.} \ & g(y) \leq 0 && \text{constraints on the output } y = h(u, w) \\ & u \in \mathcal{U} && \text{actuation bounds.} \end{aligned} \tag{6.1}$$

For a more general approach with $f(u, y)$ and consideration of underlying dynamics, see [Hau+20a]. One way to approach this decision problem is to solve (6.1) using the model $y = h(u, w)$ and then apply the resulting set-points to the system in a feedforward manner. This approach comes with several disadvantages, such as the need for an accurate model $h$ of the system and for full measurement or an estimate of the exogenous input $w$.

An alternative approach is called Online Feedback Optimization, and is based on the assumption that the output $y$ of the system can be measured in real-time, while the exogenous input $w$ is unmonitored. Real-time measurements are used to iteratively adjust the set-points $u$, based on reduced model information, in such a way that the closed-loop system converges to the solutions of the optimization problem (6.1) (hence the name).

### 6.2.1 Online Feedback Optimization Principle

The core idea behind OFO is to exploit the measurements $y$ instead of relying on the model $y = h(u, w)$. One way to do so is to dualize the output constraints and get the Lagrangian

$$\mathbf{L}(u, \lambda) = f(u) + \lambda^T g(h(u, w)), \tag{6.2}$$

where $\lambda$ is a vector of dual variables in which each dual variable corresponds to one constraint. Instead of (6.1) we consider the optimization problem

$$\max_{\lambda \geq 0} \ \phi(\lambda), \tag{6.3}$$

where the dual function $\phi(\lambda)$ is defined as

$$\phi(\lambda) := \min_{u \in \mathcal{U}} \ \mathbf{L}(u, \lambda). \tag{6.4}$$

Assuming that the feasible space of (6.1) has a non-empty interior, (6.1) and (6.3) have the same solution (Strong Duality Theorem, [Ber99, Proposition 5.3.1]).[1]

To solve (6.3) we use a gradient ascent with a fixed step size, in which the multiplier $\lambda$ is repeatedly updated in the direction of steepest ascent of $\phi(\lambda)$, while ensuring $\lambda \geq 0$. By introducing the element-wise projection operator $[a]_{\geq 0} := \max\{a, 0\}$ and the tuning parameter $\alpha$ we can write

$$\lambda(t+1) = [\lambda(t) + \alpha \nabla_\lambda \phi(\lambda)]_{\geq 0}. \tag{6.5}$$

In [Ber99, Proposition 6.1.1] it was shown that $\nabla_\lambda \phi(\lambda) = g(h(u, w))$. In other words, the gradient of $\phi$ is given by the violation of the dualized constraints $g(h(u, w))$ at the solution of the optimization problem (6.4), leading to:

$$\lambda(t+1) = [\lambda(t) + \alpha g(y(t))]_{\geq 0}. \tag{6.6}$$

Instead of computing $g(y(t))$ based on model information, we exploit the physical system to enforce the constraint $y = h(u, w)$ and measure the output $y = h(u, w)$ as feedback from the plant. The variable $\lambda$ integrates the output constraint violation with a step size of $\alpha$. Note, that this corresponds to the integral part of a PI-controller.

Using $\lambda(t+1)$, we update the set-points $u$ with the solution of (6.4), i.e.,

$$\begin{aligned} u(t+1) &= \arg\min_{u \in \mathcal{U}} \ \mathbf{L}(u, \lambda(t+1)) \\ &= \arg\min_{u \in \mathcal{U}} \ f(u) + \lambda(t+1)^T g(h(u, w)). \end{aligned} \tag{6.7}$$

Whether this optimization problem is easier to solve than the original one in (6.1) is not apparent at this point. In the next subsection we will see how, under mild assumptions, this optimization problem admits an approximation which is numerically very tractable.

To summarize, the OFO controller is realized by running the following algorithm at every time $t = 0, 1, \ldots$

**Algorithm 6.1** Online Feedback Optimization controller

1: Measure the system output $y(t)$
2: Calculate $\lambda(t+1)$ as in (6.6)
3: Solve the optimization problem in (6.7)
4: Apply the calculated set-points $u(t+1)$ to the system

See Figure 6.1 for a block diagram of a OFO controller for the Volt/VAr problem, that we derive in Section 6.2.3.

[1] This holds true if $\mathcal{U}$ is convex, and $f(u)$ and $g(h(u, y))$ are convex over $\mathcal{U}$. Convexity of $f(u)$ can be guaranteed as it is chosen by the designer and $\mathcal{U}$ usually describes box constraints which renders $\mathcal{U}$ convex. Convexity of $g(y) = g(h(u, w))$ is not guaranteed, even for convex $g(\cdot)$, when $h(u, w)$ is non-linear. However, convexity of $g(h(u, w))$ is only required over $\mathcal{U}$ and at least power systems tend to be reasonably linear within the bounds of the available actuation capacity $\mathcal{U}$.

### 6.2.2 Practical Online Feedback Optimization Design

We now make two assumptions that are not necessary, but make the OFO controller numerically more tractable. First, we assume the cost is a quadratic function $f(u) = \frac{1}{2}u^T M u$ with $M$ being square, symmetric and positive semidefinite. Second, we make the mild assumption that the constraints on the input and output are linear. We therefore get $\mathcal{U} = \{u \mid Cu \leq d\}$ and $g(y) = Ay - b$. Linearity of the constraints is often given, as in many cases the limits are upper and lower bounds of the form $u_{\min} \leq u \leq u_{\max}$. This leads to (6.1) taking the form

$$\begin{aligned} \min_u \ & \frac{1}{2}u^T M u && \text{quadratic cost of actuation} \\ \text{s.t. } & Ay \leq b && \text{linear constraints on the output } y = h(u, w) \\ & Cu \leq d && \text{linear actuation bounds.} \end{aligned} \tag{6.8}$$

Notice that the output is still a possibly nonlinear and non-convex function of the input $y = h(u)$. The dual update (6.6) for the special case (6.8) of (6.1) takes the form:

$$\lambda(t+1) = [\lambda(t) + \alpha(Ay(t) - b)]_{\geq 0}. \tag{6.9}$$

However, the major advantage of (6.8) over (6.1), lies in the evaluation of (6.7) which can now be explicitly solved. There are several ways to solve (6.7). We choose to do this in two steps that we feel are easy to understand. First, we ignore the constraint $u \in \mathcal{U}$ and calculate the critical point $u$ for which $\nabla_u \mathbf{L}(u, \lambda(t+1)) = 0$ (first order optimality condition). Then, we project this unconstrained critical point onto $\mathcal{U}$.

The derivative of the Lagrangian $\mathbf{L}(u, \lambda(t+1))$ is

$$\begin{aligned} \nabla_u \mathbf{L}(u, \lambda(t+1)) &= \nabla_u f(u) + \nabla_u \left(\lambda^T(t+1) g(h(u))\right) \\ &= Mu + \frac{\partial h(u, w)}{\partial u}^T A^T \lambda(t+1). \end{aligned} \tag{6.10}$$

The factor $\frac{\partial h(u,w)}{\partial u}$ is the sensitivity of the output $y$ with respect to the input $u$. This sensitivity is in general dependent on $u$ and $w$, but in many practical applications can be approximated by a constant matrix $H$. Furthermore, the approximation error will be compensated by the feedback nature of this scheme. The theoretical analysis of this robustness remains an open question, and is one of the main motivations for the experimental validation reported in this chapter. Under this modeling assumption we have

$$\nabla_u \mathbf{L}(u, \lambda(t+1)) \approx Mu + H^T A^T \lambda(t+1), \tag{6.11}$$

and a critical point of $\mathbf{L}(u, \lambda(t+1))$ in $u$ is approximated by

$$u_{\text{unc}} := -M^{-1} H^T A^T \lambda(t+1). \tag{6.12}$$

This is the unconstrained critical point. The solution to the constrained case is obtained by projecting $u_{\text{unc}}$ onto the set of feasible control inputs $\mathcal{U}$, that is

$$\begin{aligned} u(t+1) &= \arg\min_{u \in \mathcal{U}} \ \|u - u_{\text{unc}}\|_M^2 \\ &= \arg\min_{u \in \mathcal{U}} \ (u - u_{\text{unc}})^T M (u - u_{\text{unc}}). \end{aligned} \tag{6.13}$$

The feasible set $\mathcal{U}$ is known and described by linear inequality constraints. Therefore, this minimization is a simple convex quadratic program. Notice how both the unconstrained and the constrained solution do not depend on the unmeasured exogenous input $w$, as desired.

### 6.2.3 Online Feedback Optimization for Volt/VAr Regulation

In this section we specialize OFO to the Volt/VAr regulation problem. This problem is defined as follows: Determine the reactive power $q_h$ at every DER $h$ such that $q_{\min} \leq q_h \leq q_{\max}$ and that $v_{\min} \leq v_h(q, w) \leq v_{\max}$. Here, $v_h(q, w)$ is the steady state map of the nonlinear power flow equations that defines voltages $v_h$ as a function of both reactive powers $q_h$ and external influences $w$ (e.g., active and reactive demands, active generation). Mathematically speaking, we try to solve a feasibility problem:

$$q \in \mathcal{F} \quad \mathcal{F} := \{q \mid q_{\min} \leq q \leq q_{\max},\ v_{\min} \leq v(q, w) \leq v_{\max}\},$$

where $q$ and $v$ are the vectors of reactive power set-points and voltage magnitudes that we obtain by stacking the individual $q_h$ and $v_h$ of the DERs, respectively. We choose not to control active power with our algorithm. Due to the different cost of the two control actions one should first utilize reactive power and only afterwards use active power to control the voltage. Therefore, these two control actions can be applied individually and do not need a unified control approach. However, active power could easily be included in the controller without adding technical difficulties. In order to apply the proposed methodology, we cast this feasibility problem into the optimization problem

$$\begin{aligned} \min_q \ & \frac{1}{2} q^T M q \\ \text{s.t. } & v_{\min} \leq v_h(q, w) \leq v_{\max} \quad \forall h \\ & q_{\min} \leq q_h \leq q_{\max} \quad \forall h. \end{aligned} \tag{6.14}$$

This is a special case of (6.8), where $M$ can be used to weight the reactive power contribution of the different inverters $h$.

We introduce the dual variables $\lambda_{\min}$ and $\lambda_{\max}$ corresponding to the voltage (output) constraints. We adapt (6.9) to this specific case (namely, $A = \left[\begin{smallmatrix} -I \\ I \end{smallmatrix}\right]$, $b = \left[\begin{smallmatrix} v_{\min} \\ -v_{\max} \end{smallmatrix}\right]$) and we get

$$\lambda_{\min}(t+1) = [\lambda_{\min}(t) + \alpha(v_{\min} - v)]_{\geq 0} \tag{6.15}$$

$$\lambda_{\max}(t+1) = [\lambda_{\max}(t) + \alpha(v - v_{\max})]_{\geq 0}. \tag{6.16}$$

As we can see, we are integrating the voltage violations, which can be measured, with a gain of $\alpha$.

As discussed before, in order to calculate (6.12), we need a constant approximation of the sensitivity of the voltages with respect to the reactive power injection akin to power transfer distribution factors for active power generation on the transmission level. Under no-load conditions and the assumption of negligible cable resistances we have the approximation

$$\frac{\partial v(q,w)}{\partial q} = X, \tag{6.17}$$

where $X$ is the reduced bus reactance matrix that can be derived from the grid topology and the data in Table 6.1. The approximation is accurate for lightly loaded systems, because the nonlinearity of the power flow equations is mild near this operating point [BD15]. In our application the system can be heavily loaded, but in Section 6.6 we verify that the proposed OFO is sufficiently robust against this model mismatch.

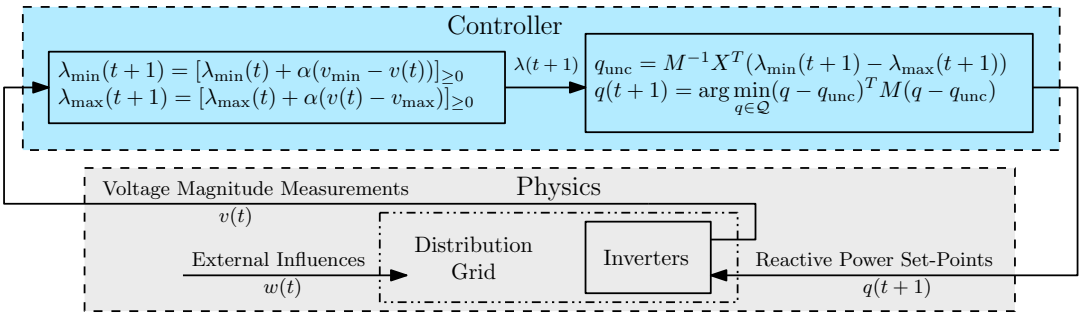


Figure 6.1: Block diagram of the controller with (6.15) and (6.16) (left block) and (6.18) and (6.19) (right block). The controller gets the voltage magnitude measurements from the inverters and determines the reactive power set-points, which are send to the inverters. The parameter $\alpha$ is the controller gain and is the only tuning knob. Note, that the left block corresponds to the integral part of a PI-controller.

The expression in (6.12) for the optimal unconstrained reactive power set-points $q_{\text{unc}}$ becomes

$$q_{\text{unc}} = M^{-1}X^T(\lambda_{\min}(t+1) - \lambda_{\max}(t+1)), \tag{6.18}$$

while the solution of the constrained optimization problem (6.13) becomes

$$q(t+1) = \arg\min_{q \in \mathcal{Q}} (q - q_{\text{unc}})^T M (q - q_{\text{unc}}), \tag{6.19}$$

where $\mathcal{Q} = \{q \mid q_{\min} \leq q \leq q_{\max}\}$.

In practice, these reactive power set-points $q(t+1)$ are to be communicated to the different DERs, which will adjust their reactive power accordingly and collect the measurement of the consequent steady state voltage magnitudes, which need to be communicated to the central control unit. Therefore, at every time step the measurement and

set-point need to be communicated by and to every inverter, respectively. The resulting centralized controller is represented in Figure 6.1 and consists of equations (6.15) and (6.16) (left block in the figure) and (6.18) and (6.19) (right block in the figure).

We can see that the OFO controller uses the same measurements as local controllers, but these measurement are processed by a central unit which coordinates the actions of the different DERs and steers the system to the optimal steady state. In comparison to the OPF-based dispatch, no nonlinear model nor knowledge of the power consumption or generation (modelled as external influences $w$) is needed.

## 6.3 Experimental Setup

The experiment has been implemented in the SYSLAB distribution grid at DTU Risø, Denmark. A small yet realistic distribution feeder has been configured in order to observe an overvoltage condition caused by local generation. The same setup was used in [Ort+20b] to analyze a distributed OFO controller for the Volt/VAr problem. Without proper reactive power control, the feeder's ability to host renewable energy injections is limited and generation has to be curtailed. This scenario was chosen because it constitutes a non-trivial voltage regulation problem which cannot be solved without a coordinated Volt/VAr control strategy, as will be demonstrated in Section 6.6.1. Note, that the applicability of the proposed OFO strategy is not limited to the chosen topology.

The setup consists of a vanadium battery, two photovoltaic systems (PV), a resistive load, and the distribution substation (PCC) connecting the distribution feeder to the remaining grid, see Figure 6.2. The different nodes are connected via cables with non-negligible resistance (Table 6.1). The cable connecting the battery to the grid has a particularly large resistance.

The active power injection $p_3$ of the battery can represent a renewable source, which should not be curtailed. In our experiments we choose the active power of the battery to be $p_3 = 10$ kW. The high cable resistance and active power injection deteriorates the approximation of the sensitivity matrix in (6.17). In Section 6.6.1 we will show that the OFO controller can cope with the model mismatch. The static load is set to an active power consumption of 15 kW ($p_1 = -15$ kW) which is larger than the local production, therefore requiring a positive active power flow from the substation. PVs are fluctuating power sources. Therefore, to facilitate repeatability of the experiments and to allow for a comparison between different controllers, the PVs do not inject active power ($p_2 = 0$kW).

The resulting voltage profile with no reactive power flows is represented in Figure 6.2, where the overvoltage at the end of the feeder is apparent.

Both the PVs and the battery can measure their voltage magnitudes, and their reactive power injections can be controlled. The PV inverters have a reactive power range of ±6 kVAr and the battery can be actuated with ±8 kVAr. The inverters at SYSLAB

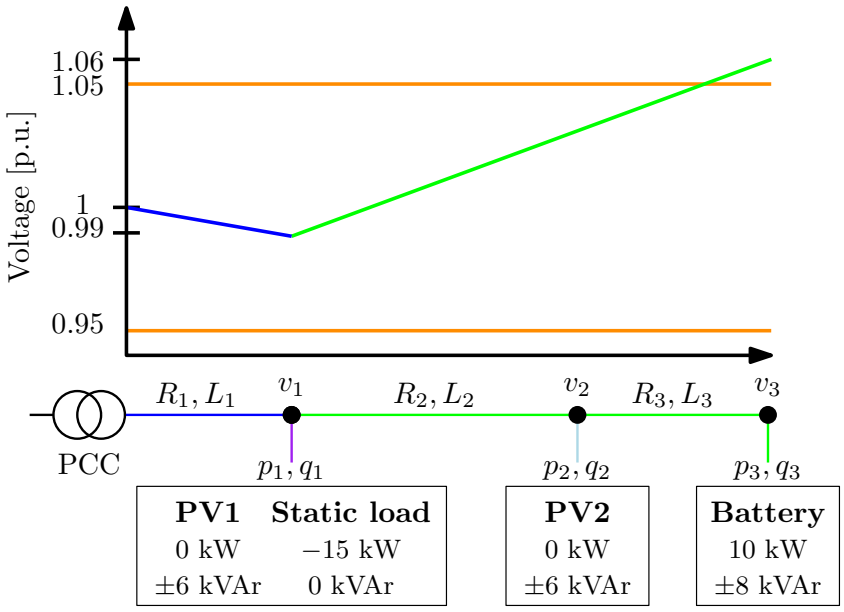


Figure 6.2: Sketch of the voltage profile and the distribution feeder. The colors of the voltage profile match the colors of the sketched feeder.

Table 6.1: Overview of the resistances and inductances in the grid.

| $R_1$ [Ω] | $L_1$ [Ω] | $R_2$ [Ω] | $L_2$ [Ω] | $R_3$ [Ω] | $L_3$ [Ω] |
|---|---|---|---|---|---|
| 0.195 | 0.124 | 0.11 | 0.027 | 0.97 | 0.093 |

are oversized such that their full reactive power range is available independently of their concurrent active power injection. The PVs and the battery can communicate with a central computational unit via a general-purpose Ethernet network, while the load is uncontrolled and unmeasured.

The voltage limits are defined to be 0.95 p.u. and 1.05 p.u. We set these limits tighter than most grid codes in order to be able to observe persistent overvoltages without hardware protections being activated.

## 6.4 Controller Implementation

The OFO controller is implemented in Matlab at a central computation unit (Figure 6.1), where it is provided with the voltage magnitude measurements from the different inverters and computes the reactive power set-points. These are send to the inverters every 10 seconds, because the PV systems in the laboratory were not to be actuated more frequently, due to special hardware constraints. In general, the controller can run more frequently.

### 6.4.1 Controller Tuning

The controller has one tuning parameters which is the scalar control gain $\alpha$ in (6.15) and (6.16). The higher its value, the faster a voltage constraint violation is integrated and the faster the DERs' reactive power set-points counteract the violation. However, as known from the optimization literature the stability of the gradient ascent we perform in (6.6) is lost if $\alpha$ is chosen too large (see [Ber99, Proposition 1.2.3]).

### 6.4.2 Anti-Windup

If the active power injections are too high (overvoltage) or too low (undervoltage) there do not exist feasible reactive power injections that lead to voltages which are inside the allowed voltage band. Therefore, the Volt/VAr problem is infeasible and at least one voltage violation is persistent. In this case the dual variable ($\lambda_{\min}$ or $\lambda_{\max}$) corresponding to the violated constraint keeps integrating, yielding a windup of this variable. We implemented the following simple anti-windup solution in which the integration of the constraint violation is inhibited if all DERs are saturated:

$$\lambda_{h,\min}(t+1) = \begin{cases} \lambda_{h,\min}(t) & \text{if } v_{\min} - v_h(t) > 0 \text{ and } q_k = q_{k,\max}\ \forall k \\ \lambda_{h,\min}(t) + \alpha(v_{\min} - v_h(t)) & \text{otherwise,} \end{cases}$$

$$\lambda_{h,\max}(t+1) = \begin{cases} \lambda_{h,\max}(t) & \text{if } v_h(t) - v_{\max} > 0 \text{ and } q_k = q_{k,\min}\ \forall k \\ \lambda_{h,\max}(t) + \alpha(v_h(t) - v_{\max}) & \text{otherwise.} \end{cases}$$

Furthermore, an active power curtailment could be triggered once all DERs are saturated.

## 6.5 Benchmark Controllers

We implement a local droop controller and an OPF-based dispatch as two benchmark solutions to compare with the proposed OFO strategy. These approaches have almost opposite features: The droop controller only needs local voltage magnitude measurements, no communication, and no model of the grid; the OPF-based dispatch is centralized, requires communication of full state measurements (all power generation and demand), and relies on an accurate nonlinear grid model.

### 6.5.1 Droop Control

The droop controller that we implement complies with the recommendations by recent grid codes [IEE; VDE18; Com16]. Every DER measures the magnitude of the voltage

at their point of connection and absorbs/injects reactive power following the piecewise linear control law

$$q_h = \begin{cases} q_{h,\max} & v_h < v_1 \\ q_{h,\max}\dfrac{v_2 - v_h}{v_2 - v_1} & v_1 \leq v_h \leq v_2 \\ 0 & v_2 \leq v_h \leq v_3 \\ q_{h,\min}\dfrac{v_h - v_3}{v_4 - v_3} & v_3 \leq v_h \leq v_4 \\ q_{h,\min} & v_4 < v_h. \end{cases}$$

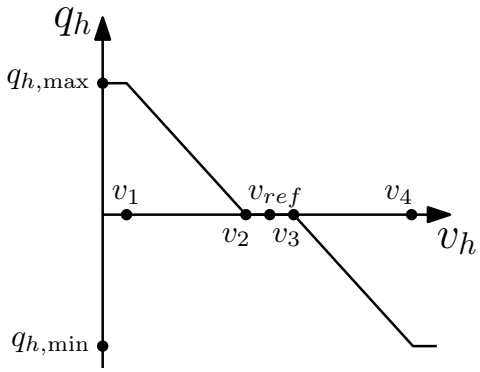


Based on the voltage band specifications of our experiment, we tune the droop curve to $v_1 = 0.95$ p.u., $v_2 = 0.99$ p.u., $v_3 = 1.01$ p.u. and $v_4 = 1.05$ p.u..

### 6.5.2 OPF-based Dispatch

We implement an OPF-based dispatch by communicating all reactive and active power consumption and generation to a centralized computation unit. There, we solve (6.14) using the OPF solver provided by Matpower [ZMT10], which we provide with a nonlinear grid model that we obtain from the grid topology and the data from Table 6.1. The reactive power set-points which are the solution of (6.14) are then given to the inverters. This approach guarantees optimality of the set-points under perfect model knowledge, but all power generation and consumption needs to be measured or estimated. This information is available at SYSLAB with a significant level of accuracy. In most distribution grids, the cable data and grid topology are not known exactly, nor are all reactive and active power consumption and generation measurements available.

## 6.6 Experimental Results

In the following experiment, we analyze two crucial features: the tracking performance when solving a time-varying voltage regulation problem, and the robustness against model uncertainty. We also contrast the proposed OFO strategy with the local droop controller and the OPF-based dispatch.

### 6.6.1 Tracking Performance

We repeat the following 21-minute experiment for the three aforementioned strategies: droop control, OPF-based dispatch, and OFO. All power inverters are initialized with

zero reactive power injection.[2]

After three minutes the controllers are activated and start regulating the voltage. After 11 minutes the active power injection of the battery is reduced to 0 kW (effectively removing the cause of the overvoltage and the need for reactive power regulation). At minute 14 the active power injection is stepped up again to 10 kW for the remaining seven minutes of the experiment.

### Droop Control

The performance of the droop controller can be seen in Figure 6.3. Once the controller is activated the reactive power of the battery drops to its lower limit which reduces the overvoltage. However, the limited reactive power capability of the battery cannot drive the voltage into the desired voltage range. The PV systems do not absorb reactive power to help reduce the overvoltage because they do not sense an overvoltage condition at their point of connection, and they will not lower their voltage below the nominal value of 1 p.u. Using a lower nominal voltage is also not possible as it will increase the occurrence of undervoltage events. This behavior is general for all local control strategies, and cannot be prevented without introducing some form of coordination between the inverters. Local control strategies are therefore inherently suboptimal; as established from a theoretical perspective in [Bol+19].

During minutes three to five, PV1 even injects reactive power to increase its voltage, because it has fallen under its deadband voltage of 0.99 p.u. This worsens the overvoltage at the battery, showing that droop control can even be detrimental.

### OPF-based Dispatch

An OPF-based strategy guarantees optimality under perfect model knowledge. This is a strong requirement which cannot be met in practice. Even in the SYSLAB distribution grid, where the setup, the cables and their parameters are accurately known, the OPF solution does not lead to feasible voltages (see the persistent voltage violation in Figure 6.4). Standard techniques such as disturbance observers, model adaptation, and state estimation could be used to alleviate the effect of model uncertainty. Also, robust optimization techniques could be used to solve the OPF problem. Nevertheless, an OPF-based dispatch requires a nonlinear grid model and knowledge of all active and reactive power consumption and production on the feeder.

[2]The plots show that the battery is injecting a small amount of reactive power at the beginning of the experiments. This is due to a measurement error. An inaccurate sensor is used for the internal reactive power controller of the battery, and a small tracking error is therefore present. The reported measurements in the figures are accurate.

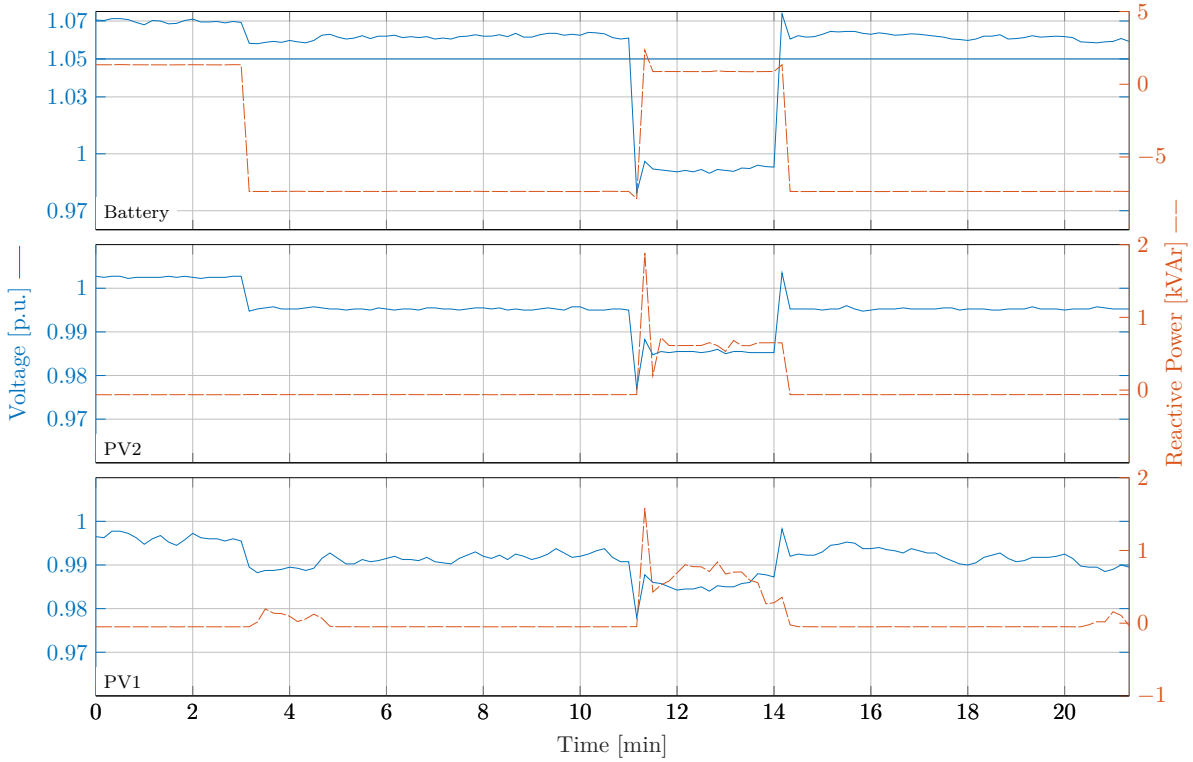


Figure 6.3: Performance of the Droop Control.

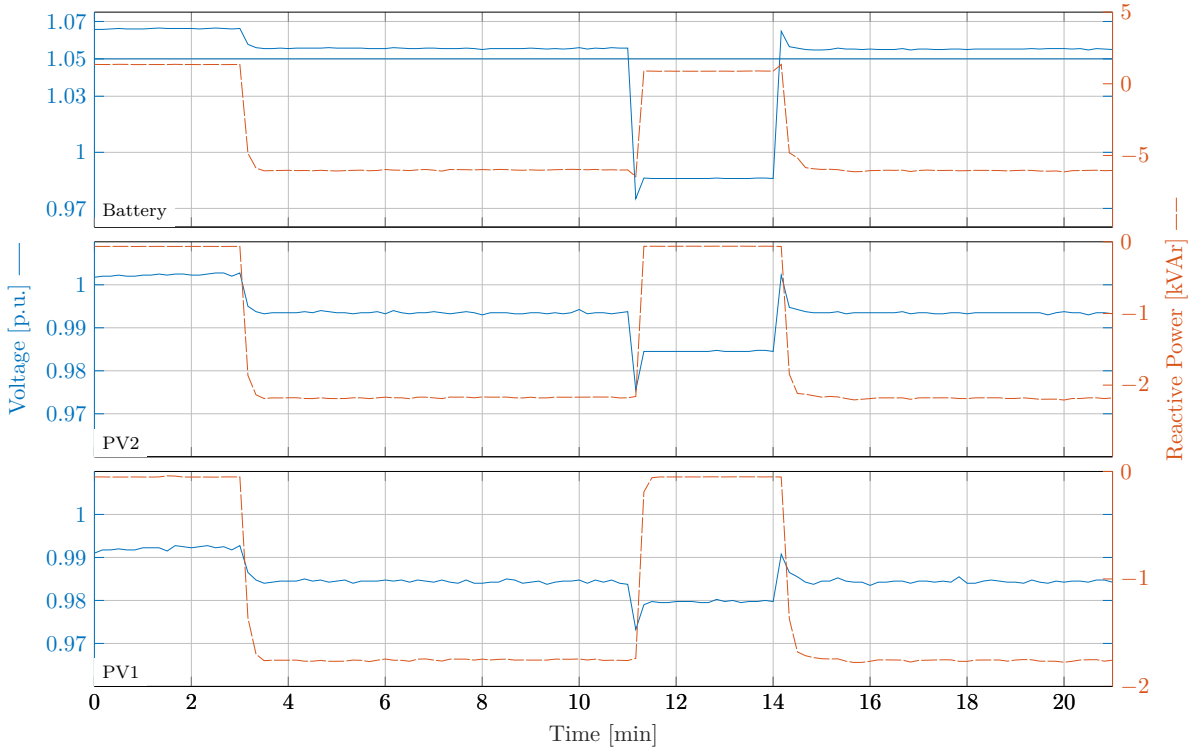


Figure 6.4: Performance of the OPF-based dispatch.

#### Online Feedback Optimization

The control gain $\alpha$ of the OFO controller is chosen to be 100, and the matrix $X$ was calculated using the data from Table 6.1. The weighting matrix of the optimization problem $M$ is a diagonal matrix with the entries being the inverse of the reactive power limits ($q_{\max}^{-1}$):

$$X = \begin{bmatrix} 0.10 & 0.09 & 0.09 \\ 0.09 & 0.11 & 0.11 \\ 0.09 & 0.11 & 0.16 \end{bmatrix}, \quad M = \begin{bmatrix} 1/6 & 0 & 0 \\ 0 & 1/6 & 0 \\ 0 & 0 & 1/8 \end{bmatrix}.$$

The control performance can be seen in Figure 6.5. When the controller is activated the central unit is provided with the voltages at the PV systems and the battery. The dual variable $\lambda_{\max,3}$ that corresponds to the violation of the upper voltage limit of the battery starts integrating the violation. This then leads to all inverters reducing their reactive power injections. As long as there is an overvoltage the dual variable keeps integrating, which leads to the inverter absorbing more reactive power which lowers the voltage. At steady state the voltage at the battery is at the upper voltage limit and the reactive power injections are at the optimal solution of (6.14).

The temporal constraint violation before the system converges to the feasible voltage band can be made shorter by using a faster sampling time. Furthermore, the power system is equipped to withstand short overvoltages.

### 6.6.2 Robustness to Model Mismatch

Due to its feedback nature, the proposed OFO approach is expected to be robust to model mismatch. However, in spite of recent theoretical insights [CSB19], the robustness of these strategies has not been analyzed experimentally before. In order to validate this claim in an experiment, we assume uncertainty in the knowledge of the grid sensitivity matrix $X$. We consider the crude approximation in which all entries of the $X$ matrix are believed to be 1. This choice corresponds to assuming that all inverters are connected to the same point on the feeder. No other model information is used, making the controller design essentially model-free. The behavior of this OFO controller with $\alpha = 10$ can be seen in Figure 6.6. Notice, that the controller is still able to drive the voltages to the feasible voltage band. The DERs are utilized differently than in Figure 6.5 due to the different $X$ matrix. This leads to a different value of the cost function, which is within 12% of the optimal value.

## 6.7 Conclusion

We have implemented three Volt/VAr control strategies on a real distribution feeder: local droop control, centralized OPF-based dispatch that guarantees optimal regulation

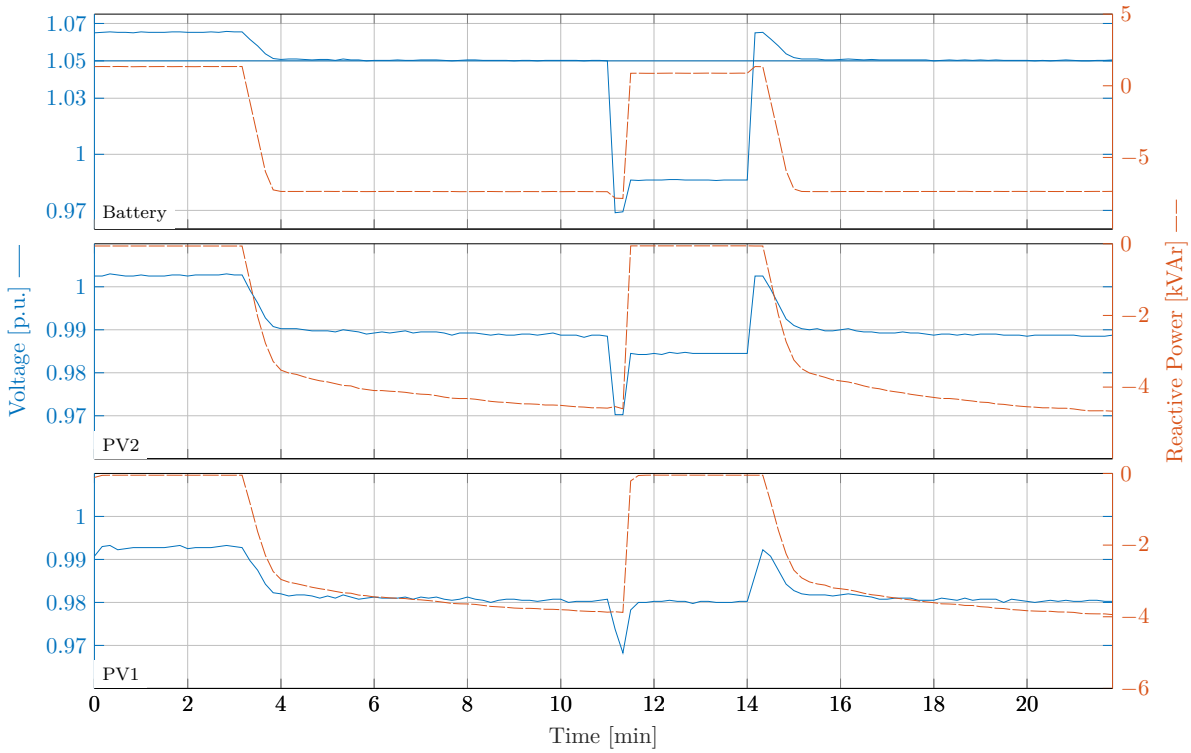


Figure 6.5: Performance of the OFO controller.

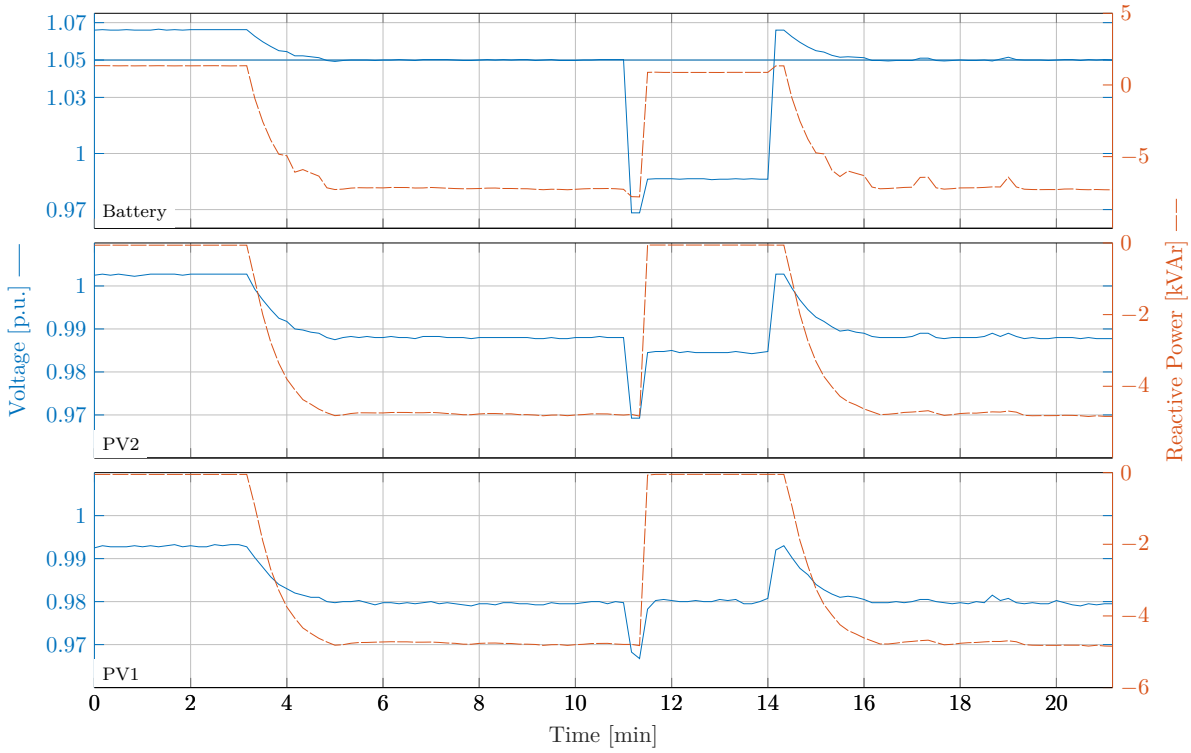


Figure 6.6: Performance of the OFO controller with no model information.

under perfect model information, and a recently proposed OFO scheme. While the droop control fails to regulate voltages in a satisfactory manner (as predicted analytically), the OPF-based dispatch exhibits substantial fragility with respect to model uncertainty. In contrast, the OFO strategy drives the system to the feasible voltage range while relying only on voltage measurements collected from the inverters (without measuring or estimating any power flows). Within our experimental setup, Online Feedback Optimization is extremely robust to model mismatch and its design and tuning is essentially model-free.

This leads us to conclude that Online Feedback Optimization is a promising approach for the real-time coordinated control of DERs in future distribution grids. We conjecture that these features of Online Feedback Optimization are not specific to this application and we plan to investigate them in the more general context of real-time control of power systems.

CHAPTER 7

# Deployment of an Online Feedback Optimization Controller for Reactive Power Flow Optimization in a Distribution Grid

This chapter describes the implementation of an Online Feedback Optimization (OFO) controller in a Swiss distribution grid for 24/7 operation. Toward that goal, the grid is retrofitted with off-the-shelf hardware and the controller uses existing inverters to optimize the reactive power flow into the subtransmission grid. At the same time, the controller is enforcing voltage limits which can allow for higher active power flow and thus virtually reinforces the grid. The gathered data shows, that the OFO controller works well within a real distribution grid.

## 7.1 Introduction

The operation of power systems comprises many tasks that can be formulated as optimization problems A famous example is Optimal Power Flow. Defining a control objective as an optimization problem is powerful, flexible, and versatile. Often, optimization problems even arise naturally e.g. when constraints, like voltage limits, need to be satisfied. It is therefore important to develop, deploy and evaluate different methods that can solve optimization problems under real operating conditions in a grid. More precisely, methods are needed that are fast and robust, and, especially in distribution grids, need to be able to work with little model information. If an exact model is available these optimization problems are solved offline on a computer by using an optimization algorithm and the model. The solution of the optimization is then deployed onto the grid, see Figure 7.1(a). However, solving these optimization problems offline can be computationally intense and they need to be robustified to be able to deal with model mismatch. Otherwise, a model mismatch could lead to a constraint violation. Unfortunately, such

This chapter is based on the publication [Ort+23c].

robustification prohibits to utilize the grid to its full capacity because some margin needs to be included to deal with a model mismatch. In distribution grids, no good system model might exist in the first place.

To circumvent these problems, Online Optimization methods have been developed that take feedback into account, see Figure 7.1(b) and consult [Mol+17] for a detailed review. One such method is called OFO. This method allows to steer a system to the solution of an optimization problem by taking decisions that are not based on an available model of the grid but on measurements collected in real-time. It is computationally light, robust to model mismatch, can utilize a grid to its full capacity, and needs very limited model information, see [Hau+21] for a review paper. In simulations, it has been applied to a vast number of power system problems [Oli+22; Oli+23; Tan+20; Ipa+22; NCW20a; GL16; DS16; BD19] and it has also been experimentally tested with hardware-in-the-loop simulations [Wan+20; Pad+21]. Experiments using a real power grid setup have also been done, however, those tests were either done in dedicated lab environments [Ort+20a; Ort+20b; Rey+18] or on microgrids [Kro+20b; Kro+20a] using a specialized hardware and communication setup. In contrast, this chapter presents the deployment of an OFO controller in a real distribution grid for 24/7 operation utilizing existing hardware. The distribution grid we chose is operated by AEW Energie AG, is located in the north of Switzerland, and supplies 100.000 people. The objective of the controller is twofold: On the one hand, it is tasked to optimize the reactive power flow at the substation, based on a TSO-DSO coordination scheme, that yields financial rewards for the distribution grids. On the other hand, it is used to regulate the voltage inside the distribution feeder. Such voltage support virtually reinforces the grid through automation and has the potential to mitigate or postpone grid reinforcements [Höf+12]. The potential of such virtual grid reinforcement through coordinated reactive power sources was analyzed in [Mat+23] and the authors concluded that 9% more active power can be conducted before voltage constraints limit the possible active power flow.

The chapter documents an example of successful TSO-DSO coordination in the Swiss power system and provides a demonstration of the effectiveness of OFO for real-time optimization problems in the power grid. Our contributions can be structured as follows: 1) we present how we retrofitted the distribution grid infrastructure both in terms of the communication and hardware setup, 2) we investigate the consequences of using off-the-shelf hardware and the interaction of a real distribution grid with an OFO controller which serves as a robustness test of OFO, 3) we give a tutorial on OFO, including potential extensions of the controller, that will assist the power system community in using this new technology for other control and optimization problems.
Overall, with this deployment for 24/7 operation in a real distribution grid, OFO has reached Technology Readiness Level (TRL) 7 ("system prototype demonstration in an operational environment") [Sta19].

## 7.2 Reactive Power Prices in Switzerland

The Swiss transmission grid operator, Swissgrid, is controlling its voltage with the help of generators and distribution grids that are connected to the transmission grid. Generators connected to the transmission grid have to participate in so-called active voltage support while subtransmission grid operators have to participate in so-called semi-active voltage support and they can opt-in for active voltage support. The basis for this voltage support scheme is that Swissgrid calculates a voltage reference for every bus in the transmission grid. This is done every 15 minutes through an Optimal Power Flow solver. All entities connected to the transmission grid are incentivized to adjust their reactive power flow such that it helps to drive the voltage at their connection point to the provided reference. The incentive scheme works as follows: Reactive power flows that are helping to drive the voltage to the reference are considered conform whereas reactive power flows that have the wrong sign and drive the voltage away from the reference are considered non-conform. In both active and semi-active voltage support, the generators and subtransmission grid operators are financially rewarded when they provide conform reactive power flows and they pay penalties when their reactive power flows are non-conform. The prices and penalties differ between active and semi-active voltage support. Furthermore, in semi-active voltage support, a tolerance band exists within which no reward nor penalty is billed. See [Swi23] for more information.
The subtransmission grid operators forward this pricing scheme to the distribution grid operators and charge or pay the distribution grids depending on the reactive power flow at the connection points between their subtransmission and the distribution grid. Hence, the distribution grid operators have a financial incentive to control their reactive power flows as well. This can be done with inverters and generators connected to the distribution grid as they can serve as reactive power sources. However, their reactive power injections have lower and upper limits ($q_{min}$ and $q_{max}$) due to the hardware limits of the inverters and generators. Furthermore, reactive power flows also affect the voltages in the grid and one needs to make sure that all voltages $v$ stay within their lower and upper limits ($v_{min}$ and $v_{max}$). Therefore, an optimization problem arises: How can reactive power injections $q$ be used to minimize the cost and maximize the reward from the subtransmission grid operator while satisfying the voltage and hardware limits. Mathematically speaking, we define the constraint optimization problem:

$$\begin{aligned} \min_{q} \; & cost(q) - reward(q) \\ \text{s.t.} \quad & q_{min} \leq q \leq q_{max} \\ & v_{min} \leq v \leq v_{max} \\ & v = h(q, d) \end{aligned} \tag{7.1}$$

We will describe the relationship between $q$ and $v$ as $v = h(q, d)$ where $h(\cdot)$ represents the power flow equations and $d$ is a vector of all active and reactive injections in the

grid. The goal of our OFO controller and its implementation in the distribution grid will be to iteratively change the reactive power injections $q$ until they converge to $q^\star$ that optimally solves the optimization problem (7.1).

## 7.3 Online Feedback Optimization

OFO is a method to solve optimization problems using measurements instead of models. This means it is a feedback control method instead of a model-based feedforward approach, compare Figure 7.1. The advantage is that a system model to evaluate $v = h(q, d)$ is not needed. Therefore, no cable and line parameters nor the topology need to be known, and also no active and reactive generation and consumption $d$ need to be measured or estimated. The only model information needed is $\nabla_q h(q, d)$, where $\nabla$ is the gradient operator. It describes how a small change in the reactive power injections $q$ will change the voltage $v$. Note that, this is not the same as knowing which voltage $v$ will result for a specific $q$. We only need to know the derivative of $v$ with respect to $q$. This is very similar to power transfer distribution factors which describe how a change in active power injections will change the line flows. We will from now on refer to this relationship between the effect of a change in $v$ for a small change in $q$ as the sensitivity.

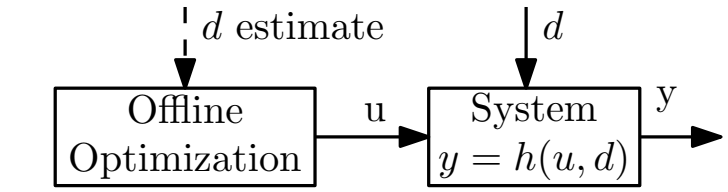


(a) Block diagram of Offline Optimization.

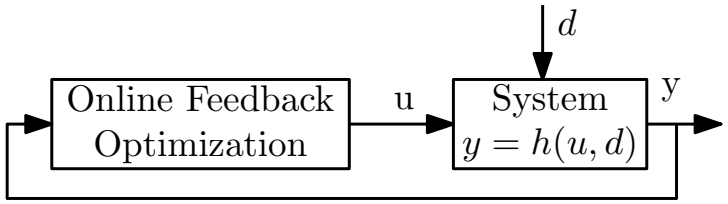


(b) Block diagram of Online Feedback Optimization.

Figure 7.1: Comparison of Offline Optimization and Online Feedback Optimization.

Now, we explain how to drive a power system to the optimal solution of an optimization problem using feedback. To do so we turn an optimization algorithm into a feedback controller, which is the core idea of OFO. This enables us to profit from closed-loop feedback control advantages such as robustness to disturbances $d$ and model mismatch in the sensitivity. This has been done with several different optimization algorithms which all lead to a different system behavior with specific advantages. For an overview see [Hau+21]. Here we explain the idea with an illustrative example, i.e. an optimization

problem with no constraints:

$$\min_{q} f(q) \tag{7.2}$$

and the optimization algorithm is gradient descent. This means to minimize a function $f(q)$ one takes gradient steps with step size $\alpha$. The gradient of $f(q)$ is $\nabla f(q)$ and a gradient step with step size $\alpha$ is:

$$q(k+1) = q(k) - \alpha \nabla f(q(k)). \tag{7.3}$$

This is an integral controller which keeps changing $q$ until the gradient of the cost function $\nabla f(q(k))$ is zero and therefore $q$ is driven to a locally optimal solution of (7.2). Just as with standard integral controllers and due to using feedback this works for a wide range of gains $\alpha$. An OFO controller based on standard gradient descent like (7.3) does not satisfy any constraints. To ensure that the constraints on the reactive power injections $q$ and voltages $v$ are satisfied, we can use projected gradient descent. An OFO controller derived from projected gradient descent was presented in [Häb+20]. We tailor the update law to our specific use case and get

$$q(k+1) = q(k) + \alpha \sigma(q(k), v(k)) \tag{7.4}$$

$$\begin{aligned} \sigma(q, v) = \arg\min_{w \in \mathbb{R}^p} \; & \|w + \nabla f(q)\|^2 \\ \text{s. t.} \quad & q_{min} \leq (q + \alpha w) \leq q_{max} \\ & v_{min} \leq (v + \alpha \nabla_q h(q, d) w) \leq v_{max} \end{aligned} \tag{7.5}$$

with $p$ being the number of reactive power setpoints. This is also an integral controller and it drives $\sigma(q, v)$ to zero, which is only zero when either $\nabla f(q)$ is zero or if the cost function $f(q)$ cannot be further decreased because constraints on $q$ or $v$ are reached. In both cases, the controller has iteratively changed $q$ until a local optimum has been reached, which is exactly what the controller is designed for. In our implementation in the distribution grid, we were not able to control the reactive power injections directly. However, we can control the power factor $\cos(\phi)$ of the power injections instead. The commands we can send are 0.8 ind., 0.85 ind., 0.9 ind., 0.95 ind., 1, 0.95 cap., 0.9 cap., 0.85 cap., 0.8 cap. This means our control input has to be a discrete value which we can enforce by adding integer constraints. We adapt the controller proposed in [Ort+23b] which results in:

$$\cos(\phi)(k+1) = \cos(\phi)(k) + \alpha \sigma(\cos(\phi(k)), v(k)) \tag{7.6}$$

$$\begin{aligned} \sigma(\cos(\phi), v) = \arg\min_{w \in \mathbb{R}^p} \; & \|w + \nabla f(q)\|^2 \\ \text{s.t.} \quad & \cos(\phi)_{min} \leq (\cos(\phi) + \alpha w) \leq \cos(\phi)_{max} \\ & v_{min} \leq (v + \alpha \nabla_{cos(\phi)} q(\cos(\phi), p) \nabla_q h(q, d) w) \leq v_{max} \\ & \frac{w}{0.05} \in \mathbb{Z}, \end{aligned} \tag{7.7}$$

where $\mathbb{Z}$ is the set of all integer variables and therefore w/0.05 can only take values of 0.05, -0.05, 0.1, etc. This is the control algorithm we implement on the distribution grid. Problem (7.7) is a mixed integer quadratic optimization problem (MIQP) that needs to be solved at every time step. Without integer constraints, it is easy and fast to solve even for large systems. With integer constraints, the problem is harder to solve but easier than solving the overall problem (7.1) including these integer constraints that the hardware setup demands.

### 7.3.1 Necessary Model Information

The controller used in the implementation needs to know how a change in the $\cos(\phi)$ setpoint is going to affect the voltage. This can be split into two parts. First how a change in $\cos(\phi)$ changes the reactive power injections $q$ ($\nabla_{\cos(\phi)} q(\cos(\phi))$) and second how the reactive power injections affect the voltage ($\nabla_q h(q, d)$). Such sensitivities can either be derived experimentally by changing an input and observing the change in the output or the same can be done using a simulation model of the grid. Furthermore, the sensitivity can be derived mathematically using the admittance matrix of the grid, and the power flow equations [BD15].

The sensitivity $\nabla_q h(q, d)$ depends on both the topology and line impedances as well as $q$ and $d$. Therefore, the sensitivity changes over time and is generally hard to compute exactly. One has to work with approximations which poses a challenge to any kind of optimization. In such conditions of uncertainty, OFO controllers are particularly effective due to their feedback nature. Approximating the sensitivity with a constant matrix has proven to work well [Ort+20a] and most importantly, even with an approximate sensitivity, the controller will enforce the constraints on both the input ($q$ or $\cos(\phi)$) and output ($v$) in steady-state. Also, temporary constraint violations [Häb+20] and the suboptimality are bounded [CSB19]. Last but not least, the sensitivity can be learned online from measurements [Pic+22b] and OFO controllers exist that rely on zeroth order optimization algorithms and therefore do not need any sensitivity [He+22].

### 7.3.2 Possible Extensions

OFO controllers offer great flexibility and possible extensions. We show some that are helpful in power grids.

#### State estimation

Instead of feeding the raw voltage measurements into the OFO controller one can run the measurements through a state estimation and provide the result of the state estimation to the controller instead. The convergence of this feedback system was proven in [PBD20].

This also enables to control voltages that are not directly measured and get estimated instead.

#### Time-varying constraints

The constraints in the control law (7.7) can be different at every time step. This allows to include time-varying constraints of the overarching optimization problem (7.1). For example, with certain inverters, one can directly command reactive power injections $q$. Given that an inverter has a current limit the available capacity for reactive power injections would depend on the active power injections which change over time. In other applications, time-varying constraints could be dynamic line ratings or they could be used to temporarily block taps changers, make the controller reduce the power flow on a line, or lower the voltage angle over a circuit breaker.

#### Updating the sensitivity

The sensitivity depends on the topology, tap changer positions, line parameters, generation, and consumption. These may change over time and therefore also the sensitivity can change over time. If for example, the topology has changed the sensitivity could be recomputed or the results of a new state estimation could be used to update the sensitivity.

## 7.4 Distribution Grid Deployment

### 7.4.1 Hardware and Communication Setup

The area of the grid under control by the OFO controller is visualized in Figure 7.2. We control 16 inverters located at point 2 which is approximately 9.2 km away from the connection to the subtransmission grid. Their total rated apparent power is 800 kVA and with our maximum power factor of 0.8, this corresponds to 640 kW and 480 kVAr. These inverters operate at 400 V and are located close to a transformer which transforms the power to the 16 kV radial grid whose topology is depicted in the figure. Voltage magnitude and power measurements are taken throughout the grid and communicated to the SCADA system of the distribution grid operator.
To implement our controller we retrofitted this infrastructure as depicted in Figure 7.3. Our controller gets measurements from the SCADA system through an existing Archive Data Server in a CSV file once every minute. It then calculates the new power factor setpoints for the inverters which are collected in a data storage and given to a Modbus server. This Modbus server communicates the setpoints to a protocol converter which transmits the setpoints to the SCADA system over an IEC104 protocol. We equip the

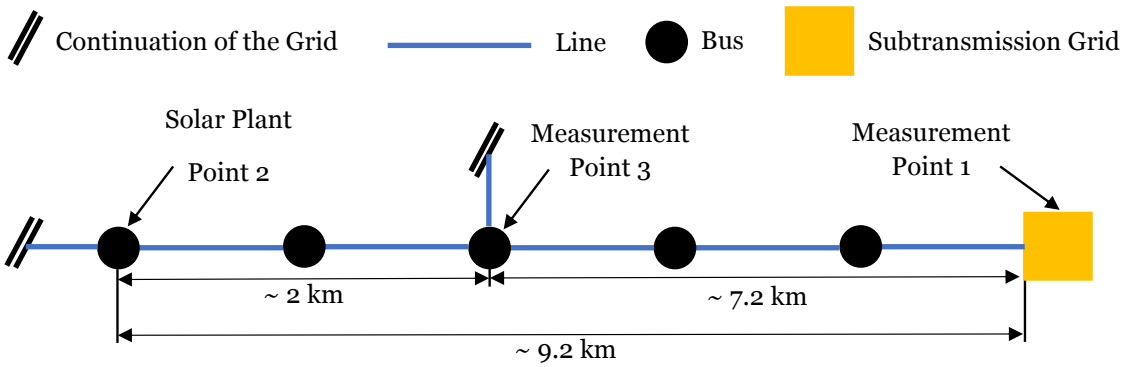


Figure 7.2: The part of the grid controlled by OFO with the connection to the subtransmission grid operator, the measurement points, and the grid topology.

inverters with a Siemens Smartgrid-Box A8000 to be able to send them these setpoints. The SCADA system communicates with this A8000 through an IEC 60870-5-104 protocol. Data logging at the inverters is done with an ADL-MXSpro from Meier-NT. A dashboard visualizes the measurements and setpoints and it can be used to enable, disable, and reset the controller or for manually choosing the setpoints. To enable these features the dashboard crawls data from the data storage and communicates with the Modbus server.
The OFO controller, the dashboard, and the data storage are implemented on a virtual machine inside the control room. Figure 7.4 shows an overview of the programs running and interacting on the virtual machine. The code was written in Python and its execution is computationally very light, meaning no large computation power is needed.

### 7.4.2 Controller Setup

The controller is implemented as follows. The SCADA system provides the controller with voltage magnitude measurements of the three points shown in Figure 7.2. At measurement point 1 we also get the reactive power flow which is needed to calculate $\nabla f(q)$. The goal is to optimize the reactive power flow at the connection point to the external grid (measurement point 1). The cost function $f(q)$ is based on the pricing scheme of the subtransmission grid operator and it is a piece-wise linear function, see Figure 7.5. Due to the linearity the derivative $\nabla f(q)$ is constant in each area. There is a high cost for capacitive reactive energy and a small reward for inductive reactive energy (MVArh). A deadband with no cost nor reward exists and is of size 0.25% $S_n$ where $S_n$ is the sum of the apparent power of all transformers at the connection point to the subtransmission grid. Recall that, $\sigma = \nabla f(q)$ when no constraints are active and note that the derivative of the cost function $\nabla f(q)$ is zero in the gray area. Hence, $\sigma$ would therefore be zero in the gray area (as long as there are no voltage violations) and the

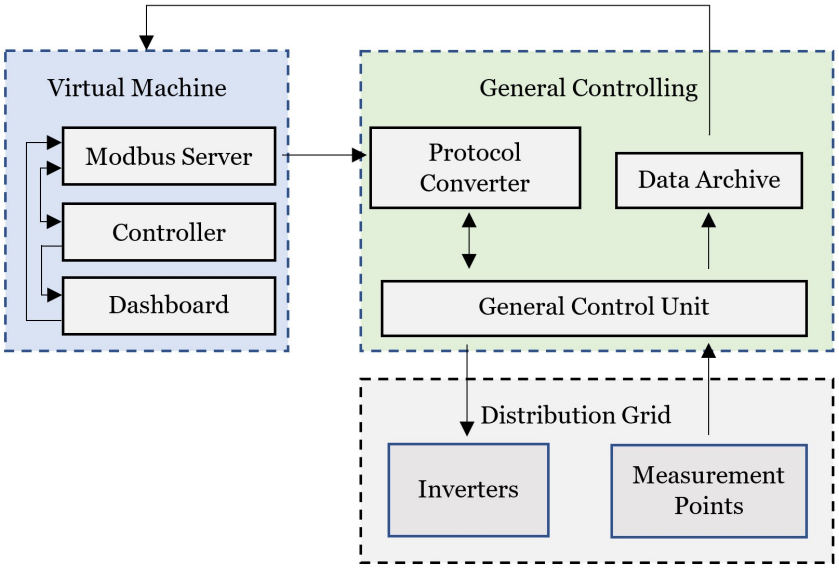


Figure 7.3: High-level overview of the system including interfaces and communication links.

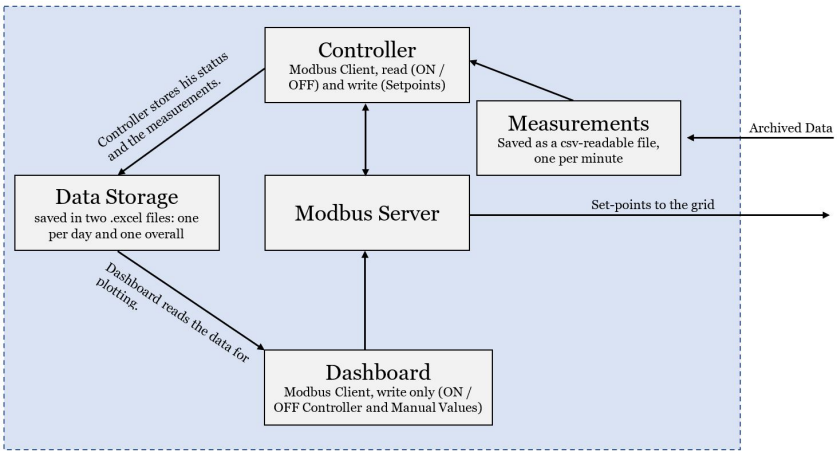


Figure 7.4: Overview of the programs inside the virtual machine.

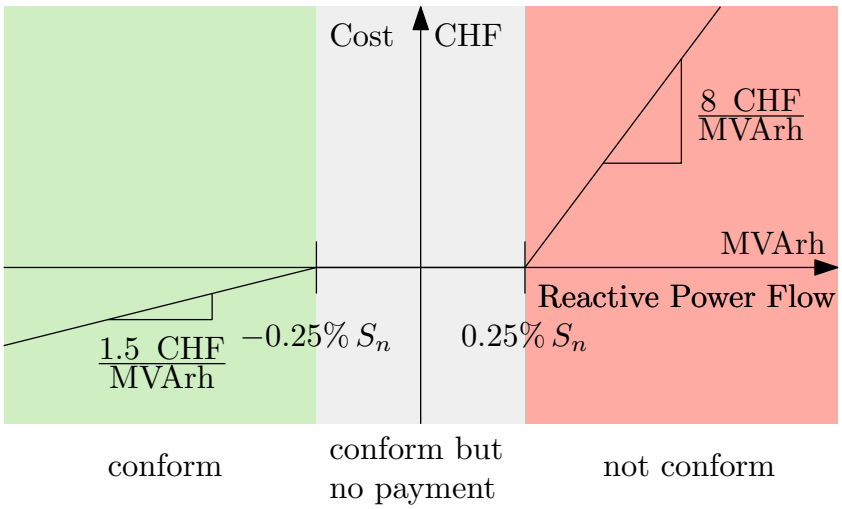


Figure 7.5: Cost function for reactive power flows into the subtransmission grid based on the pricing scheme of the subtransmision grid operator. The distribution grid operator has to pay a high penalty for capacitive flows and gets a small amount of money for inductive flows.

controller would not change the setpoints. To circumvent this, we artificially change the cost function to have a small gradient in the gray area which ensures that the controller tries to drive the reactive power flows into the conform (green) area. The sensitivity $\nabla_q h(q, d)$ was calculated based on a model and is kept constant.

Given that our control approach is relying on communication infrastructure, it is necessary to define a fallback strategy in case the communication breaks down. In case the controller does not receive measurements for five minutes it instructs the inverter to operate at a power factor of 1. If the inverters do not receive commands from the controller anymore, they also set their power factor to 1.

## 7.5 Results and Data Analysis

In this section, we analyze the consequences of using off-the-shelf hardware, the interaction of an OFO controller with a real distribution grid, and the behavior of the controller. The controller went live in December 2022 and the data analysis of the first months revealed the following.

The controller gives power factor setpoints $\cos(\phi)$ to the inverters. Figure 7.6 shows the active and reactive power injections of the inverters for a power factor setpoint of 0.8 inductive. The figure shows that the inverters do not track the setpoint well. Especially for low active power injections the reactive power injection is capacitive even though the controller was asking for a power factor of 0.8 inductive. This happens because old norms only required reactive power tracking for active power generation of larger than 5% of the

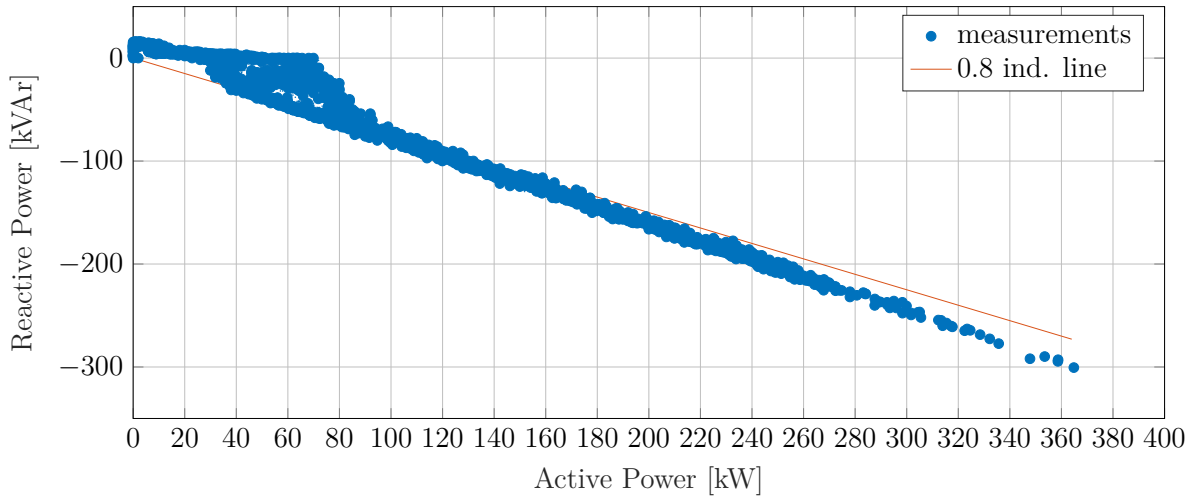


Figure 7.6: Active and reactive power injections of the inverters in the month of January together with a line indicating a power factor of 0.8 inductive.

rated power. These measurements highlight how important it is to utilize measurements as feedback because not only a grid model can be wrong, but also actuators might not follow their reference.

In 2022, the pricing scheme of the subtransmission grid operator was different from the one in Figure 7.5 and was dependent on the time of day. Therefore, the optimization problem changed at certain times and the controller automatically adjusted the setpoints to drive them to the optimal solution of the new optimization problem. Figure 7.7 shows the behavior of the controller when the cost function changes. Note that, the controller iteratively changes the setpoints over several steps. This iterative behavior is at the core of OFO as it allows to work with minimal model information. It can also be seen that there is a time delay of approximately four minutes between the setpoints being changed and the inverters adjusting their reactive power injections. The presence of this time delay means that voltage violations could persist for up to four minutes before the controller is able to mitigate them. Currently, the VDE 4105 norm is allowing temporary voltage violations for up to one minute [VDE18]. We conclude that a sampling time of the controller of fewer than 10 seconds should be chosen for future implementations to guarantee that voltage violations are cleared within one minute.

The sensors in the grid only send a new measurement to the control room when the measured value has changed by more than 1%. The gathered data suggests that the controller does not have a problem with the measurements being triggered.

Note that, the distribution grid is currently not experiencing voltage violation and hence the virtual reinforcement feature of the controller could not be evaluated.

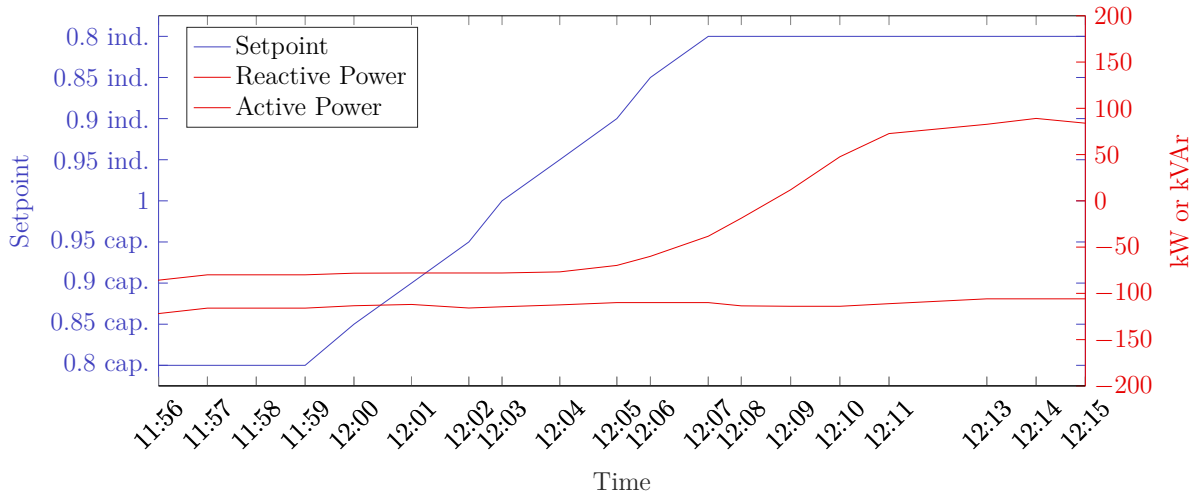


Figure 7.7: Change of the setpoint and reactive power when the cost function changes at noon.

## 7.6 Conclusion

In this chapter, we presented the retrofitting of existing grid infrastructure to optimize reactive power flows in a distribution grid using an OFO controller that controls reactive power injections of PV inverters. The controller also enforces voltage limits by adjusting the reactive power injections which means there exists potential to virtually reinforce the grid by mitigating voltage limit violations. The implementation shows that the controller is robust against model mismatch, is compatible with the legacy grid infrastructure, and can work with triggered measurements. We consider this 24/7 implementation to be a system prototype demonstration in an operational environment and conclude that the OFO control method has therefore reached technology readiness level 7.
Further investigations are needed to quantify the monetary value of the virtual grid reinforcement that voltage control through reactive power can provide. Also, given the high technology readiness level, OFO might be considered for commercial control room software. Finally, the principle of defining a control problem as an optimization problem and then using an OFO controller to solve the optimization and therefore the control problem could be applied to more problems, e.g. active power curtailment, curative actions and automatic redispatch, disaggregation of flexibility commands onto several resources.

CHAPTER 8

# Conclusions and Outlook

## Conclusions

The research in this thesis achieved the following goals: 1) evaluating the applicability of Online Feedback Optimization (OFO) controllers to solve several power system problems, 2) further developing and tailoring OFO controllers for power system applications, and 3) demonstrating that OFO controllers work well with real power grid hardware, as shown in two OFO controller implementations in a laboratory setup and one in a real distribution grid. Overall, the research in this thesis helped to show that the OFO control method is a suitable tool to solve power system problems, and the implementations have brought the method to Technology Readiness Level (TRL) level 7.

Finally, the research in this thesis allows for the following statement:

> *OFO controllers can operate the power grid in real-time with minimal model information and computation power, are robust against model mismatch, converge to the optimal solution, their tuning is limited to few parameters, and defining the control goal through an optimization problem is powerful and versatile. It can be concluded that OFO has become a viable tool with which engineers can solve power system problems.*

## Future research

The potential future research in this area can be divided into work concerning the application to power systems and the theory behind OFO.

**Power System Problems**

The research in this thesis showed that OFO controllers have the potential to calculate curative actions in real-time for grids that are operated according to a curative $N-1$ philosophy. The potential is large, however, this thesis analyzed a very specific use case, and therefore more research should be conducted. Open questions are: 1) in what other kinds of scenarios can OFO controllers be used to derive curative actions, 2) what are

suitable optimization problems for the OFO controllers that lead to them calculating effective curative actions for these scenarios, and 3) how could such OFO controllers be integrated into existing control methods and how do they interact?

Similar to the calculation of curative actions, OFO controllers could be used to derive redispatch decisions in real-time. This could ultimately help to operate the power system infrastructure at its limit, with redispatch decisions only being calculated and implemented when a contingency has occurred.

OFO controllers guarantee the satisfaction of input constraints at all times. Satisfaction of output constraints is guaranteed in steady state. Therefore, temporary constraint violations are possible, and their size depends on the choice of OFO controller. Research should be conducted on which constraints in which power system problems can be temporarily violated and for how long. If no violations can be permitted, it needs to be analyzed by how much the corresponding constraints have to be adjusted to eliminate temporary violations as well.

### Theoretical Questions

Applying an OFO controller to a physical system leads to the interconnection of two dynamic systems. The stability of this interconnection can be guaranteed if the physical system is sufficiently faster than the dynamics of the OFO controller. This is the case when the step size of the OFO controller is small enough. There does exist a method based on timescale separation that can calculate a value for the step size that guarantees stability [Hau+20a]. However, the method yields highly conservative results for the step size, which would lead to controllers that are not fast enough to be used in practice. Therefore, more research efforts should be aimed at finding a better upper bound on the OFO controller step size that still guarantees stability and convergence.

The main tuning parameters of an OFO controller are its step size and the sampling time with which it is implemented. Both parameters influence the overall system behavior, and their tuning can be non-trivial as they also influence each other. The faster the sampling time is, the less time the physical system has to settle to a steady state. The longer the sampling time is, the longer it takes until new measurements are collected, which increases the time that, e.g., constraint violations can persist. The higher the step size and the lower the sampling rate, the faster the controller converges, but temporary constraint violations increase in size. Finding guidelines for the controller tuning would facilitate the use of OFO controller by practitioners.

Another open theoretical research question is what happens when several OFO controllers are operating in the same physical system and therefore interact with each other. Questions worth answering are: 1) do they affect each other's stability, 2) which operating point do they converge to, and 3) what are potential coordination schemes between the OFO controllers that enable an overall more desirable system behavior?

# Bibliography


[Age21] I. E. Agency. *World Energy Outlook 2021*. Tech. rep. IEA, 2021.

[Age22] T. I. R. E. Agency. *Renewable Energy Statistics 2022*. Tech. rep. 2022.

[BS85] E. Bai and S. Sastry. "Persistency of excitation, sufficient richness and parameter convergence in discrete time adaptive control". In: *Systems & Control Letters* 6.3 (1985), pp. 153–163.

[Bec+14] C. Beckel, W. Kleiminger, R. Cicchetti, T. Staake, and S. Santini. "The ECO Data Set and the Performance of Non-Intrusive Load Monitoring Algorithms". In: *Proc. 1st ACM Conf. on Embedded Systems for Energy-Efficient Buildings*. Nov. 2014.

[BDS19] A. Bernstein, E. Dall'Anese, and A. Simonetto. "Online primal-dual methods with measurement feedback for time-varying convex optimization". In: *IEEE Trans. Signal Process.* 67.8 (2019), pp. 1978–1991.

[BD19] A. Bernstein and E. Dall'Anese. "Real-time feedback-based optimization of distribution grids: A unified approach". In: *IEEE Transactions on Control of Network Systems* 6.3 (2019), pp. 1197–1209.

[Ber99] D. P. Bertsekas. *Nonlinear programming*. 2nd. Belmont (MA): Athena Scientific, 1999.

[Ber97] D. P. Bertsekas. "Nonlinear programming". In: *Journal of the Operational Research Society* 48.3 (1997), pp. 334–334.

[Bia+21a] G. Bianchin, J. Cortes, J. I. Poveda, and E. Dall'Anese. "Time-varying optimization of LTI systems via projected primal-dual gradient flows". In: *IEEE Transactions on Control of Network Systems* (2021).

[Bia+21b] G. Bianchin, M. Vaquero, J. Cortes, and E. Dall'Anese. "Data-Driven Synthesis of Optimization-Based Controllers for Regulation of Unknown Linear Systems". In: (Dec. 2021).

[Bol18] S. Bolognani. "Grid Topology Identification Via Distributed Statistical Hypothesis Testing". In: *Big Data Application in Power Systems*. Ed. by R. Arghandeh and Y. Zhou. Elsevier, 2018, pp. 281–301.

[Bol+13] S. Bolognani, N. Bof, D. Michelotti, R. Muraro, and L. Schenato. "Identification of power distribution network topology via voltage correlation analysis". In: *52nd Conference on Decision and Control*. 2013, pp. 1659–1664.

[Bol+15] S. Bolognani, R. Carli, G. Cavraro, and S. Zampieri. "Distributed reactive power feedback control for voltage regulation and loss minimization". In: *IEEE Transactions on Automatic Control* 60.4 (Apr. 2015).

[Bol+19] S. Bolognani, R. Carli, G. Cavraro, and S. Zampieri. "On the Need for Communication for Voltage Regulation of Power Distribution Grids". In: *IEEE Transactions on Control of Network Systems* 6.3 (Sept. 2019), pp. 1111–1123.

[BD15] S. Bolognani and F. Dörfler. "Fast power system analysis via implicit linearization of the power flow manifold". In: *53rd Annual Allerton Conference on Communication, Control, and Computing (Allerton)*. 2015, pp. 402–409.

[BZ15] S. Bolognani and S. Zampieri. "On the existence and linear approximation of the power flow solution in power distribution networks". In: *IEEE Transactions on Power Systems* 31.1 (2015), pp. 163–172.

[COC+12] M. B. Cain, R. P. O'neill, A. Castillo, et al. "History of optimal power flow and formulations". In: *Federal Energy Regulatory Commission* 1 (2012), pp. 1–36.

[CC17] G. Cavraro and R. Carli. "Local and Distributed Voltage Control Algorithms in Distribution Networks". In: *IEEE Transactions on Power Systems* 33.2 (2017), pp. 1420–1430.

[CPL21] X. Chen, J. I. Poveda, and N. Li. "Model-Free Optimal Voltage Control via Continuous-Time Zeroth-Order Methods". In: (Dec. 2021).

[Che+21] X. Chen, G. Qu, Y. Tang, S. Low, and N. Li. "Reinforcement learning for decision-making and control in power systems: Tutorial, review, and vision". In: *arXiv preprint arXiv:2102.01168* (2021).

[CDB19] M. Colombino, E. Dall'Anese, and A. Bernstein. "Online optimization as a feedback controller: Stability and tracking". In: *IEEE Transactions on Control of Network Systems* 7.1 (2019), pp. 422–432.

[CSB19] M. Colombino, J. W. Simpson-Porco, and A. Bernstein. "Towards robustness guarantees for feedback-based optimization". In: *58th Conference on Decision and Control (CDC)*. 2019, pp. 6207–6214.

[Com16] E. Commission. "Commission Regulation (EU) 2016/631 of 14 April 2016 establishing a network code on requirements for grid connection of generators". In: *OJ* L112 (2016), pp. 1–68.

[Com17] E. Commission. *Commission Regulation (EU) 2017/1485 of 2 August 2017, establishing a guideline on electricity transmission system operation*. 2017.

[CLD19] J. Coulson, J. Lygeros, and F. Dörfler. "Data-enabled predictive control: In the shallows of the DeePC". In: *2019 18th European Control Conference (ECC)*. IEEE. 2019, pp. 307–312.

[DS16] E. Dall'Anese and A. Simonetto. "Optimal power flow pursuit". In: *IEEE Transactions on Smart Grid* 9.2 (2016), pp. 942–952.

[DC18] D. Deka and M. Chertkov. "Topology Learning in Radial Distribution Grids". In: *Big Data Application in Power Systems*. Ed. by R. Arghandeh and Y. Zhou. Elsevier, 2018, pp. 261–279.

[Dom+23] A. D. Dominguez-Garcia, M. Zholbaryssov, T. Amuda, and O. Ajala. "An Online Feedback Optimization Approach to Voltage Regulation in Inverter-Based Power Distribution Networks". In: *arXiv preprint arXiv:2303.08164* (2023).

[Dör+19] F. Dörfler, S. Bolognani, J. W. Simpson-Porco, and S. Grammatico. "Distributed Control and Optimization for Autonomous Power Grids". In: *Proc. European Control Conference (ECC)*. June 2019.

[EGH16] V. A. Evangelopoulos, P. S. Georgilakis, and N. D. Hatziargyriou. "Optimal operation of smart distribution networks: A review of models, methods and future research". In: *Electric Power Systems Research* 140 (2016), pp. 95–106.

[FZC15] M. Farivar, X. Zho, and L. Che. "Local voltage control in distribution systems: An incremental control algorithm". In: *2015 IEEE international conference on smart grid communications (SmartGridComm)*. 2015.

[GL16] L. Gan and S. H. Low. "An online gradient algorithm for optimal power flow on radial networks". In: *IEEE Journal on Selected Areas in Communications* 34.3 (2016), pp. 625–638.

[Guo+23] Y. Guo, X. Zhou, C. Zhao, L. Chen, G. Hug, and T. H. Summers. "An Online Joint Optimization–Estimation Architecture for Distribution Networks". In: *IEEE Transactions on Control Systems Technology* (2023).

[Häb+20] V. Häberle, A. Hauswirth, L. Ortmann, S. Bolognani, and F. Dörfler. "Non-convex feedback optimization with input and output constraints". In: *IEEE Control Systems Letters* 5.1 (2020), pp. 343–348.

[Hal+22] S. Hall, L. Ortmann, M. Picallo, and F. Dörfler. "Real-time Projected Gradient-based Nonlinear Model Predictive Control with an Application to Anesthesia Control". In: *2022 IEEE 61st Conference on Decision and Control (CDC)*. IEEE. 2022, pp. 6193–6198.

[HUJ21] H. Haugdal, K. Uhlen, and H. Jóhannsson. "An open source power system simulator in python for efficient prototyping of wampac applications". In: *2021 IEEE Madrid PowerTech*. IEEE. 2021, pp. 1–6.

[Hau+20a] A. Hauswirth, S. Bolognani, G. Hug, and F. Dörfler. "Timescale separation in autonomous optimization". In: *IEEE Transactions on Automatic Control* 66.2 (2020), pp. 611–624.

[Hau+21] A. Hauswirth, S. Bolognani, G. Hug, and F. Dörfler. "Optimization algorithms as robust feedback controllers". In: *arXiv:2103.11329* (2021).

[Hau+20b] A. Hauswirth, L. Ortmann, S. Bolognani, and F. Dörfler. "Limit behavior and the role of augmentation in projected saddle flows for convex optimization". In: *IFAC-PapersOnLine* 53.2 (2020), pp. 5511–5517.

[Hau+17] A. Hauswirth, A. Zanardi, S. Bolognani, F. Dörfler, and G. Hug. "Online optimization in closed loop on the power flow manifold". In: *2017 IEEE Manchester PowerTech*. 2017, pp. 1–6.

[He+22] Z. He, S. Bolognani, J. He, F. Dörfler, and X. Guan. "Model-Free Nonlinear Feedback Optimization". In: *arXiv:2201.02395* (2022).

[Hel] HelioClim-3. *HelioClim-3 Database of Solar Irradiance*. http://www.soda-pro.com/web-services/radiation/helioclim-3-archives-for-free. Accessed: 2017-12-01.

[Hin13] P. Hintjens. *ZeroMQ: Messaging for many applications*. " O'Reilly Media, Inc.", 2013.

[Höf+12] B. Höflich, P. Richard, J. Völker, C. Rehtanz, M. Greve, B. Gwisdorf, J. Kays, T. Noll, J. Schwippe, A. Seack, et al. "dena-Verteilnetzstudie Ausbau-Und Innovationsbedarf der Stromverteilnetze in Deutschland bis 2030". In: *Deutsche Energie-Agentur: Berlin, Germany* (2012).

[Hot21] G. Hotz. "Online Feedback Optimization for Emergency Power System Operation". MA thesis. ETH Zurich, 2021.

[IEE] IEEE 1547-2018. *Standard for Interconnection and Interoperability of Distributed Energy Resources with Associated Electric Power Systems Interfaces*. Standard.

[Ipa+22] H. Ipach, L. Fisser, C. Becker, and A. Timm-Giel. "Distributed utility-based real-time power flow optimization in ICT-enabled low voltage distribution grids". In: *IET Generation, Transmission & Distribution* (2022).

[IA09] A. Ipakchi and F. Albuyeh. "Grid of the future". In: *IEEE power and energy magazine* 7.2 (2009), pp. 52–62.

[IM10] R. Isermann and M. Münchhof. *Identification of dynamic systems: an introduction with applications*. Springer Science & Business Media, 2010.

[Jaz70] A. H. Jazwinski. “Mathematics in science and engineering”. In: *Stochastic processes and filtering theory* 64 (1970).

[KAH19] S. Karagiannopoulos, P. Aristidou, and G. Hug. “Data-driven Local Control Design for Active Distribution Grids using off-line Optimal Power Flow and Machine Learning Techniques”. In: *IEEE Transactions on Smart Grid* (2019).

[Ker91] W. Kersting. “Radial distribution test feeders”. In: *IEEE Transactions on Power Systems* 6.3 (1991), pp. 975–985.

[Kle+23] F. Klein-Helmkamp, F. Böhm, L. Ortmann, A. Winkens, F. Schmidtke, S. Bolognani, F. Dörfler, and A. Ulbig. “Providing Curative Distribution Grid Flexibility Utilizing Online Feedback Optimization - Laboratory Evaluation”. In: *submitted to IEEE PES ISGT EUROPE 2023* (2023).

[KND22] T. Kolster, S. Niessen, and M. Duckheim. “Providing Distributed Flexibility for Curative Transmission System Operation Using a Scalable Robust Optimization Approach”. In: *Electric Power Systems Research* 211 (2022), p. 108431.

[KP12] S. G. Krantz and H. R. Parks. *The implicit function theorem: history, theory, and applications*. Springer Science & Business Media, 2012.

[Kro+20a] B. Kroposki, A. Bernstein, J. King, and F. Ding. “Good grids make good neighbors”. In: *IEEE Spectrum* 57.NREL/JA-5D00-78521 (2020).

[Kro+20b] B. Kroposki, A. Bernstein, J. King, D. Vaidhynathan, X. Zhou, C.-Y. Chang, and E. Dall’Anese. “Autonomous energy grids: Controlling the future grid with large amounts of distributed energy resources”. In: *IEEE Power and Energy Magazine* 18.6 (2020), pp. 37–46.

[LSM20] L. S. Lawrence, J. W. Simpson-Porco, and E. Mallada. “Linear-convex optimal steady-state control”. In: *IEEE Transactions on Automatic Control* 66.11 (2020), pp. 5377–5384.

[Len99] L. Lennart. “System identification: theory for the user”. In: *PTR Prentice Hall, Upper Saddle River, NJ* 28 (1999).

[LWL22] S. Li, W. Wu, and Y. Lin. “Robust Data-driven and Fully Distributed Volt/VAR Control for Active Distribution Networks with Multiple Virtual Power Plants”. In: *IEEE Transactions on Smart Grid* 13.4 (2022), pp. 2627–2638.

[LSZ17] H. J. Liu, W. Shi, and H. Zhu. “Distributed voltage control in distribution networks: Online and robust implementations”. In: *IEEE Transactions on Smart Grid* 9.6 (2017), pp. 6106–6117.

[Lof04] J. Lofberg. "YALMIP: A toolbox for modeling and optimization in MATLAB". In: *IEEE International Conference on Robotics and Automation*. 2004, pp. 284–289.

[Low14] S. H. Low. "Convex relaxation of optimal power flow—Part I: Formulations and equivalence". In: *IEEE Transactions on Control of Network Systems* 1.1 (2014), pp. 15–27.

[MFL19] S. Magnusson, C. Fischione, and N. Li. "Optimal Voltage Control Using Event Triggered Communication". In: *Proc. 10th ACM Intl. Conf. Future Energy Systems*. 2019, pp. 343–354.

[Mag+19] S. Magnússon, G. Qu, C. Fischione, and N. Li. "Voltage control using limited communication". In: *IEEE Transactions on Control of Network Systems* 6.3 (Sept. 2019), pp. 993–1003.

[MQL20] S. Magnússon, G. Qu, and N. Li. "Distributed Optimal Voltage Control with Asynchronous and Delayed Communication". In: *IEEE Transactions on Smart Grid* (2020). In press.

[Mat+23] J. G. Matt, L. Ortmann, S. Bolognani, and F. Dörfler. "Virtual Power Grid Reinforcement via Coordinated Volt/VAr Control". In: *arXiv preprint arXiv:2305.04666* (2023).

[MER] MERRA-2. *The Modern-Era Retrospective analysis for Research and Applications, Version 2 (MERRA-2) Web service*. http://www.soda-pro.com/web-services/meteo-data/merra. Accessed: 2017-12-01.

[MBV20] K. Moffat, M. Bariya, and A. Von Meier. "Unsupervised Impedance and Topology Estimation of Distribution Networks—Limitations and Tools". In: *IEEE Transactions on Smart Grid* 11.1 (2020), pp. 846–856.

[MH19] D. K. Molzahn and I. A. Hiskens. "A Survey of Relaxations and Approximations of the Power Flow Equations". In: *Foundations and Trends in Electric Energy Systems* 4.1-2 (Feb. 2019), pp. 1–221.

[Mol+17] D. K. Molzahn, F. Dörfler, H. Sandberg, S. H. Low, S. Chakrabarti, R. Baldick, and J. Lavaei. "A survey of distributed optimization and control algorithms for electric power systems". In: *IEEE Transactions on Smart Grid* 8.6 (2017), pp. 2941–2962.

[MPG87] A. Monticelli, M. Pereira, and S. Granville. "Security-constrained optimal power flow with post-contingency corrective rescheduling". In: *IEEE Trans. on Power Systems* 2.1 (1987), pp. 175–180.

[Mug+16] C. Mugnier, K. Christakou, J. Jaton, M. De Vivo, M. Carpita, and M. Paolone. "Model-less/measurement-based computation of voltage sensitivities in unbalanced electrical distribution networks". In: *2016 Power Systems Computation Conference (PSCC)*. IEEE. 2016, pp. 1–7.

[NER20] NERC. *Glossary of Terms Used in NERC Reliability Standards*. 2020.

[NCW20a] S. Nowak, Y. C. Chen, and L. Wang. "A Measurement-based Gradient-descent Method to Optimally Dispatch DER Reactive Power". In: *2020 47th IEEE Photovoltaic Specialists Conference (PVSC)*. IEEE. 2020, pp. 0028–0032.

[NCW20b] S. Nowak, Y. C. Chen, and L. Wang. "Measurement-based optimal DER dispatch with a recursively estimated sensitivity model". In: *IEEE Transactions on Power Systems* 35.6 (2020), pp. 4792–4802.

[Oli+23] J. C. Olives-Camps, Á. R. del Nozal, J. M. Mauricio, and J. M. Maza-Ortega. "A holistic model-less approach for the optimal real-time control of power electronics-dominated AC microgrids". In: *Applied Energy* 335 (2023), p. 120761.

[Oli+22] J. C. Olives-Camps, Á. R. del Nozal, J. M. Mauricio, and J. M. Maza-Ortega. "A model-less control algorithm of DC microgrids based on feedback optimization". In: *International Journal of Electrical Power & Energy Systems* 141 (2022), p. 108087.

[Oli+16] F. Olivier, P. Aristidou, D. Ernst, and T. Van Cutsem. "Active Management of Low-Voltage Networks for Mitigating Overvoltages Due to Photovoltaic Units". In: *IEEE Transactions on Smart Grid* 7.2 (Mar. 2016), pp. 926–936.

[Ort22] L. Ortmann. *Gitlab repository*. https://gitlab.ethz.ch/ortmannl/online-feedback-optimization-for-transmission-grid-operation. 2022.

[Ort23] L. Ortmann. *SimulinkMATPOWER*. https://github.com/Lukas738/SimulinkMATPOWER. 2023.

[Ort+20a] L. Ortmann, A. Hauswirth, I. Caduff, F. Dörfler, and S. Bolognani. "Experimental validation of feedback optimization in power distribution grids". In: *Electric Power Systems Research* 189 (2020), p. 106782.

[Ort+23a] L. Ortmann, G. Hotz, S. Bolognani, and F. Dörfler. "Real-time Curative Actions for Power Systems via Online Feedback Optimization". In: *accepted at PowerTech* (2023).

[Ort+23b] L. Ortmann, J. Maeght, P. Panciatici, F. Dörfler, and S. Bolognani. "Online Feedback Optimization for Subtransmission Grid Operation". In: *arXiv preprint arXiv:2212.07795* (2023).

[Ort+20b] L. Ortmann, A. Prostejovsky, K. Heussen, and S. Bolognani. "Fully distributed peer-to-peer optimal voltage control with minimal model requirements". In: *Electric Power Systems Research* 189 (2020), p. 106717.

[Ort+23c] L. Ortmann, C. Rubin, A. Scozzafava, J. Lehmann, S. Bolognani, and F. Dörfler. "Deployment of an Online Feedback Optimization Controller for Reactive Power Flow Optimization in a Distribution Grid". In: *arXiv preprint arXiv:2305.06702* (2023).

[Pad+21] H. Padullaparti, A. Pratt, I. Mendoza, S. Tiwari, M. Baggu, C. Bilby, and Y. Ngo. "Peak load management in distribution systems using legacy utility equipment and distributed energy resources". In: *2021 IEEE Green Technologies Conference (GreenTech)*. IEEE. 2021, pp. 435–441.

[PBD20] M. Picallo, S. Bolognani, and F. Dörfler. "Closing the loop: Dynamic state estimation and feedback optimization of power grids". In: *Electric Power Systems Research* 189 (2020), p. 106753.

[Pic+22a] M. Picallo, D. Liao-McPherson, S. Bolognani, and F. Dörfler. "Cross-layer design for real-time grid operation: Estimation, optimization and power flow". In: *Electric Power Systems Research* 212 (2022), p. 108378.

[Pic+22b] M. Picallo, L. Ortmann, S. Bolognani, and F. Dörfler. "Adaptive real-time grid operation via Online Feedback Optimization with sensitivity estimation". In: *Electric Power Systems Research* 212 (2022), p. 108405.

[Pro+16] A. M. Prostejovsky, O. Gehrke, A. M. Kosek, T. Strasser, and H. W. Bindner. "Distribution Line Parameter Estimation Under Consideration of Measurement Tolerances". In: *IEEE Transactions on Industrial Informatics* 12.2 (2016), pp. 726–735.

[QL19] G. Qu and N. Li. "Optimal distributed feedback voltage control under limited reactive power". In: *IEEE Transactions on Power Systems* 35.1 (2019), pp. 315–331.

[Rey+18] L. Reyes-Chamorro, A. Bernstein, N. J. Bouman, E. Scolari, A. M. Kettner, B. Cathiard, J.-Y. Le Boudec, and M. Paolone. "Experimental validation of an explicit power-flow primary control in microgrids". In: *IEEE Transactions on Industrial Informatics* 14.11 (2018), pp. 4779–4791.

[RTE19] RTE. *Schéma décennal de développement du réseau (SDDR) 2019 - Rapport complet*. Tech. rep. RTE Réseau de transport d'électricité, 2019.

[RO23] C. Rubin and L. Ortmann. *Neplan to PandaPower*. https://gitlab.ethz.ch/ortmannl/neplan-to-pandapower. 2023.

[SR16] M. Schmidthaler and J. Reichl. "Assessing the socio-economic effects of power outages ad hoc". In: *Computer Science-Research and Development* 31.3 (2016), pp. 157–161.

[Sem19] D. Semitsoglou-Tsiapos. "Evaluation of Distributed Algorithms for Electric Power Systems Applications". English. MA thesis. Technical University of Denmark (DTU), 2019.

[Sim+20] A. Simonetto, E. Dall'Anese, S. Paternain, G. Leus, and G. B. Giannakis. "Time-varying convex optimization: Time-structured algorithms and applications". In: *Proceedings of the IEEE* 108.11 (2020), pp. 2032–2048.

[Sta19] I. O. for Standartization. *ISO 16290:2013 Space systems — Definition of the Technology Readiness Levels (TRLs) and their criteria of assessment*. 2019.

[SHD21] I. Subotic, A. Hauswirth, and F. Dorfler. "Quantitative sensitivity bounds for nonlinear programming and time-varying optimization". In: *IEEE Transactions on Automatic Control* (2021).

[Swi23] Swissgrid. *Swiss Voltage Support*. https://www.swissgrid.ch/en/home/customers/topics/ancillary-services/voltage-support.html. Accessed: 2023-04-23. 2023.

[TDL17] Y. Tang, K. Dvijotham, and S. Low. "Real-time optimal power flow". In: *IEEE Transactions on Smart Grid* 8.6 (2017), pp. 2963–2973.

[Tan+20] Z. Tang, E. Ekomwenrenren, J. W. Simpson-Porco, E. Farantatos, M. Patel, and H. Hooshyar. "Measurement-based fast coordinated voltage control for transmission grids". In: *IEEE Transactions on Power Systems* 36.4 (2020), pp. 3416–3429.

[THL20] Z. Tang, D. J. Hill, and T. Liu. "Distributed coordinated reactive power control for voltage regulation in distribution networks". In: *IEEE Transactions on Smart Grid* 12.1 (2020), pp. 312–323.

[TSO19] G. TSOs. "Netzentwicklungsplan Strom 2030 (Version 2019), Zweiter Entwurf". In: *Berlin, Dortmund, Bayreuth, Stuttgart: 50Hertz Transmission GmbH, Amprion GmbH, TenneT TSO GmbH, TransnetBW GmbH* (2019).

[TR76] Tzyh-Jong Tarn and Y. Rasis. "Observers for nonlinear stochastic systems". In: *IEEE Transaction on Automatic Control* 21.4 (Aug. 1976), pp. 441–448.

[UCT04] UCTE. *Final Report of the Investigation Committee on the 28 September 2003 Blackout in Italy*. 2004.

[VDE18] VDE. *VDE-AR-N 4105: Generators connected to the LV distribution network – Technical requirements for the connection to and parallel operation with low-voltage distribution networks*. 2018.

[Wan+20] J. Wang, M. Blonsky, F. Ding, S. C. Drew, H. Padullaparti, S. Ghosh, I. Mendoza, S. Tiwari, J. E. Martinez, J. J. Dahdah, et al. "Performance evaluation of distributed energy resource management via advanced hardware-in-the-loop simulation". In: *Innovative Smart Grid Technologies Conference (ISGT)*. IEEE. 2020, pp. 1–5.

[Wes+19] D. Westermann, S. Schlegel, F. Sass, R. Schwerdfeger, A. Wasserrab, U. Haeger, S. Dalhues, C. Biele, A. Kubis, and J. Hachenberger. "Curative actions in the power system operation to 2030". In: *International ETG-Congress 2019; ETG Symposium*. VDE. 2019, pp. 1–6.

[Wil+05] J. C. Willems, P. Rapisarda, I. Markovsky, and B. L. De Moor. "A note on persistency of excitation". In: *Systems & Control Letters* 54.4 (2005), pp. 325–329.

[Yam+09] K. Yamashita, J. Li, P. Zhang, and C.-C. Liu. "Analysis and control of major blackout events". In: *2009 IEEE/PES Power Systems Conference and Exposition*. 2009.

[Zag+23] M. Zagorowska, M. Degner, L. Ortmann, A. Ahmed, S. Bolognani, E. del Rio Chanona, and M. Mercangöz. "Online Feedback Optimization of Compressor Stations with Model Adaptation using Gaussian Process Regression". In: *Journal of Process Control* 121 (2023), pp. 119–133.

[ZMT10] R. D. Zimmerman, C. E. Murillo-Sánchez, and R. J. Thomas. "MATPOWER: Steady-state operations, planning, and analysis tools for power systems research and education". In: *IEEE Transactions on power systems* 26.1 (2010), pp. 12–19.